ISTANBUL TECHNICAL UNIVERSITY ★ GRADUATE SCHOOL

NUMERICAL INVESTIGATION OF RUNNING DYNAMICS OF A FREIGHT WAGON BOGIE WITH VARIABLE GAUGE WHEELS

M.Sc. THESIS

Gökhan KARAKAŞ

Department of Railway Systems Engineering

Railway Systems Engineering Programme

FEBRUARY 2022

ISTANBUL TECHNICAL UNIVERSITY ★ GRADUATE SCHOOL

NUMERICAL INVESTIGATION OF RUNNING DYNAMICS OF A FREIGHT WAGON BOGIE WITH VARIABLE GAUGE WHEELS

M.Sc. THESIS

Gökhan KARAKAŞ
(526181011)

Department of Railway Systems Engineering

Railway Systems Engineering Programme

Thesis Advisor: Assoc. Prof. Dr. Emin SÜNBÜLOĞLU

FEBRUARY 2022

ISTANBUL TEKNİK ÜNİVERSİTESİ ★ LİSANSÜSTÜ EĞİTİM ENSTİTÜSÜ

AKS AÇIKLIĞI DEĞİŞTİRİLEBİLİR BİR YÜK VAGONU BOJİSİNİN SEYİR DİNAMİĞİNİN SAYISAL OLARAK İNCELENMESİ

YÜKSEK LİSANS TEZİ

Gökhan KARAKAŞ
(526181011)

Raylı Sistemler Mühendisliği Anabilim Dalı

Raylı Sistemler Mühendisliği Programı

Tez Danışmanı: Doç. Dr. Emin SÜNBÜLOĞLU

ŞUBAT 2022

Gökhan KARAKAŞ, an M.Sc. student of ITU Graduate School student ID 526181011, successfully defended the thesis entitled "NUMERICAL INVESTIGATION OF RUNNING DYNAMICS OF A FREIGHT WAGON BOGIE WITH VARIABLE GAUGE WHEELS", which he prepared after fulfilling the requirements specified in the associated legislations, before the jury whose signatures are below.

Thesis Advisor :	**Assoc. Prof. Dr. Emin SÜNBÜLOĞLU** Istanbul Technical University	.....
Jury Members :	**Prof. Dr. Cemal BAYKARA** Istanbul Technical University	.....
	Assoc. Prof. Dr. Semih SEZER Yildiz Technical University	.....

Date of Submission : 14 January 2022
Date of Defense : 08 February 2022

To my family,

FOREWORD

Endless thanks to my advisor, Assoc. Prof. Dr. Emin SÜNBÜLOĞLU for his teachings on the subject of this study, his patience and his precious time on this thesis. His genuine and constructive approach to my work helped me at the highest level.

I am grateful to my mother Aynur and my father Rıdvan, who deserve the most credit for their support to me for the achievements in my education.

Many thanks Res. Assis. Fatih YAMAK, Azamet KARAOĞLAN, Cenk AKKAYA and Furkan Taha UĞURLUBİLEK for their help on many issues.

Thanks to the authors of all the references for the knowledge and contribution provided to study.

February 2022

Gökhan KARAKAŞ
(Railway Engineer)

TABLE OF CONTENTS

Page

ABBREVIATIONS

MBS **:** Multibody Simulation
BS : British Standard
EN **:** European Norms
DOF **:** Degrees of Freedom
UIC **:** International Union of Railway
GUI **:** Graphical User Interface

LIST OF TABLES

Page

LIST OF FIGURES

Page

NUMERICAL INVESTIGATION OF RUNNING DYNAMICS OF A FREIGHT WAGON BOGIE WITH VARIABLE GAUGE WHEELS

SUMMARY

Many innovations have been made on the basis of vehicles, rails and track structure in railway systems, which are of great importance for humanity. One among of a vast, axle groups called bogies are used to increase the performance of tractive and hauling stock to adapt curves on railway tracks. Thanks to bogies, the wheels provide a better positioning to the rails during their movements.

The distance between two rails on railway line varies among various countries and regions around the world. The wheels on the vehicles also have to change and adapt to track according to this track gauge if the start and final points of the intended travel are on different gauge stations. Therefore, there is an additional labour and time loss in the track gauge changing situations of vehicles on railway routes passing over two different gauge. Variable gauge bogies are one of the best solutions to minimizing the cost and time of adaptation.

This thesis aims to examine the running behaviour of a bogie design with variable gauge wheels using Numerical Multibody Dynamics Analysis. Wheel-rail interactions and many inter-vehicle interactions can be simulated with multibody simulation software platforms.

A conventional three-piece bogie and the new design bogie are analyzed and compared in terms of stability, twisted track analysis and bogie yaw resistance according to the specified standards. “Method 1” was applied to the twisted track and the Nadal criteria were examined. The running safety was checked by staying below the limit values in the standard.

On-track dynamic tests were performed only for the new design bogie. These dynamic tests were analyzed separately for various combinations of loading and vehicle length conditions using four differend classes of track according to their curve radii. The variable gauge distance bogie was also tested in two separate track gauges of 1435 mm and 1520 mm, as in the previous tests.

Some parts of the studied bogie design were modeled in CATIA V5. In addition, wheel profile, rail profile, tracks in three-dimensional space, wheel-rail pairs and contacts are created in SIMPACK environment. Track and vehicle configurations where dynamic tests are carried out are modeled according to the requirements specified in EN 14363 and EN 16235 standards.

An important recommendation was made to the design while performing all the tests. When the proposed design for the bogie was modeled exactly, derailment was observed in the wheels inside the curves. The problem has been solved by connecting the two inner axleboxes in the design to limit relative lateral movements to each other.

As a result, while the new design exhibits a different character in terms of stability, it succesfully met the criteria examined in this study in terms of running safety of freight wagons.

AKS AÇIKLIĞI DEĞİŞTİRİLEBİLİR BİR YÜK VAGONU BOJİSİNİN SEYİR DİNAMİĞİNİN SAYISAL OLARAK İNCELENMESİ

ÖZET

Demiryolları; hem yük hem de yolcu taşımacılığında sürdürülebilir, ekonomik, enerji etkin ve emniyetli oluşuyla ulaşım modları içerisinde önemli bir yer tutmaktadır.

Demiryolu sistemlerinin var olduğu ilk günden bugüne dek teknik gereksinimlerini ve iyileştirmelerini karşılamak amacıyla taşıtlar, raylar ve hat yapısı bazında birçok yenilik yapılmıştır.

Çeken ve çekilen demiryolu taşıtlarının, demiryolu hattında kurp ismiyle bilinen geometrik dönüşlere uyum sağlama performansını artırmak için boji adı verilen dingil grupları kullanılmaktadır. Bojiler en az iki dingil üzerine oturtulmuş şasiler olup taşıtların gövdeleri bojilerin merkezindeki mafsala oturtulur. Bu sayede kurplarda seyreden taşıtlar, tekerlekler için daha uygun bir konumlanış sağlarlar. Bojiler seyir emniyet ve konforuna katkılarının yanı sıra fren sistemleri gibi trenler için kritik önemdeki düzenekleri taşırlar.

Demiryolu hattında yük taşıyan iki tren rayı arasındaki mesafe dünya üzerinde çeşitli bölgeler arasında değişiklik gösterirken araçlardaki her dingil için iki tekerlek arasındaki mesafe de hat açıklığına göre değişmek durumundadır. Dolayısıyla farklı açıklıklara sahip iki bölge arasındaki yük ve yolcu seferlerinde kullanılan bojilerin veya taşınan konteyner yüklerinin sefer esnasında değişimi için özel kurulmuş tesislerde ilave iş gücü ve zaman kaybı durumu ortaya çıkmaktadır. Maliyetli bir çözüm olarak bazı bölgelerde çift hat açıklıklı yollar da kullanılabilmektedir. Hat açıklıkları farklı belirli iki bölge arasında yapılan tren seferleri için etkin bir çözüm olarak her iki bölgeye de uyum sağlayabilen aks açıklığı değişebilir bojiler kullanılabilmektedir. Bu bojiler sayesinde aynı dingil eksenine ait iki farklı tekerleğin birbirine göre yatay eksendeki mesafesi değişebilirken, trenler hat açıklığının değiştiği esnada durma yaşamadan seyrine devam edebilmektedir.

Bu tez çalışmasında aks açıklığı değiştirilebilir bir yük vagonu bojisinin seyir davranışlarının incelenmesi amacıyla bilgisayar ortamında çoklu gövde benzetimi amaçlanmıştır. Boji şasisi ve vagon gövdesi arasındaki süspansiyon boji yan çerçevesinin merkezinde konumlandığı için söz konusu model Amerikan tipi döküm bojinin dinamik karakteristiklerine benzemektedir. Bu tip bojiler üç parçalı boji olarak bilinmekte olup normalde iki yan çerçeve ve bir boji traversinden oluşur. Bu üç ayrı parça birbirine elastik bağlar ve sönüm elemanları ile irtibatlıdır. Boji traversinin bir diğer ismi bolster olup taşıt gövdesi ve boji irtibatını sağlayan pivotu da taşımaktadır. Düşey ve yatay eksenlerde oluşan ivmelenmeler bolster ve yan çerçevelere sürtünen sürtünme kamaları sayesinde sönümlemektedir.

Demiryolu taşıtlarının seyir davranışlarında kritik göreve sahip olan tekerlek-ray etkileşimleri, süspansiyon bileşenleri; sonuç olarak da yük vagonlarının dinamik davranışları çok gövdeli benzetim yazılımları kullanılarak benzetilebilir ve bu da

yüksek maliyetli fiziksel testler için geçerli bir alternatif sağlayabilir. Bu noktada seyir dinamiğinin benzetimi içi rijit veya esnek gövdeleri mafsallar ve kuvvet elemanları gibi bileşenler yardımıyla ilişkilendiren ve dinamik denklemleri kullanarak çözümleyebilen MBS yazılımları oldukça kullanışlıdır.

Aks açıklığı değiştirilebilir bojinin benzetiminden önce bojinin yan çerçeveleri, sürtünme kamaları, bolster ve tekerlek milleri tasarım parametrelerine uygun olarak CATIA V5 yazılımında parça dosyası olarak modellenmiştir. Bu parçalar MBS için kullanılan SIMPACK paket yazılımına aktarılmıştır. Vagonlarda çok sayıda tekrar eden tekerlek setleri ve tekerlek setlerinin bulunduğu bojiler alt modeller kullanılarak oluşturulup birleştirilmiştir. Bu parçalar üç parçalı bojilerin içerdiği tekerlek-boji arasındaki birincil süspansiyon, boji-taşıt gövdesi arasındaki merkezi süspansiyon, boji göbek mafsalları ve yan yasıklar vasıtasıyla irtibatlanmıştır.

Yazılımda tekerlek profili, ray profili, üç boyutlu uzayda demiryolu hatları, tekerlek-ray çiftleri ve temasları oluşturulmuştur.

Dinamik davranışların testleri için kullanılan demiryolu hat kısımları EN 14363 "Demiryolu uygulamaları – Demiryolu taşıtları seyir niteliklerinin kabul deneyleri – Seyir davranışlarının denenmesi ve durağan deneyler" standardında belirtilen isterlere göre tanımlamıştır. Ayrıca standartta belirtildiği gibi, test koşullarına göre taşıtların uzunluk, ağırlık ve sürat konfigürasyonu gibi parametreleri işlenmiştir.

Standart bir Amerikan tipi boji ve aks açıklığı değişebilen bojiler çok gövdeli mekanizmalar mantığıyla modellenmiştir. Dinamik analizi yapılan aks açıklığı değişebilen boji 1435 mm ve 1520 mm olmak üzere iki ayrı hat açıklığında çalışmaktadır. Her iki açıklık durumu için de yatay eksende konumlanabilen tekerlekler test edildiği açıklıklığa göre yataklanmıştır. Gerçekleştirilen testler sonrasında iki ayrı açıklık durumunda da ilgili EN standartlarının isterlerine göre mukayese edilmiştir. Bojiler ve vagon arasındaki açısal yer değiştirmelere göre küresel mafsalda oluşan momentler EN 16235 "Demiryolu uygulamaları – Demiryolu araçlarının seyir karakteristiklerinin kabul deneyleri – Yük vagonları – EN 14363'e göre hat üstü deneylerde belirlenen özelliklere sahip yük vagonlarının muafiyet koşulları" standardı çerçevesinde incelenmiştir.

Aks açıklığı değiştirilebilir boji düz yolda ivmelendirilerek kritik hız açısından incelenmiştir. Konvansiyonel bir üç parçalı bojiye göre aks yapısının ve birincil süspansiyon yönteminin farkından kaynaklanarak instabilite karakterinde farklılık gözlemlenmiştir.

Bükülmüş test yol analiziyle her iki açıklık için de "Metod 1" uygulanmıştır. Tekerlek başına gelen düşey ve yatay kuvvet değerleri incelenmiştir. Taşıtın derayman analizi Nadal kriterince değerlendirilmiştir. Tekerlek yükselmesi değeri standarttaki limitine göre kontrol edilmiştir.

Hat üstü dinamik testler ilgili yol kısımlarının kurp yarıçaplarına göre dört ayrı sınıfta yapılmaktadır. Bu dört farklı yarıçapta deversiz düz yolda standartta belirtilen maksimum dever eksiklik değeri oluşturularak maksimum hız altındaki taşıt karakterleri analiz edilmiştir. Maksimum hızlar yüksek yarıçaplı kurplarda veya geometrik olarak aliyman olarak bilinen düz yollarda instabilite riskini ve taşıt ivmelenmelerini kontrol etme amacı taşımaktadır. Daha küçük kurp yarıçaplı yollarda ise yüksek değerlerde tekerlek kuvvetleri (yatayda ve düşeyde) oluşturulması amaçlanıp dönüş yay merkezinin geometrik olarak daha uzağında kalan ön tekerleğe ve raylara etkisi incelenir.

Dinamik testler dört ayrı yol sınıfında taşıtın boş/dolu vagon ve kısa/dolu vagon durumları ayrı ayrı bakılarak iki açıklık için gerçekleştirilmiştir.

Bahsedilen testler tamamlanarak tekerlekleri dar açıklıkta (1435 mm) olan aks açıklığı değiştirilebilir yük vagonu bojisi ve tekerlekleri geniş açıklıkta olan (1520 mm) aks açıklığı değiştirilebilir yük vagonu bojisi seyir dinamiği açısından standartları karşılamıştır. İlgili benzetimler ve sonuçlarındaki çıktılardan faydalanılarak önceden önerilen konsept kapsamında tavsiyeler oluşturulmuştur. Stabilite ve tekerlek-ray etkileşimleri açısından çıkarımlar ve kıyaslamalar yapılmıştır.

Aks açıklığı değiştirilebilir boji için önerilen dizayn birebir modellenip kurpta hareketlendiğinde, tekerleklerin limitleyici elemanlarına rağmen kurpların iç tarafında kalan tekerleklerde derayman gözlemlenmiştir. Tasarımdaki iki iç tekerleğin birbirine göre yatay hareketlerini kısıtlamak amacıyla içeride kalan aks kutuları birbirine her iki uçta da rijit kirişlerle bağlanmıştır. Sonuç olarak derayman problem çözülmüştür.

Standart bir üç parçalı boji artan hızlarla birlikten yükselen instabilite sorunuyla karşılaşırken önerilen yeni tasarımın modelinde bu daha az gözlemlenmiştir.

Tekerlek-ray arası kuvvetler, süspansiyon yükleri ve deraymanla ilgili katsayılar gerekli standartları sağlamıştır ve modellenmiş olan aks aralığı değiştirilebilir boji seyir dinamiği açısından simülasyonları başarıyla tamamlamıştır.

1. INTRODUCTION

Railways have multiple advantages in freight transportation and remain as an indispensable important sector. Railway transportation systems contribute greatly to the economies of countries although the financial losses of many railway operations in the world are covered by states. There are factors that can be preferred in terms of sustainability, energy efficiency, safety and security. These advantages have led to a wide range of applications for railway systems all over the world. In the use of certain factors, standardization have been inevitable for manufacturers and operators.

One of a mentioned standardization is railway line span. The span distance between the rails in rail transport terminology is named track gauge (Figure 1.1). Measuring range is between the inner faces of two load-bearing rails. This range varies in use by countries or regions. Dominantly used track gauge is known as “Standart gauge” which measured 1435 mm. The second common track gauge in continent of Europe is 1520 mm which mostly used by former Soviet Union countries. (Figure 1.2).

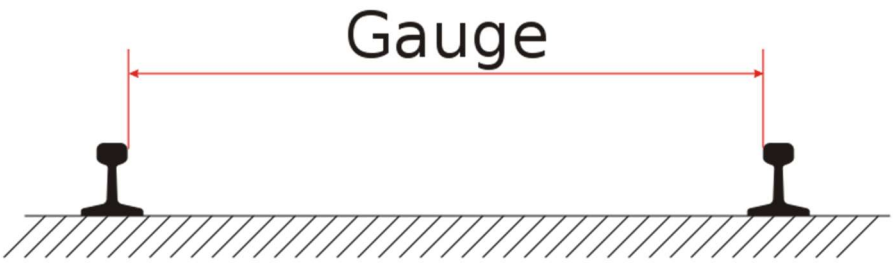

Figure 1.1 : Railway track gauge definition [1].

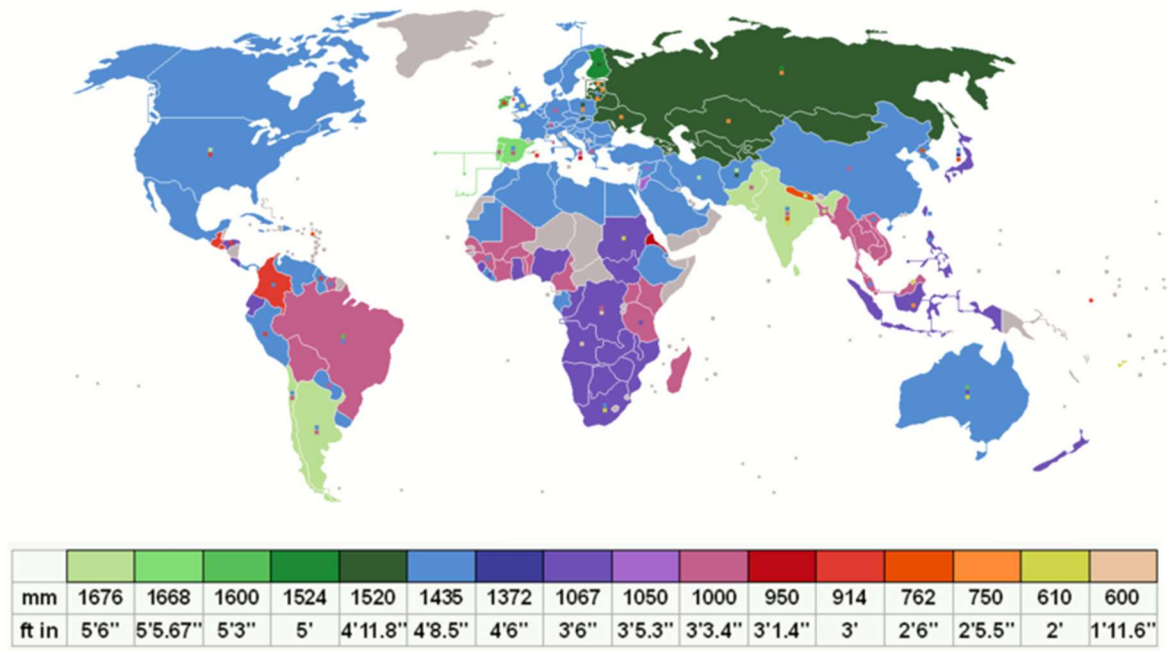

Figure 1.2 : Global track gauges map [2].

Track gauge is one of the main identifying elements for design of the railway vehicles and trains. Wheels must be positioned on the axle according to this value. Therefore, conventional railway vehicles and trains can only operate in countries which their design gauge is compatible. Different track gauges on routes appear as an obstacle during transportation via railways. This situation requires additional labour and time to make the rolling stock fit for new track section with particular solutions such as bogie changing or transporting container loads to new platform wagons, etc... .

Although a small portion of freight wagons consist of only two axles, most of them include bogies. Bogies consist of chassis and wheels, they are used for railway vehicles to adapt better to curves in movement. Seperately, they also allows further loading to be carried with more bearing points created by more wheels. Freight wagon bogies consist of springs, dampers, braking devices and mechanisms of other systems with relatively simple features in terms of design, production and maintenance along various improvements that have been made according to some purposes. Variable gauge axles and bogies are special examples and it is an optimised solution to the problem of adapting to different track gauge dimensions en route as mentioned before. Considering the transcontinental rail link projects that are popular today, variable gauge axle systems would become need beyond improvement in the future.

1.1 Purpose of Thesis

It is seen that variable gauge bogies might have interesting running dynamics characteristics when they are examined depending on the design of the gague-adaptation system. Varying quantities and DOFs are seen for axles and other main parts. In this thesis it is aimed that performing dynamic tests, examining running behaviour and simulations on a proposed design for freight bogie with variable gauge. It is intended to be modeled correct in terms of MBS in SIMPACK software and examine running behaviour.

2. BOGIES IN RAILWAY VEHICLES

Economic and safe freight transport is the first priority and necessity in rail systems. The load carried in a wagon must be further as much as possible for an economic transportation. In order to carry more load, longer than early-stage wagons were considered and implemented. Due to the permitted values for axle loads on the wheelsets used in these, more than two axles had to be used per wagon. To adapt the wagons with more axles and long chassis as well as to the curves, additional sub-structures with axle groups called bogies have been created. A bogie consists of a small chassis mounted on at least two axles. The wagon carbody is generally mounted on a rotational joint to the centre pivot of the bogie (Figure 2.1).

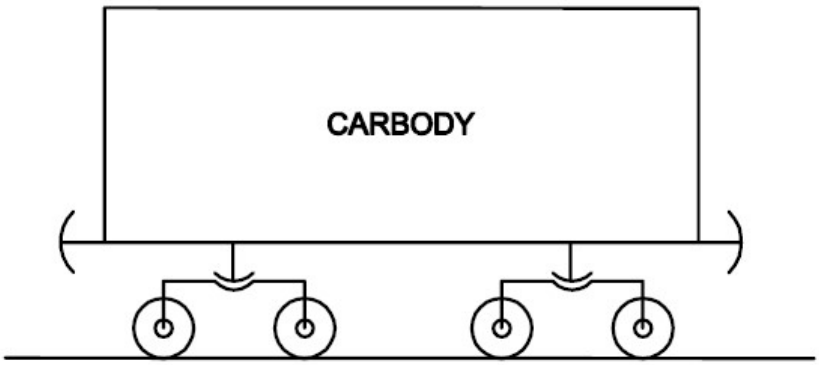

Figure 2.1 : Bogie and wagon schematic representation.

Bogies allow the wheelsets to more closely follow the direction of the rails when traveling around a curve in the railroad [3], thus adaptation of wagons to the curves have considerably increased (Figure 2.2).

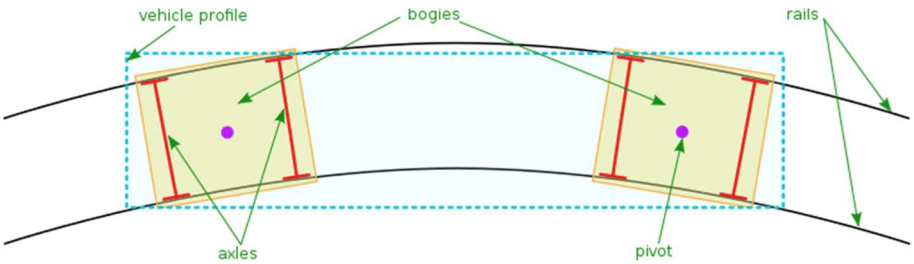

Figure 2.2 : Bogie positioning on curves.

Bogies are usually manufactured with two axles which have benefits such as better running characteristics, less wear on the rail and less risk of derailment though for special purposes 3 or more axles can be included. Damping methods and suspension elements of the bogies vary according to the railway vehicle classification which is passenger or freight train. Furhermore, in order to provide sufficient traction force, locomotive bogies with more than two axles are also made. Likewise, special designs with more than two bogies in a single one or Jacobs type bogies commonly are with articulated railcars can be used. The bogie to be used is determined by considering the running conditions. Consequently classification of the bogies is not independent of them either.

2.1 Carbody to Bogie Connection

Connection of the bogie and the rolling stock carbody allows the angular movement of the bogie relatively to the carbody. It must transmit the inter-vehicle forces and provide stability of rolling stock. Connection types are various, basically spherical or cylindrical parts and joints are often seen.

Car body to bogie connection appears in following:

- Flat Centre Plate
- Spherical Centre Bowl
- Centre Pivot
- Watts Linkage
- Pendulum Linkage
- Connection for Bolsterless Bogies

Flat centre plate is the most common connection for three-piece freight bogies. Flat circular centre plate is secured by pin at the center (Figure 2.3). It has simple installation but yields to basic problems such as wear on support surfaces and the connection itself on the curves and slopes. It is an assembly that increases lateral wheel-rail forces. Clearances exist in the lateral and longitudinal directions. Spherical bowls connect the base to the carbody in a similar way with flat centre plate but works with elastic side bearers between bogie and carbody and it is a spherical joint (Figure 2.4) with more freedom of motion. Spherical centre bowls case is more feasible in

comparison with flat centre plates, since low levels of contact stress provides long term service life. Spherical centre bowls are widely used in UIC freight bogies [4].

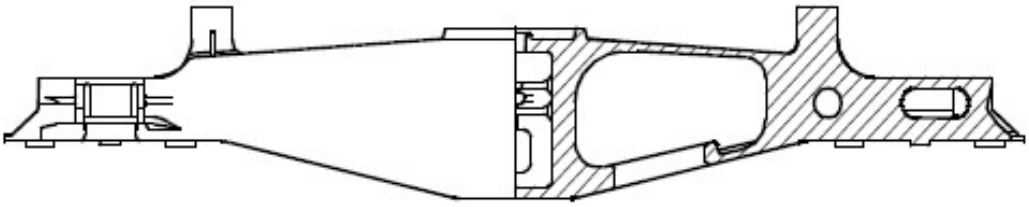

Figure 2.3 : Flat centre plate.

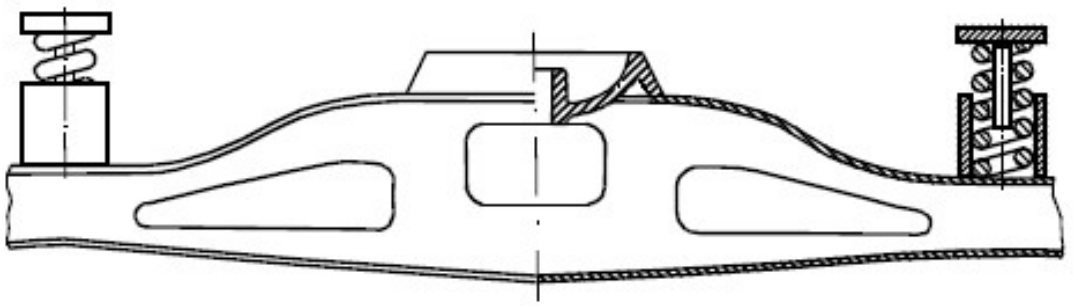

Figure 2.4 : Spherical centre bowl.

2.2 Structure of Freight Wagon Bogies

Freight wagon bogies generally have (apparently) single stage suspensions. Main types of single stage suspensions are axle box suspension and central suspension. Axle box suspensions provide damping of vibrations between the bogie frame and the wheels, close to the axle bearing zones. Central suspensions perform the same task between bogie frames and bolster. Freight wagon bogies with double stage suspensions in advanced design are also available but they are rare in comparison.

Similar to the previous classification, bogies can also be grouped as one-piece (H-Frame Y25 or similar) and three-piece bogies. In this way, it has more self-explanatory denotation. One-piece bogies have only a main rigid body while three-piece bogies have two seperate side frames both right and left side and the bolster that are elastically connected by coil spring nests and damping systems with friction wedges. Friction wedge suspensions are seen in three-piece bogie types.

Freight wagons have to operate between tare and laden loading conditions. Springs in the three-piece bogies generally have independent stiffness to the load while one-piece

bogies which they are commonly used in Europe and linkage for primary suspension provides lower stiffnes in tare than in laden.

2.3 Three-Piece Bogies

Three-piece bogies are common in countries which are largest by area like the USA, Canada, Australia, China and Russia. Simple and lower cost design of these bogies made it selection element in mentioned countries due to their conditions. It also known as “American bogie” (Figure 2.5 and Figure 2.6).

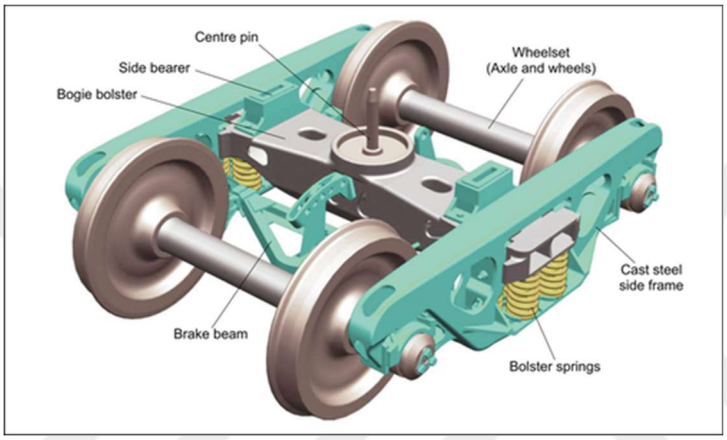

Figure 2.5 : A standard American three-piece bogie.

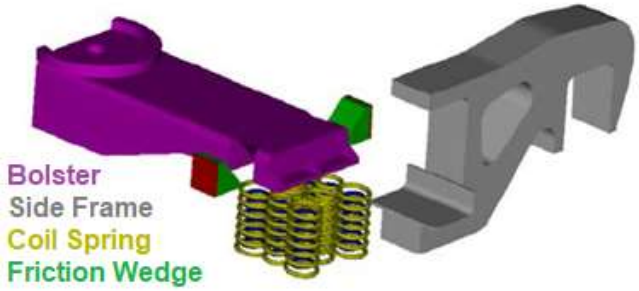

Figure 2.6 : Main components of the three-piece bogie [5].

Support points of side frames are wheels then again side frames are support provider for bolster. Simple design of three-piece bogie is an advantage while it brings many non-linear interactions which are effortful to computate. Rolling stock performance is crucially depends on friction wedges. Relative motions of bolster and side frames create frictions on these wedges in vertical and lateral dimensions. This method provides damping in the mentioned directions. Friction wedges act according to two different approaches: variable column damping and constant column damping (Figure 2.7).

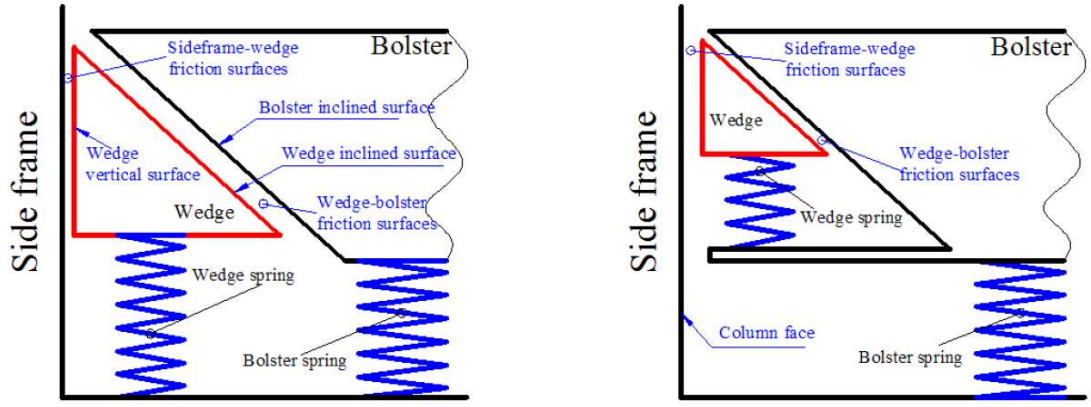

Figure 2.7 : Variable (left) and constant (right) damping [6].

In constant damping method, wedge carrier springs do not compensate the vehicle loads. It provides constant friction forces on side frames and bolster surfaces. The other one, variable damping method changes the wedge spring forces due to vehicle's static and dynamic loads.

2.3.1 Variable gauge bogie

In this thesis, a special bogie concept has been studied and examined in terms of running dynamics. There are some important points to note when comparing this bogie concept to an original three-piece bogie. The variable gauge purpose has brought changes of the components in their design.

In this bogie frame, there are inner and outer side frames in both left and right sides. Instead of a single monobloc shaft, two concentric shafts are placed in an axle row. These shafts, which will be released laterally from the axle boxes at the gauge change stations will be able to make relative lateral movement. The wheels lock at the station exits into the new gauge states [7]. This design eliminates the need for extending shafts such as ELH Y25Lsd1-Spw bogie (Figure 2.8) [8].

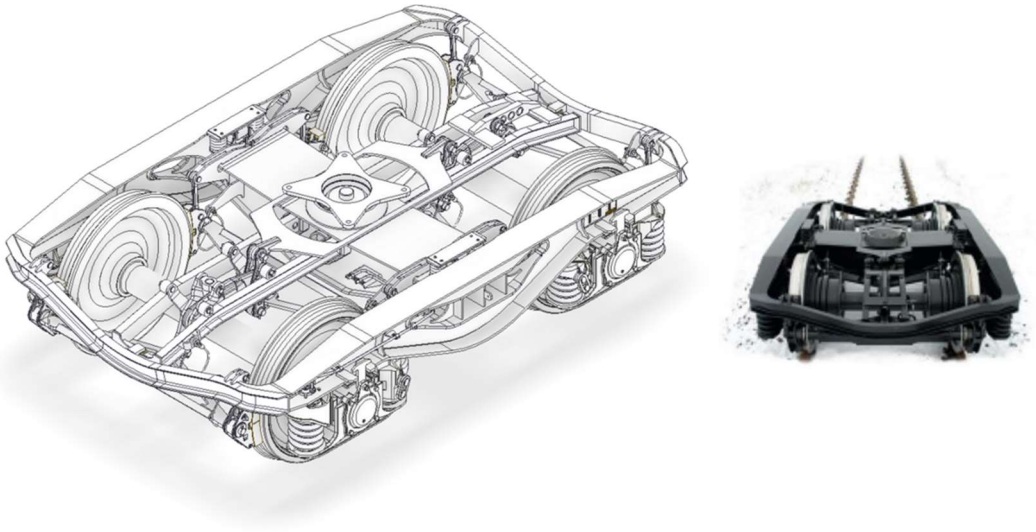

Figure 2.8 : Variable Gauge Bogie With Extending Shafts.

Variable gauge bogie without extending shafts is shown in Figure 2.9. Number of components of original three-piece bogie and this variable axle distance bogie is compared in Table 2.1.

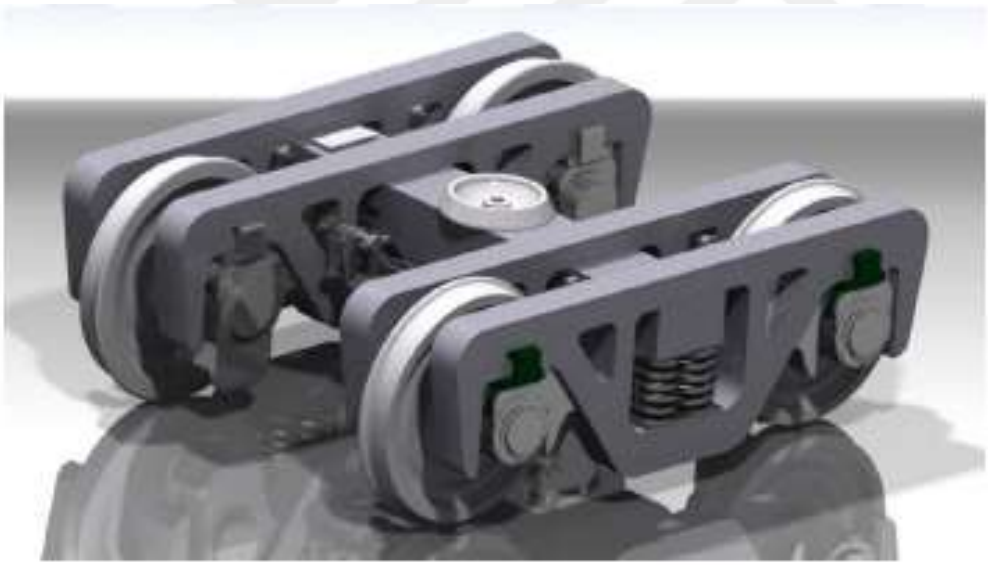

Figure 2.9 : Variable Gauge Bogie.

There are no comprehensive and definite recomendations for suspension in the concept design instead it has central suspension system which have coil spring sets in the middle of side frames. Friction wedges to provide dry friction for vibration damping of the vehicle and coil spring sets are proposed in this thesis study.

Table 2.1 : Component numbers of three-piece and variable gauge bogies.

	Three-Piece Bogie	Variable Gauge Bogie
Number of axles	2 (long)	4 (short)
Number of wheels	4	4
Number of axle boxes	4	8
Number of bolsters	1	1
Number of side frames	2	4
Number of wedges	4	8

2.4 Literature Review

In the modern railway environment, software solutions has become an important instrument in the design and acceptance stages. Performing simulations that is an alternative to high-cost experimental tests is properly a trade-off situation. Simulations will achieve accurate results as experimental tests, but only with the correct modeling. Especially wheel-rail contact and many inter-vehicle interactions are non-linear situations that are difficult to modelling. Nevertheless all types of freight bogies have specific and common fundamentals in a wide sense.

Stichel and Jönsson examined the dynamic characteristics of wagons with single axle running gear. Carbody hunting is correlated with resonance between kinematic motions of the wheelsets and eigenmodes of the vehicle. These studies have shown the relationship between hunting mode and damping although mostly on UIC link characteristics [9,10].

Eickhoff has shown modeling techniques for railway vehicles in the related review, in particular he studied primary and secondary suspensions and vehicle coactions except wheel-rail contacts [11].

Iwnicki's book [4] gives comprehensive information about dynamics of rolling stock. Significant knowledge that shaped the project initially is most of freight bogies are with friction damping instead of viscous damping.

Bosso has shown that Lenoir link mechanism in certain type of bogies and friction wedges in three-piece type bogies provides lateral and vertical damping against the distruptive effect of the track [12].

The variable gauge bogie frame concept studied for dynamic analysis in this project is three-piece bogie categorically from running behaviour wise. Additional parallel

sideframe bodies are added for bearing of two concentric axles instead of standard single axle. All the axles which move laterally in the gauge changing with movement freedom for axle gauge change. Secondary suspension between bogie and wagon is positioned in center of sideframes [7].

Wu gives comprehensive information about friction wedges, friction damping theory and modeling in different MBS models, quasi-static analyses and force element combinations in the related article. The method of representation of friction surfaces in software is described and is a very important basis for the modeling [6].

Shabana's book [13] helps in terms of theoretical explanations of transformation matrices and equation of motion in his comprehensive book on multibody dynamics and multibody simulations.

3. BASICS OF MULTIBODY DYNAMICS

Multibody Dynamic System modeling is a numerical examination method for kinematic and dynamic analysis of systems consisting of various rigid and/or elastic bodies. Connections between bodies can be modeled by various selection of kinematic joints, force elements, control devices and constraints (Figure 3.1). Multibody dynamics is widely used in engineering systems such as automotive, railway systems, biomechanics, robotics, aviation, space structures, engines, wind turbines, etc.

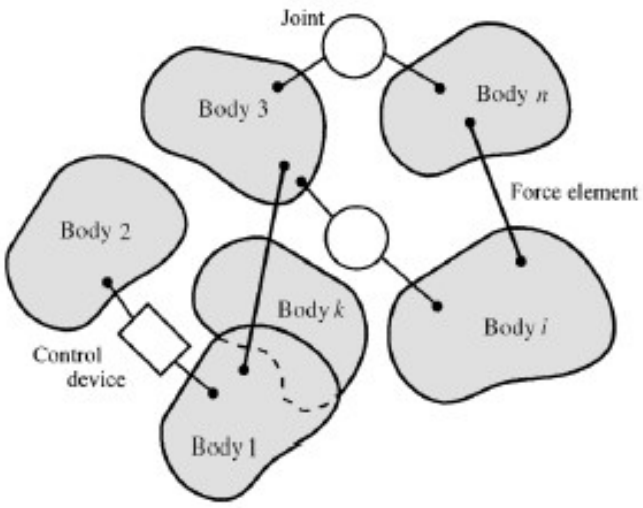

Figure 3.1 : Multibody systems.

While studying rigid bodies, the kinematics of the body is completely defined by the body reference coordinate system because the particles of a rigid body do not move relative to its fixed body reference system. It is possible to define purely geometric correlations between axes and all points. In creating equations of motion that define the positions of bodies and their relative to each other, reference kinematics are used [13].

Reference kinematics for rigid models, equations of motion in accordance with the Lagrangian approach, wheel-rail contact algorithm, multibody dynamics solver properties and Coulomb frictions of friction wedges are described in the continuation of this section which MBS package softwares take as theoretical basis.

3.1 Reference Kinematics

Any particle of a moving rigid body remains in the same position according to reference coordinate system of the body. Components express local positions also used as components of moving coordinate system as remain constant. It constitutes an important distinction in terms of the study of flexibe bodies.

This type of examination consists in terms of the translation of the origin and/or rotation around an axis. The reference system is explained by an orhogonal axis system defined on the body. Assuming that the origin of the reference system is fixed at some point, the movement occurs only with translations and rotations around the axes. Therefore, the reference system is fixed at any point on the rigid body and the orientation of this reference system is explained with the help of transformation matrices. After defining these transformation matrices, the translational displacement of the origin is defined in terms of components along the axes of the moving reference. As a result, translations and rotations are represented.

3.1.1 The transformation matrix

There are six variables for definiton of the position of a coordinate system ($\mathbf{X}_1^i\mathbf{X}_2^i\mathbf{X}_3^i$ axes system of origin O^i) for a rigid body with respect to another $\mathbf{X}_1\mathbf{X}_2\mathbf{X}_3$ coordinate system of origin O (Figure 3.2).

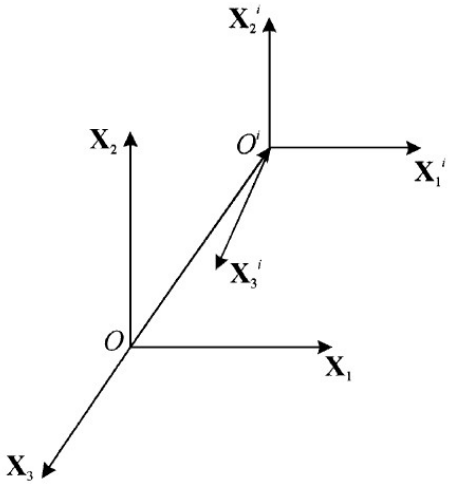

Figure 3.2 : Coordinate systems.

Three variables can define translation. Position vector of $\boldsymbol{O}^i$ represents this definiton and it is respected to $\mathbf{X}_1\mathbf{X}_2\mathbf{X}_3$ coordinate system. As a result, the vector $\bar{\mathbf{r}}$ is the position

vector of the point $\bar{Q}$ which is fixed in the coordinate system $\mathbf{X}_1^i\mathbf{X}_2^i\mathbf{X}_3^i$. Also considering the rotation about axis OC amount of angle θ in Figure 3.3, the $\bar{Q}$ is translated to the Q point with the help of $\Delta\mathbf{r}$ vector. $\Delta\mathbf{r}$ is sum of $\mathbf{b_1}$ and $\mathbf{b_2}$ vectors in representation of rotational motion (3.1).

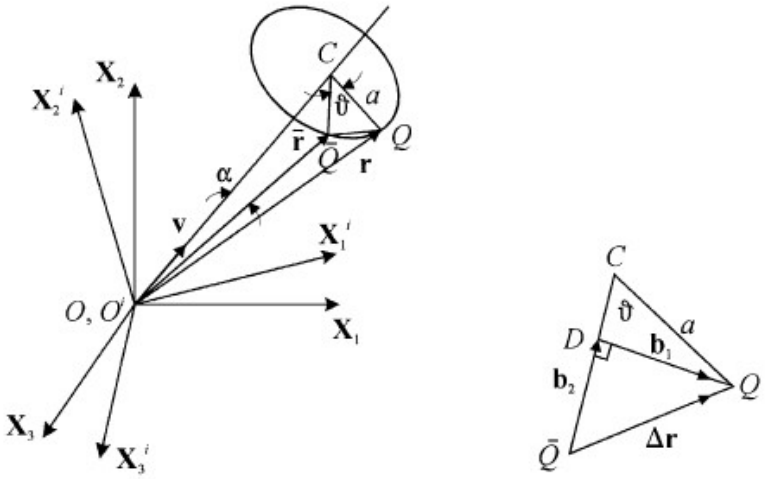

Figure 3.3 : Rotation about axis (left) and vector evaluation of rotation (right).

The motion finally changes to the vector $\mathbf{r}$, and the new vector can be expressed as in (3.2).

$$\Delta\mathbf{r} = \mathbf{b}_1 + \mathbf{b}_2 \tag{3.1}$$

$$\mathbf{r} = \bar{\mathbf{r}} + \Delta\mathbf{r} \tag{3.2}$$

The magnitude of the vector $\mathbf{b}_1$ which is perpendicular to the $OC\bar{Q}$ plane is (3.3) and the magnitude of the vector $\mathbf{b}_2$ which is perpendicular to the unit vector of $\mathbf{v}$ and $\boldsymbol{DQ}$ vector is (3.4).

$$|\mathbf{b}_1| = a\sin\theta \tag{3.3}$$

$$|\mathbf{b}_2| = 2a\sin^2\frac{\theta}{2} \tag{3.4}$$

Direction of $\mathbf{b}_1$ is $(\mathbf{v}\times\bar{\mathbf{r}})$ and direction of $\mathbf{b}_2$ is the same as the unit vector $(\mathbf{v}\times\bar{\boldsymbol{r}})/a$. One can see that from the Figure 3.3, $a = |\bar{\mathbf{r}}|\sin\theta = |\mathbf{v}\times\bar{\mathbf{r}}|$. The vector expressions (3.5) and (3.6) are created based on directions and magnitudes of $\mathbf{b}_1$ and $\mathbf{b}_2$. Hence,

$$\mathbf{b_1} = a \sin\theta \frac{\mathbf{v} \times \bar{\mathbf{r}}}{|\mathbf{v} \times \bar{\mathbf{r}}|} = (\mathbf{v} \times \bar{\mathbf{r}}) \sin\theta \tag{3.5}$$

$$\mathbf{b_2} = 2a \sin^2\frac{\theta}{2} \cdot \frac{\mathbf{v} \times (\mathbf{v} \times \bar{\mathbf{r}})}{a} = 2[\mathbf{v} \times (\mathbf{v} \times \bar{\mathbf{r}})] \sin^2\frac{\theta}{2} \tag{3.6}$$

By combining previous equations in this chapter, $\mathbf{r}$ vector can be formed to (3.7).

$$\mathbf{r} = \bar{\mathbf{r}} + (\mathbf{v} \times \bar{\mathbf{r}}) \sin\theta + 2[\mathbf{v} \times (\mathbf{v} \times \bar{\mathbf{r}})] \sin^2\frac{\theta}{2} \tag{3.7}$$

Let the components of the $\mathbf{v}$ unit vector are $\mathbf{v}_1$, $\mathbf{v}_2$, $\mathbf{v}_3$ and the components of the $\bar{\mathbf{r}}$ vector are $\bar{\mathbf{r}}_1$, $\bar{\mathbf{r}}_2$, $\bar{\mathbf{r}}_3$. Equation (3.8) is a typical vector expression.

$$\mathbf{v} \times \bar{\mathbf{r}} = \tilde{\mathbf{v}}\bar{\mathbf{r}} = -\tilde{\bar{\mathbf{r}}}\mathbf{v} \tag{3.8}$$

In (3.8), $\tilde{\mathbf{v}}$ and $\tilde{\bar{\mathbf{r}}}$ are skew symmetric matrices given in (3.9) and (3.10).

$$\tilde{\mathbf{v}} = \begin{bmatrix} 0 & -v_3 & v_2 \\ v_3 & 0 & -v_1 \\ -v_2 & v_1 & 0 \end{bmatrix} \tag{3.9}$$

$$\tilde{\bar{\mathbf{r}}} = \begin{bmatrix} 0 & -\bar{r}_3 & \bar{r}_2 \\ \bar{r}_3 & 0 & -\bar{r}_1 \\ -\bar{r}_2 & \bar{r}_1 & 0 \end{bmatrix} \tag{3.10}$$

Equation (3.7) becomes as (3.11).

$$\mathbf{r} = [\,\mathbf{I} + \tilde{\mathbf{v}} \sin\theta + 2(\tilde{\mathbf{v}})^2 \sin^2\frac{\theta}{2}\,]\bar{\mathbf{r}} \tag{3.11}$$

$\mathbf{I}$ is 3x3 identity matrix. Equation (3.11) can be written as (3.12). In conclusion, transformation matrix A is shown in (3.13).

$$\mathbf{r} = \mathbf{A}\bar{\mathbf{r}} \tag{3.12}$$

$$\mathbf{A} = \mathbf{A}(\theta) = [\,\mathbf{I} + \tilde{\mathbf{v}} \sin\theta + 2(\tilde{\mathbf{v}})^2 \sin^2\frac{\theta}{2}\,] \tag{3.13}$$

This transformation matrix is completed with three different variables. It is also possible to express this transformation method in terms of Euler parameters. Euler

parameters which consist of four different values, are as in equations (3.14) and provide the relation in equation (3.15).

$$\theta_0 = \cos\frac{\theta}{2}, \qquad \theta_1 = v_1 \sin\frac{\theta}{2}, \quad \theta_2 = v_2 \sin\frac{\theta}{2}, \qquad \theta_3 = v_3 \sin\frac{\theta}{2} \tag{3.14}$$

$$\sum_{k=0}^{3} (\theta_k)^2 = \theta^T \theta = 1 \tag{3.15}$$

Where $\boldsymbol{\theta}$ is a vector consists from θ_0, θ_1, θ_2 and θ_3 is (3.16)

$$\boldsymbol{\theta} = [\theta_0 \quad \theta_1 \quad \theta_2 \quad \theta_3]^T \tag{3.16}$$

In terms of Euler parameters, the transformation matrix can be written as four different parameters with 3x3 matrix in equation (3.17) [13].

$$\mathbf{A} = \begin{bmatrix} 1-2(\theta_2)^2-2(\theta_3)^2 & 2(\theta_1\theta_2-\theta_0\theta_3) & 2(\theta_1\theta_3+\theta_0\theta_2) \\ 2(\theta_1\theta_3+\theta_0\theta_3) & 1-2(\theta_1)^2-2(\theta_3)^2 & 2(\theta_2\theta_3-\theta_0\theta_1) \\ 2(\theta_1\theta_3-\theta_0\theta_2) & 2(\theta_2\theta_3+\theta_0\theta_1) & 1-2(\theta_1)^2-2(\theta_2)^2 \end{bmatrix} \tag{3.17}$$

It is possible to determine position, velocity and acceleration vectors by the help of derivative relations of the transformation matrices. Apart from this statement, the transformation matrices are orthogonal and orthogonality expression proves (3.18) and (3.19).

$$\mathbf{A}\mathbf{A}^{\mathrm{T}} = \mathbf{I} \tag{3.18}$$

$$\dot{\mathbf{A}}\mathbf{A}^{\mathrm{T}} + \mathbf{A}\dot{\mathbf{A}}^{\mathrm{T}} = 0 \tag{3.19}$$

3.2 Generalized Coordinates

Generalized coordinates are used to determine the exact location and orientation in a multibody system. Three parameters are used according to the dimensions x, y and z for translational displacement. There are three or four different parameters in addition to the parameters caused by translational displacement, depending on whether Euler angles, Rodriguez paramaters or Euler parameters will be used in spatial analysis [13].

Since Euler parameters are mentioned in the theoretical explanation part of this study, generalized coordinates are explained with 7 different coordinates.

The position of a point P on the rigid body named i in the system is expressed as in the equation (3.20).

$$\mathbf{r}_P^i = \mathbf{R}^i + \mathbf{A}^i \overline{\mathbf{u}}^i \tag{3.20}$$

$\mathbf{R}^i$ is the position of the origin of the i-th body that uses $\mathbf{X}_1^i \mathbf{X}_2^i \mathbf{X}_3^i$ body reference. $\mathbf{A}^i$ is the transformation matrix, according to the global coordinate system. $\overline{\mathbf{u}}^i$ is local position of point P. Representations are shown in Figure 3.4.

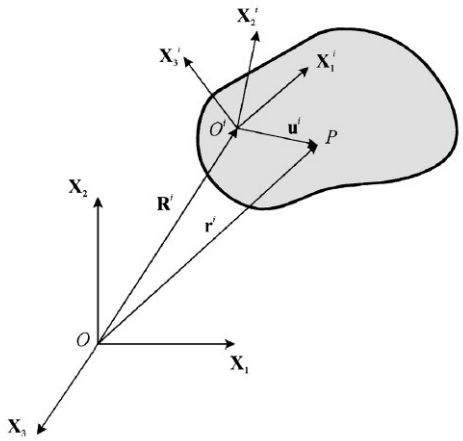

Figure 3.4 : Reference coordinates of the rigid body [13].

The notation of $\mathbf{q}_r^i$ can be used to define the translation and rotation coordinates of the body reference and it is indicated by the components "**R**" and "**θ**" in (3.21).

$$\mathbf{q}_r^i = [\mathbf{R}^{i^T} \quad \boldsymbol{\theta}^{i^T}] \tag{3.21}$$

General equations of motion of rigid bodies can be shown by reference kinematics and general coordinates in multibody systems.

3.3 Equations of Motion

3.3.1 Equations of Motion of unconstrained bodies

The general equation of motion of an unconstrained body is shown in (3.22) [14].

$$\mathbf{M}^i \ddot{\mathbf{q}}^i = \mathbf{Q}_e^i + \mathbf{Q}_v^i, \quad i = 1,2,\dots,n \tag{3.22}$$

According to this notation, $\mathbf{M}^i$ is represents the mass matrix, $\mathbf{q}^i$ is vector of coordinates of the body with 7 Euler parameters components. $\mathbf{Q}_e^i$ vector consists of generelized external forces of translations and orientations. $\mathbf{Q}_v^i$ is the vector for generalized inertia forces. If equation (3.22) in the simplified form is detailed into the matrix form, it gets the state as in equation (3.23).

$$\begin{bmatrix} m_{RR}^i & 0 \\ 0 & m_{\theta\theta}^i \end{bmatrix} \begin{bmatrix} \ddot{\mathbf{R}}^i \\ \ddot{\boldsymbol{\theta}}^{\mathbf{i}} \end{bmatrix} = \begin{bmatrix} (\mathbf{Q}_e^i)_R \\ (\mathbf{Q}_e^i)_\theta \end{bmatrix} + \begin{bmatrix} 0 \\ (\mathbf{Q}_v^i)_\theta \end{bmatrix}, \quad i = 1,2,\dots,n \tag{3.23}$$

Components containing the index "R" and "RR" are related to translational movements while the ones are with the index "θ" and "$\theta\theta$" are related to rotations. (3.23) is a matrix equation which governs the unconstrained motion of the rigid body "i" in centroidal case. The center of mass is on the body reference coordinate system and the rotation matrix described in the previous section is not yet visible. If the sub-matrices in the equation (3.23) are opened, equation (3.24) can be expressed.

$$\begin{bmatrix} m^i\mathbf{I} & 0 \\ 0 & \mathbf{I}_{cog}^i\mathbf{G}^i \\ 0 & \boldsymbol{\theta}^{iT} \end{bmatrix} \begin{bmatrix} \ddot{\mathbf{R}}^i \\ \ddot{\boldsymbol{\theta}}^i \end{bmatrix} = \begin{bmatrix} \sum_{j=1}^{n_f} \mathbf{f}_j^i \\ \mathbf{G}^{iT}\left[\sum_{k=1}^{n_m} \mathbf{m}_j^i + \sum_{j=1}^{n_f} \mathbf{u}_k^i \times \mathbf{f}_k^i\right] \end{bmatrix} + \begin{bmatrix} 0 \\ -\begin{bmatrix} \mathbf{I}_{cog}^i\dot{\mathbf{G}}^i\dot{\boldsymbol{\theta}}^i - (\mathbf{G}^i\dot{\boldsymbol{\theta}}^i \times \mathbf{I}_{cog}^i\mathbf{G}^i\dot{\boldsymbol{\theta}}^i) \\ \dot{\boldsymbol{\theta}}^{iT}\dot{\boldsymbol{\theta}}^i \end{bmatrix} \end{bmatrix}, \quad i = 1,2,\dots,n \tag{3.24}$$

In here, m is mass of the i-th body, $\mathbf{I}$ is 3x3 identity matrix, $\mathbf{f}^i$ is applied external forces vector, $\mathbf{u}_k$ is position vector of the point P, n_f is the number of total external forces, $\mathbf{m}^i$ is applied external torques and n_m is the total number of the torques. Equations (3.25), (3.26) and (3.27) express inertia matrix defined in global coordinate system and products of the transformation matrix in (3.17) defined in global and local coordinate system respectively.

$$\mathbf{I}_{cog} = \mathbf{A}\bar{\mathbf{I}}_{cog}\mathbf{A}^T \tag{3.25}$$

$$\mathbf{G} = 2\begin{bmatrix} -\theta_1 & \theta_0 & -\theta_3 & \theta_2 \\ -\theta_2 & \theta_3 & \theta_0 & -\theta_1 \\ -\theta_3 & \theta_2 & \theta_1 & \theta_0 \end{bmatrix} \tag{3.26}$$

$$\overline{\mathbf{G}} = 2\begin{bmatrix} -\theta_1 & \theta_0 & -\theta_3 & \theta_2 \\ -\theta_2 & -\theta_3 & \theta_0 & -\theta_1 \\ -\theta_3 & \theta_2 & \theta_1 & \theta_0 \end{bmatrix} \tag{3.27}$$

3.3.2 Equations of motion of constrained bodies

The bodies are connected with kinematic joints in multibody systems. Kinematics relationship is usually denoted by equation (3.28)

$$C(q,t) = 0 \tag{3.28}$$

Equations of motion of systems with consist of N bodies are shown in (3.29) with the help of Jacobian matrix $\mathbf{C}_q$.

$$\begin{bmatrix} \mathbf{M} & \mathbf{C}_q^T \\ \mathbf{C}_q & 0 \end{bmatrix}\begin{bmatrix} \ddot{q} \\ -\lambda \end{bmatrix} = \begin{bmatrix} \mathbf{Q}_e + \mathbf{Q}_v \\ \mathbf{Q}_d \end{bmatrix} \tag{3.29}$$

It is written in a different form in (3.30).

$$\begin{bmatrix} \mathbf{M}^1 & 0 & \cdots & 0 & \mathbf{C}_{q^1}^T \\ 0 & \mathbf{M}^2 & \cdots & 0 & \mathbf{C}_{q^2}^T \\ \vdots & \vdots & \ddots & \vdots & \vdots \\ 0 & 0 & \cdots & \mathbf{M}^N & \mathbf{C}_{q^N}^T \\ \mathbf{C}_{q^1} & \mathbf{C}_{q^2} & \ldots & \mathbf{C}_{q^N} & 0 \end{bmatrix}\begin{bmatrix} \ddot{q}^1 \\ \ddot{q}^2 \\ \vdots \\ \ddot{q}^N \\ \lambda \end{bmatrix} = \begin{bmatrix} Q_e^1 + Q_v^1 \\ Q_e^2 + Q_v^2 \\ \vdots \\ Q_e^N + Q_v^N \\ Q_d \end{bmatrix} \tag{3.30}$$

Generalized coordinates are shown by q. Jacobian matrix (3.31) defined as derivatives of constraint with respect to generalized coordinates.

$$\mathbf{C}_q = \begin{bmatrix} \dfrac{\partial C_x}{\partial q^1} & \cdots & \dfrac{\partial C_x}{\partial q^N} \\ \dfrac{\partial C_y}{\partial q^1} & \cdots & \dfrac{\partial C_y}{\partial q^N} \\ \dfrac{\partial C_z}{\partial q^1} & \cdots & \dfrac{\partial C_z}{\partial q^N} \end{bmatrix} \tag{3.31}$$

$\mathbf{Q}_d$ absorbs terms quadratic in the velocities and defined in equation (3.32). r represents number of constraint in the model [15].

$$\mathbf{Q}_d = \begin{bmatrix} -\sum_{a=1}^{N}\sum_{j=1}^{N} \frac{\partial^2 C_1}{\partial q_j \partial q_a}\dot{q}_j\dot{q}_a \\ -\sum_{a=1}^{N}\sum_{j=1}^{N} \frac{\partial^2 C_2}{\partial q_j \partial q_a}\dot{q}_j\dot{q}_a \\ \vdots \\ -\sum_{a=1}^{N}\sum_{j=1}^{N} \frac{\partial^2 C_r}{\partial q_j \partial q_a}\dot{q}_j\dot{q}_a \end{bmatrix} \tag{3.32}$$

3.4 Wheel-Rail Interaction

The basis of rail vehicle dynamics is the modeling of wheel and rail contact which is usually non-linear. Various wheel-rail contact models have been developed to examine the contact interaction between the wheel and the rail. Wheel-rail interaction analysis is based on theories such as Hertz and Kalker theories [16].

3.4.1 Hertzian contact theory

Hertz theory examines the contact of two parts with round surfaced bodies interacting with each other and the resulting deformation due to internal forces. The interface stresses occured on these contact surfaces are due to the so-called “Hertz Contact Pressure”. This theory occurs with following assumptions:

- The material is homogeneous and isotropic.
- Hooke’s Law applies.
- Only normal forces are assumed at the point of contact which is considered in a small area.
- Shear stress (at the interface) is not taken into account.
- The strain in the contact state is assumed to be small compared to other dimensions of the body.
- The force is evenly distributed over the entire contact area [17,18].

3.4.2 Kalker’s theory

Kalker’s theories have gained wide use of wheel-rail contact modelling in simulations of railways. This theories examine the rolling contact states of three-dimensional

elastic bodies. In addition to studies have been developed such as two-dimensional contact theories, Kalker's linear theory and Kalker's contact theory; there is also a simplified approach which called FASTSIM [19]. The software used in this thesis study was analyzed by means of the FASTSIM algorithm.

There are 4 different contact configurations when the movement of the wheel on the rail is examined. Due to track conditions in curves, superelevation differences cause one of these 4 situations at a time instant which are represented in Figure 3.5.

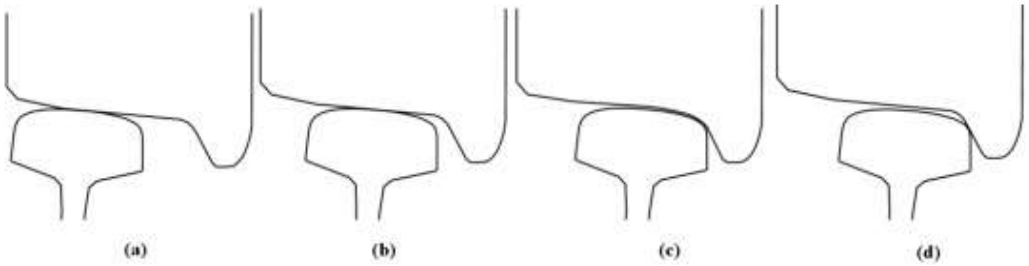

Figure 3.5 : Wheel and Rail Contact States [20].

The wheel-rail contact conditions illustrated in Figure 3.5 are classified as

- Field tread side-rail head contact (a)
- Tread-Rail head contact (b)
- Flange root-gauge corner contact (c)
- Flange-gauge corner contact (d)

Simulations along the line take into account these contact states considering rail wand wheel geometries. Possible contact points between the S1002 profiled wheel with 0.46 m radius used in the models and the UIC60 rail profile with 1:40 inclination as follows in Figure 3.6.

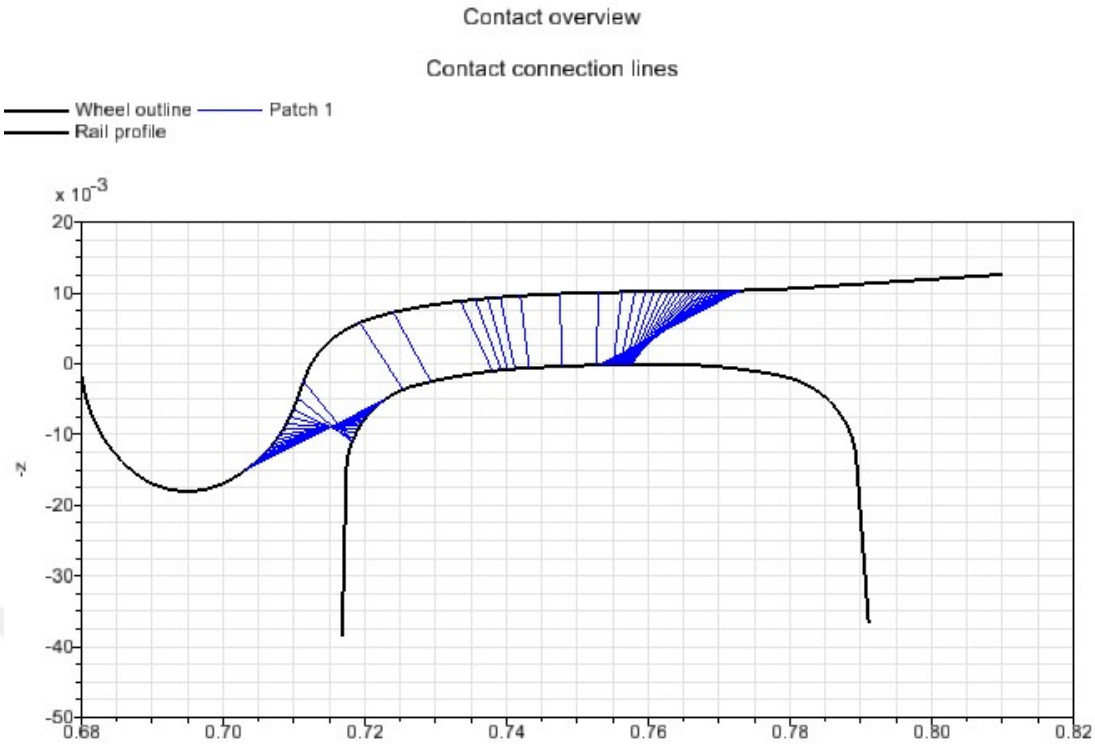

Figure 3.6 : Contact points for wheel-rail pair.

3.4.2.1 FASTSIM

There are certain differences with the Hertz and FASTSIM approaches while both have common assumptions. FASTSIM algorithm is faster in comparison to other programs and this is a great advantage for simulation purposes. This has made it the most preferred for the computation of wheel/rail tangential forces. FASTSIM method requires the contact surface to be considered elliptical. According to algorithm, mesh elements are created in the contact ellipse (Figure 3.7). Creep is calculated at the contact patch in each direction. The pressure and elementary forces are considered in the center of each contact patch.

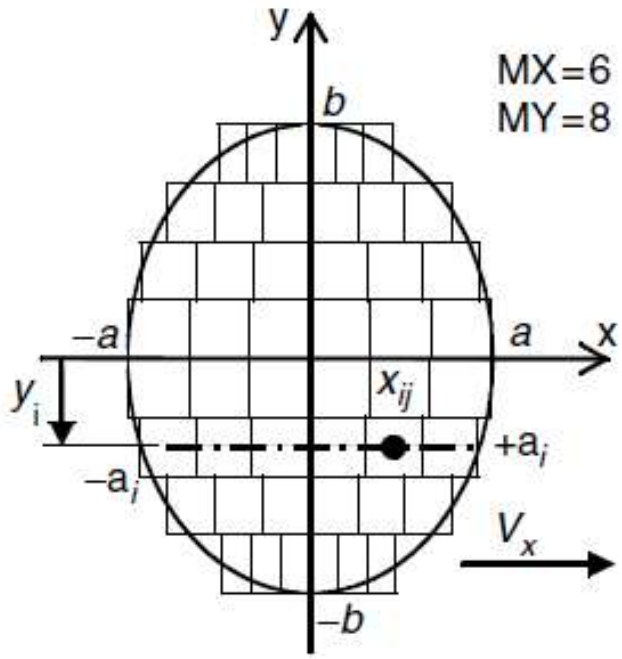

Figure 3.7 : MX x MY sized discretization within the contact ellipse [4].

According to the simplified theory, unsaturated stress distribution in the x direction is in (3.33) and in the y direction is in (3.34).

$$p_x(\mathrm{x}, y_i) = \left(\frac{v_x}{L_1} - y_i \frac{\varphi}{L_3}\right)(\mathrm{x} - a_i) \tag{3.33}$$

$$p_y(x, y_i) = \frac{v_y}{L_2}(\mathrm{x} - a_i) + \frac{\varphi}{2L_3}(x^2 - {a_i}^2) \tag{3.34}$$

In this notation, a_i is the coordinate of the leading edge of the strip. L_1, L_2, L_3 represent elasticity coefficients. v_x is longitudinal, v_y is lateral and φ is spin creepage [4].

Elasticity coefficients are given in (3.35).

$$L_1 = \frac{8a}{3c_{11}G}, \qquad L_2 = \frac{8a}{3c_{22}G}, \qquad L_3 = \frac{\pi a\sqrt{a/b}}{4c_{23}G} \tag{3.35}$$

Where c_{11}, c_{22} and c_{23} are Kalker's coefficients according to Kalker Linear Model in Kalker's book which gives theoretical explanations [19]. Kalker's coefficients are shown in Table 3.1.

Table 3.1 : Kalker's coefficient tables [1,18].

		c_{11}			c_{22}			$c_{23} = -c_{32}$			c_{33}		
	g	$\sigma = 0$	1/4	1/2	$\sigma = 0$	1/4	1/2	$\sigma = 0$	1/4	1/2	$\sigma = 0$	1/4	1/2
	0.0	$\pi^2/4(1-\sigma)$			$\pi^2/4 = 2,47$			$\pi\sqrt{g}/3$	-	-	$\pi^2/16(1-\sigma)g$		
a/b	0.1	2.51	3.31	4.85	2.51	2.52	2.53	0.334	0.473	0.731	6.42	8.28	11.7
	0.2	2.59	3.37	4.81	2.59	2.63	2.66	0.483	0.603	0.809	3.46	4.27	5.66
	0.3	2.68	3.44	4.80	2.68	2.75	2.81	0.607	0.715	0.889	2.49	2.96	3.72
	0.4	2.78	3.53	4.82	2.78	2.88	2.98	0.72	0.823	0.977	2.02	2.32	2.77
	0.5	2.88	3.62	4.83	2.88	3.01	3.14	0.827	0.929	1.07	1.74	1.93	2.22
	0.6	2.98	3.72	4.91	2.98	3.14	3.31	0.93	1.03	1.18	1.56	1.68	1.86
	0.7	3.09	3.81	4.97	3.09	3.28	3.48	1.03	1.14	1.29	1.43	1.50	1.60
	0.8	3.19	3.91	5.05	3.19	3.41	3.65	1.13	1.25	1.40	1.34	1.37	1.42
	0.9	3.29	4.01	5.12	3.29	3.54	3.82	1.23	1.36	1.51	1.27	1.27	1.27
b/a	1.0	3.40	4.12	5.20	3.40	3.67	3.98	1.33	1.47	1.63	1.21	1.19	1.16
	0.9	3.51	4.22	5.30	3.51	3.81	4.16	1.44	1.59	1.77	1.16	1.11	1.06
	0.8	3.65	4.36	5.42	3.65	3.99	4.39	1.58	1.75	1.94	1.10	1.04	0.954
	0.7	3.82	4.54	5.58	3.82	4.21	4.67	1.76	1.95	2.18	1.05	0.965	0.852
	0.6	4.06	4.78	5.80	4.06	4.50	5.04	2.01	2.23	2.50	1.01	0.892	0.751
	0.5	4.37	5.10	6.11	4.37	4.90	5.56	2.35	2.62	2.96	0.958	0.819	0.650
	0.4	4.84	5.57	5.57	4.84	5.48	6.31	2.88	3.24	3.70	0.912	0.747	0.549
	0.3	5.57	6.34	7.34	5.57	6.40	7.51	3.79	4.32	5.01	0.868	0.674	0.446
	0.2	6.96	7.78	8.82	6.96	8.14	9.79	5.72	6.63	7.89	0.828	0.601	0.341
	0.1	10.7	11.70	12.9	10.7	12.8	16.0	14.6	18.0	0.795	0.795	0.526	0.228

a and b values in the equation (3.35) and Table 3.1 are longitudinal radius and traverse radius of the ellipse respectively. Poisson's ratio is shown as σ and b/a ratio is shown as g. The c_{ij} coefficients are a given function of the b/a ratio of the ellipse. Their values are not far from π for b/a close to 1. As a result, the calculation of contact forces are subtracted by integration operations of the surface stresses. Contact forces are shown in the following equations of (3.36) and (3.37).

$$F_x = -\iint p_x(x)\,\mathrm{d}x\,\mathrm{d}y = \frac{-8a^2 b v_x}{3L_1} \tag{3.36}$$

$$F_y = -\iint p_y(x)\,\mathrm{d}x\,\mathrm{d}y = \frac{-8a^2 b v_y}{3L_2} - \frac{\pi a^3 b \varphi}{4L_3} \tag{3.37}$$

The use of FASTSIM can also be applied with other models other than Hertzian cases. Adaptation is made by changing creepage and L values according to the underlying models.

CONTACT computer software [21] is an another alternative of FASTSIM. CONTACT is an advanced simulation program for the detailed study of three-dimensional frictional contact which is based on the complete theory of elasticity. It can take into account several body shapes, including the railway case. Several methods are available to calculate the tangent stresses and/or internal stresses. However, the calculation of one case takes several seconds and it is limited to half space bodies. CONTACT was not found suitable for use in the simulations for this thesis study due to long computation time of the program.

However, FASTSIM is not preferred over CONTACT in intention to reach more accurate calculations in other cases. CONTACT is more adapted to such studies. The wear coefficients are adjusted from experiments [4].

3.5 Tasks in Dynamic Analysis Simulation

Vehicle dynamics in railways have typical analyses. Computer simulation procedures which are used in examination of running safety, track loading, ride characteristics and comfort of the vehicle are shown in Figure 3.8. There are 3 main different calculation methods:

- Eigenvalue analysis
- Quasi-static analysis
- Simulations on track analysis

The simulation results are summed up according to particular standards or specifications.

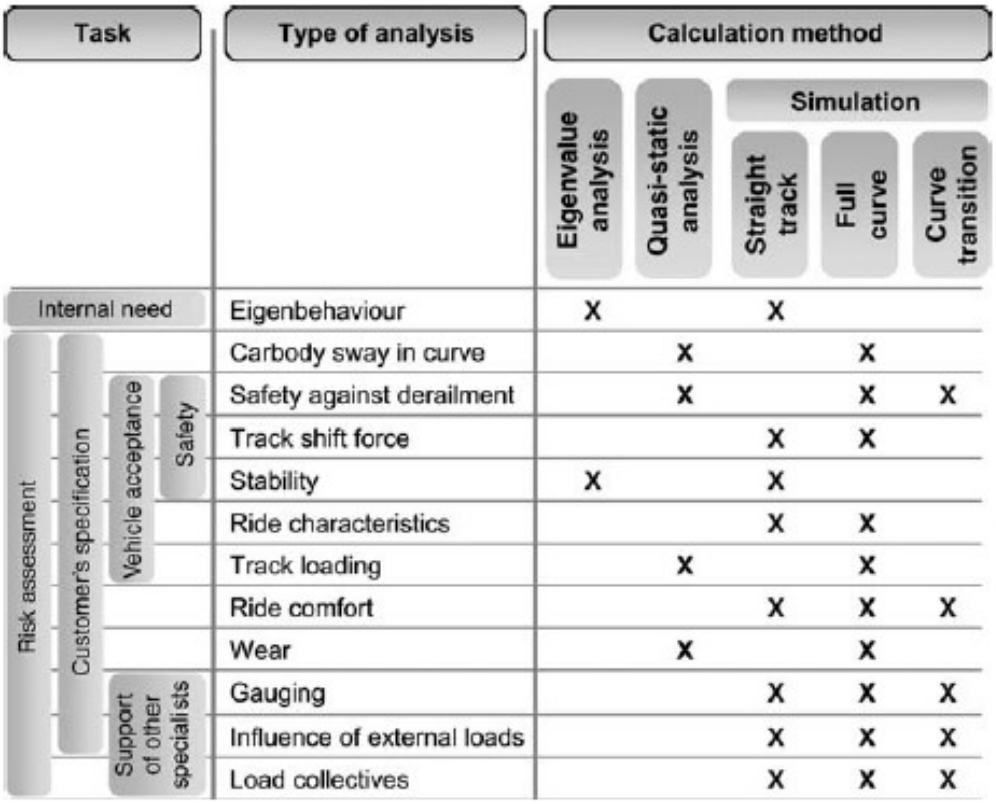

Figure 3.8 : Typical dynamic analyses and calculation methods in railways [4].

3.5.1 Eigenvalue analysis

Eigenvalue analysis is functional for the first impression of the rail vehicle in terms of suspension characteristics in frequency domain. What kind of vibration pattern the rolling stock will create at which frequency and its damping at the relevant frequency are obtained as result of eigenbehaviour analysis.

Eigenvalues, eigenmodes, eigenfrequencies and/or eigenenergies are examined in simulation tools with tare and full load conditions of the wagons. Calculations are generally done with low velocities [4]. Eigenbehaviour analyses are based on longitudinal oscillations, lateral oscillations, bouncing, rolling, pitching and yawing in carbody modes and these are shown in Figure 3.9.

Eigenvalue analysis is performed for the following purposes:

- Quick overwiev on the model's resonance and damping behaviour
- Root locus analysis of mechanical and control systems
- Finding the maximum eigenfrequency for tuning the time integration settings
- Checking the model for plausibility [22].

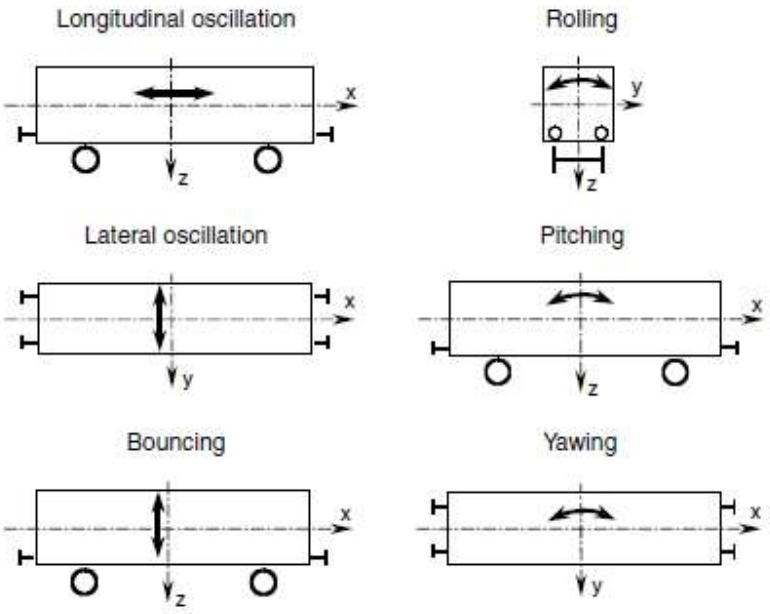

Figure 3.9 : Carbody modes and axis nomenclature [4].

3.5.2 Quasi-static analysis

Quasi-static analyses examine processes in the dynamic systems with with assuming the process is happening infinitely slowly. Thus, static principles are applicable. It can be used for static equilibrium calculations. It is an analysis that can used for rail vehicles moving at constant velocities and constant curve radii. There should also be no excitations caused by the road. Therefore the static assumption will fit on a meaningful basis in this way.

Reactive forces on wheels, suspensions, friction wedges, sidebearings can be detected with quasi-static analysis.

3.5.3 Simulations and time integration

An important mathematical procedure in which dynamic equations of motion can be applied in the simulations of multibody systems is time integration. Time integration solvers advance the equation of motions in the time domain. Time integration solution is an initial value problem. The initial state values are defined by the modeling state of the model and the modifications applied during the solver initialization.

Time integration solver is capable for determining the complete behaviour of non-linear models, by solving the full set of non-linear equations of motion. It writes the time history of the state vectors as output.

SIMPACK's default was used to solve the time integration which known as accurate, very fast and very robust. It has an implicit multistep integration scheme [22].

Vehicle-track dynamic relationships are available for analysis in the time domain because they are non-linear. Stability and safety against derailment are investigated through time integration in the thesis.

3.6 Friction Wedge Models

It is possible to represent the frictional behaviour of the friction wedges with the side frame and bolster in many different ways. The most widely used Colomb's law adapted for friction force has been applied. Representation of the friction force in (3.38)

$$F_f = \mu N sign(v) \tag{3.38}$$

F_f is the friction force, μ is the coefficient of friction, N is the normal force and v is the relative velocity of contacting bodies.

This formulation occurs to numerical simulation problems due to discontinuity introduced by the friction force behaviour. There is no continuity of Coulomb friction functions if the relative velocities are close to zero (see Figure 3.10).

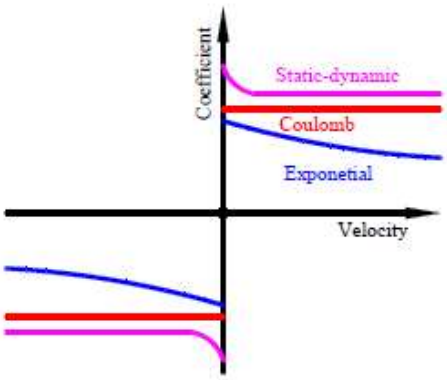

Figure 3.10 : Friction Model Patterns [6].

The discontinuity mentioned is eliminated if viscous and Coulomb friction models are combined. This can expressed by the following equation (3.39). Friction model becames the similar pattern of Figure 3.11.

$$F_f = \begin{cases} \mu N sign(v) \ , & v > v_{ref} \ \vee \ v < -v_{ref} \\ \dfrac{\mu N}{v_{ref}} v \ , & -v_{ref} \leq v \leq v_{ref} \end{cases} \tag{3.39}$$

v_{ref} is the velocity where the force law switches between Coulomb and viscous laws.

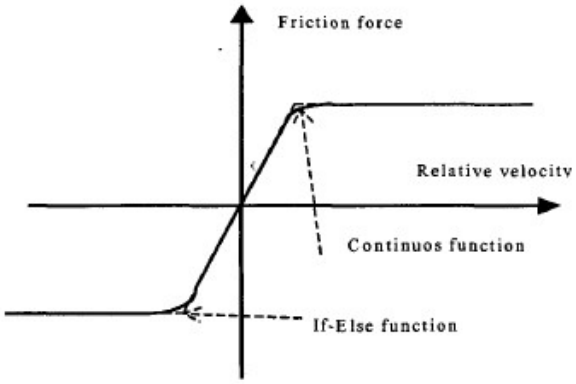

Figure 3.11 : An example of combined Friction Force Pattern [7].

Contact models are modeled with normal forces and friction forces in multibody systems and simulations, as in theory. Modeling of contact forces is a large topic. Contacts for friction wedges are modeled as elastic contacts with a stiffness and a damping values in this study. In addition to this, stick-slip models are more accurate for simulations. When the frictions on the wedge sufaces are also calculated in 2 dimension, sufficient accuracy is provided for the model.

If the contact of two bodies which represented in Figure 3.12 is adapted to simplified version of the LuGre model and equations (3.40) and (3.41) [23, 24].

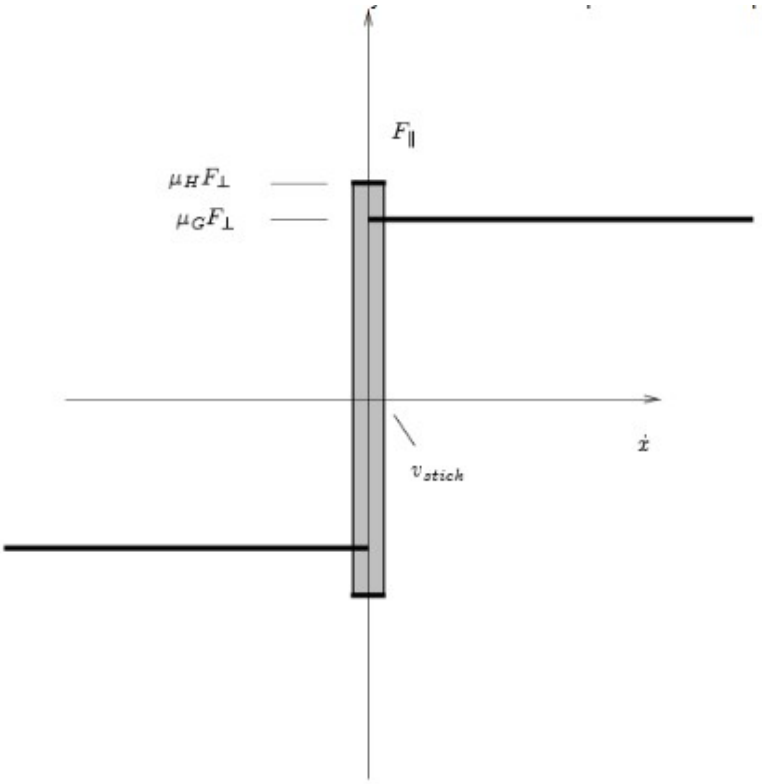

Figure 3.12 : Stick-Slip Model.

$$\begin{cases} N = 0 & \delta > 0 \\ N = c_z\delta + d_z\dot{\delta} & \delta < 0 \end{cases} \tag{3.40}$$

$$\begin{cases} F_f = 0 \quad , & \delta > 0 \\ F_f = \sigma_1 \Delta x + \sigma_2 v \ , & \delta < 0, |v| \leq v_{slip} \\ F_f = \mu_k N sign(v) \, , & \delta < 0, |v| \geq v_{slip} \ or \ |F_f| \geq \mu_s * N \\ \Delta x = \int \Delta v \end{cases} \tag{3.41}$$

N is the normal force. c_z, d_z are the stiffness and damping coefficients for the contact, respectively. δ is the penetration length of the contacting bodies. σ_1 and $\sigma_2$are stiffness and damping coefficients for the stick state. μ_k is the kinematic friction coefficient of friction and μ_k is the static coefficient of friction.

Figure 3.13 gives the logic scheme for the contact forces for the related force element in the software.

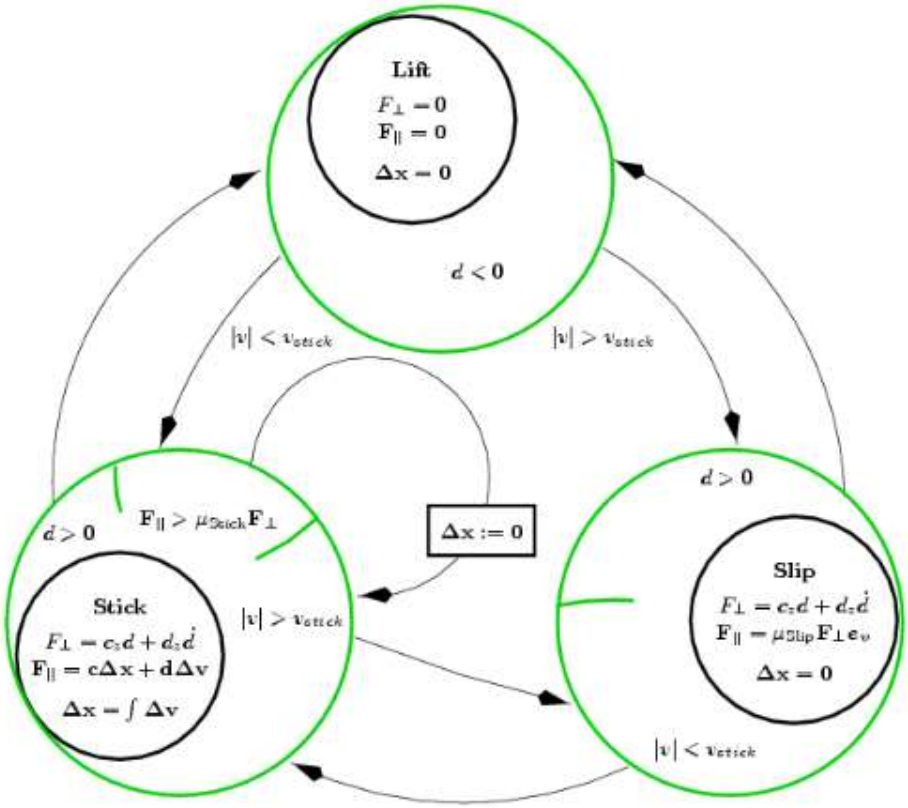

Figure 3.13 : Schematics of the stick-slip friction contact force [22].

4. SIMULATION MODEL

Tests and simulations for railway vehicles are prepared within certain standards or general procedures. Consistent and accurate results can be obtained by following a certain methodology in computer calculation tools for the railway vehicle tests. The structure of railway vehicles and tracks can be examined under wide range definitions and parameters. Outputs from the models can be checked according to relevant standards and regulations. Figure 4.1 gives a schematic summary of the main aspects of the simulation process.

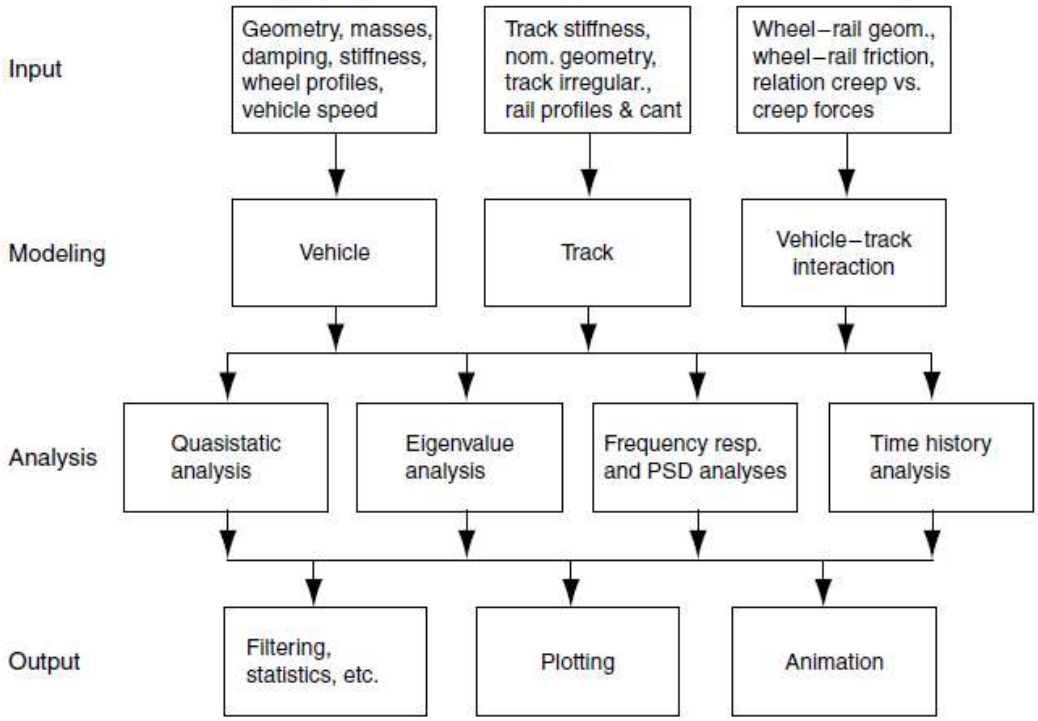

Figure 4.1 : Process of computer MBS simulation in the railway system [4].

A conventional three-piece bogie and versions of the variable axle that correspond to three-piece bogie in principle were modeled to carry out the thesis project. The masses, inertia tensors and suspension elements have similar characteristics but vary quantitatively. Some of these components are modeled with the help of CAD software of CATIA V5 and imported to MBS software of SIMPACK. Wheel profiles which are

subject to vehicle design are modeled from the package software. Accurate design and modelling of the three-piece bogies is challenging due to the fact that elastic connections introduce many non-linearities. Friction surfaces, wheel-rail interactions, bumpstops and clearances are also among vehicle inputs in the system.

Structures that repeat more than once can be modeled as sub-models in the main model. This feature is very practical for railway application models.

Single carbody weight is transferred to two equivalent bogies in the analyses to be carried out in all wagon models. In the same way, bogies transfer their own load to two equivalent wheelsets. Total weight of the wagon reaches the rails and railway infrastructure.

4.1 Vehicle Model of Three-Piece Bogie

The MBS modeling of the three-piece bogie whose structure is explained in the second section will be detailed in this chapter. The GUI image of the MBS model is shown below (Figure 4.2).

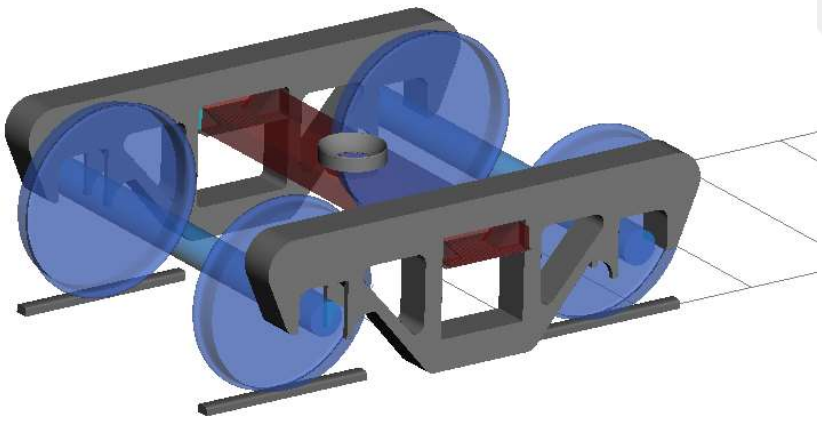

Figure 4.2 : Three-Dimensional View of Modeled Three-Piece Bogie.

Wheels have a nominal radius of 0.46 meters. The selected wheels have S1002 profile from the standard UIC 510-2 “Trailing Stock: Wheels and Wheelsets. Conditions Concerning the Use of Wheelsets of Various Diameters” and the wheel profile is shown in the Figure 4.3.

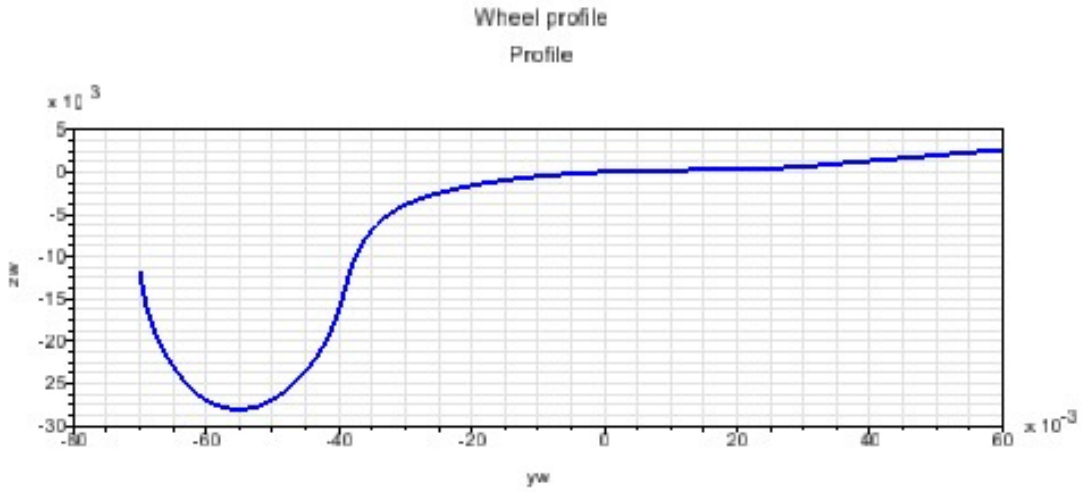

Figure 4.3 : S1002 Wheel Profile

Main features of the modeled three-piece bogie which is made up of several bodies (wheelsets, sideframes, bolster and friction wedges) and connected to each other with kinematic joints and force elements will be considered according to Table 4.1.

Table 4.1 : Modeled Three-Piece Bogie Properties.

Characteristics	Value	Unit
Wheel Diameter	920	mm
Track Gauge	1435	mm
Wheel Base	1800	mm
Side Bearers' Distance to Pivot	635	mm
Max Axle-Load	22500	kg
Total Weight	4134	kg
Max Speed	100	km/h

A single bogie of three-piece type consists of 9 seperate bodies. The use of constraint is avoided while modeling the bogie. The three-piece bogie model also did not require any kinematic constraints here, since the bodies were connected with the force elements. All of the 2 wheelsets, 1 bolster, 2 sideframes and 4 friction wedges have 6 DOF.

The mass properties of the elements relative to the their center of gravities are shown in Table 4.2.

The center of gravitiy for the bolster has a 660 mm height above the track centerline. Center of gravities for sideframes, friction wedges and wheelsets has the values of 460 mm, 560 mm and 460 mm respectively. The positions of center of gravity of each elements are shown in Figure 4.4.

Table 4.2 : Three-Piece Bogie Element Mass Properties.

Element Name	I_{xx} [kg m^2]	I_{yy} [kg m^2]	I_{zz} [kg m^2]	m [kg]
Bolster	320	23	320	662
Sideframe	99	245	180	522
Friction Wedge	0.01	0.01	0.01	7
Wheelset	625.7	13.92	625.7	1200

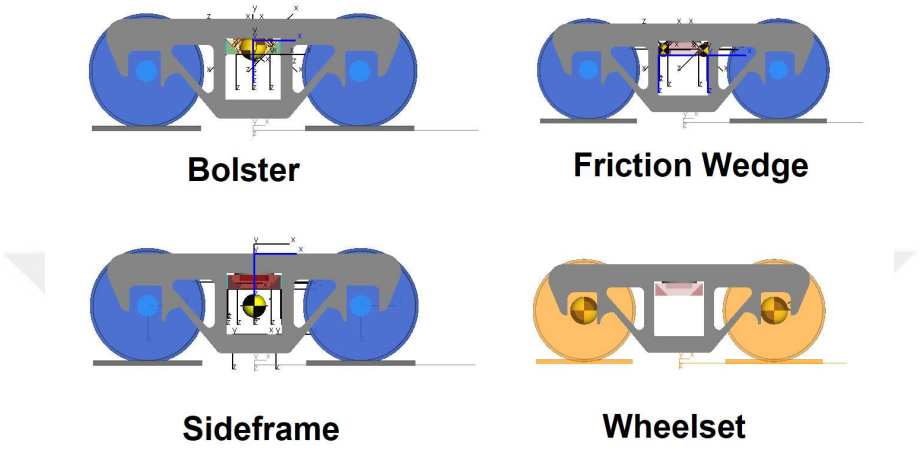

Figure 4.4 : Locations of Element Center of Gravities.

4.1.1 Primary suspension for three-piece bogie

Primary suspensions are modeled using force elements of springs and dampers. Longitudinally ±4 mm and laterally ±10 mm clearances are defined for the primary suspension model. The viscous damping approach was used here, as the axle box movements were damped by rubber bushings.

These clearances and stiffness values of non-linear springs are defined by input functions. An example function is used for clearances, as in Figure 4.5. This type of input function has been used in all bumpstops located located in certain parts of the bogie to simplify the model and reduce the calculation costs.

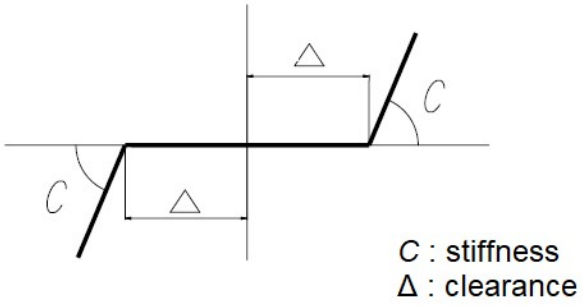

Figure 4.5 : Input for bumpstop and force elements with clearances [25].

4.1.2 Central suspension for three-piece bogie

Central suspension consists of a set of non-linear springs and wedge friction dampers working in vertical and lateral direction. Friction wedges are modelled as dry Coulomb friction where the friction force is proportional to the normal load. The model for friction wedges include two-dimensional friction in the vertical and lateral directions. [25].

Spring sets between bolster and sideframes are modeled as non-linear springs. There are two seperate input configurations available that include and do not include helper inner spring. Spring sets with helper inner springs continue to behave with the equivalent stiffness of the two springs in case of compression exceeding a certain displacement. Figure 4.6 shows the positions of the coil spring types on the bogie.

The force-displacement relation for the one with inner spring and and the input function configuration for the one without inner spring is shown in Figure 4.7.

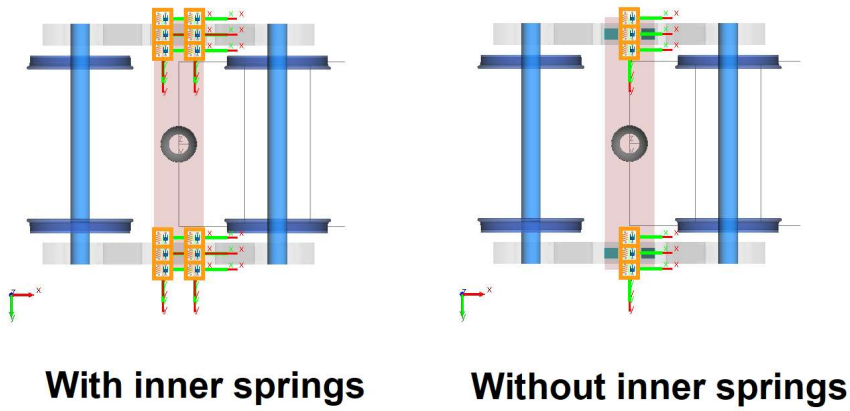

Figure 4.6 : Coil spring locations in the bogie.

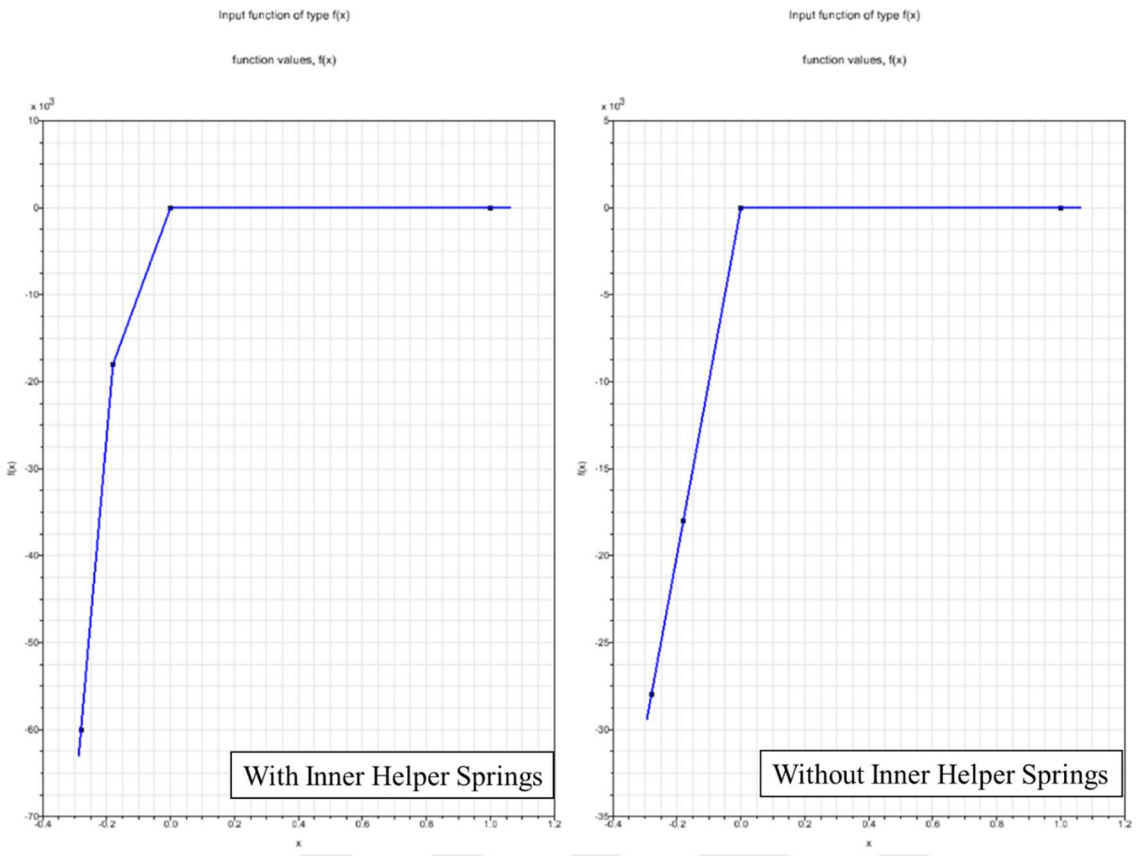

Figure 4.7 : Force-displacement characteristics of coil springs.

While bolsters are sitting on this spring sets at the both side of the bogie, the springs on the underside of the wedges are connected to the wedges. Friction wedges also make frictional damping with the bolster from its inclined surface and with sideframe from its vertical surface. The theory and algorithm of the friction force elements were explained in Chapter 3. Relevant force element in the software is used.

4.1.3 Side bearers for three-piece bogie

It is possible to model side bearings as sub-models, exactly like the wheelsets and the entire bogie. There are bump stops and contacts which will increase the solution time. However, it is modeled as non-linear massless springs in order to reduce the solution times that the solver will spend. Side bearers provide damping in the XY plane. The vertical springs have an operating range of 12 mm, depending on the tare and laden conditions of the wagon. The vertical characteristics are as in the Figure 4.8.

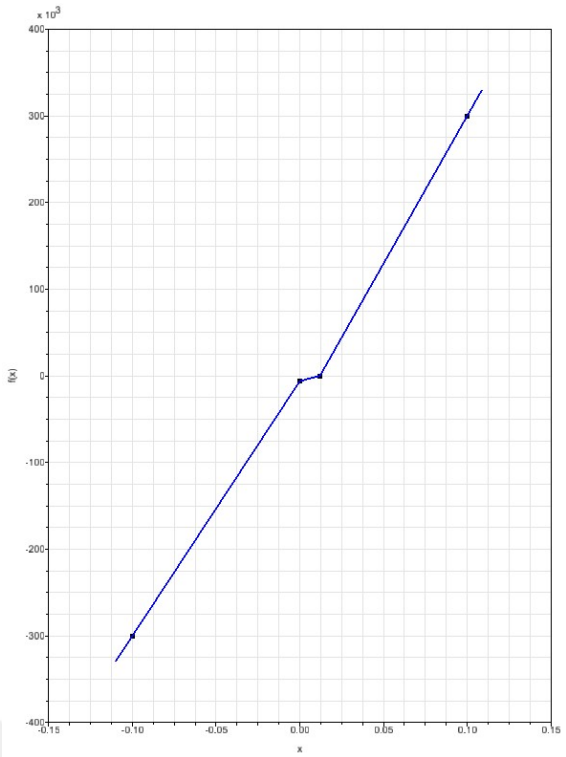

Figure 4.8 : Displacement-Force Relation in Vertical Axis for Side Bearers.

4.2 Vehicle Model of Bogie With Variable Gauge

The aim of this thesis is to examine the dynamics of a bogie with variable gauge. In order to make the correct comparisons, the elements of the three-piece bogie and the elements of the bogie with variable gauge were selected equivalent. The properties of the elements of three-piece bogie were stated in Table 4.2 and these values are the same in this topic except the wheelset which related to the bogie with variable gauge. The wheel profile is S1002 and the wheel nominal radius is 0.46 meters. The body properties for elements are shown in Table 4.3. The centers of gravity are located at the same heights as in the three-piece bogie model.

Table 4.3 : Variable Gauge Bogie Element Mass Properties.

Element Name	I_{xx} [kg m^2]	I_{yy} [kg m^2]	I_{zz} [kg m^2]	m [kg]
Bolster	320	23	320	662
Sideframe	99	245	180	522
Friction Wedge	0.01	0.01	0.01	7
Wheelset	19.5	36.3	19.5	370

In this model, the sources of differences in terms of vehicle dynamics are the number of elements, the design of the new bogie and possible track gauge differences.

The axle design explained by Igde in the bogie design (see Figure 4.9) is seen as the most obvious difference. The contact state of this axle on the right rail in SIMPACK is seen in Figure 4.10 and Figure 4.11.

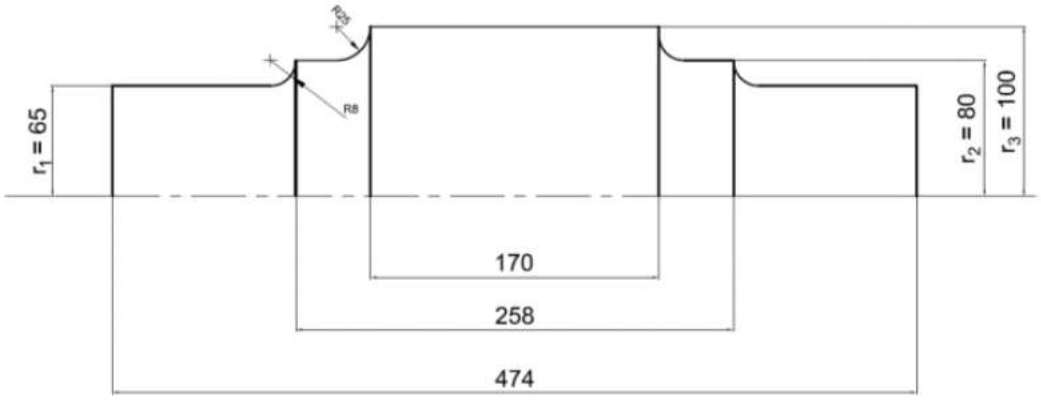

Figure 4.9 : Drawing of the Axle of Bogie With Variable Gauge [7].

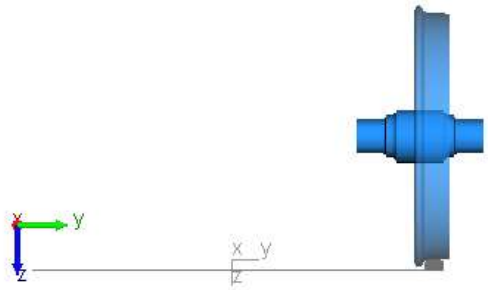

Figure 4.10 : Right-Side Axle and Wheel-Rail Contact.

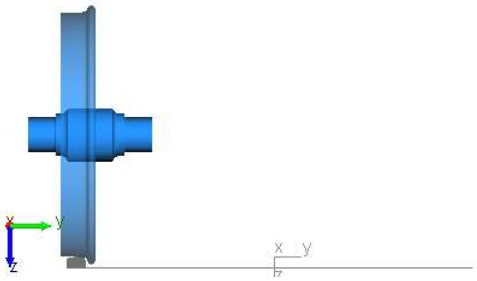

Figure 4.11 : Left-Side Axle and Wheel-Rail Contact.

MBS modeling of the bogie has been completed in accordance with the numbers mentioned in Table 2.1. The bogie is seen as in Figure 4.12 and 4.13 with various views and technical drawings.

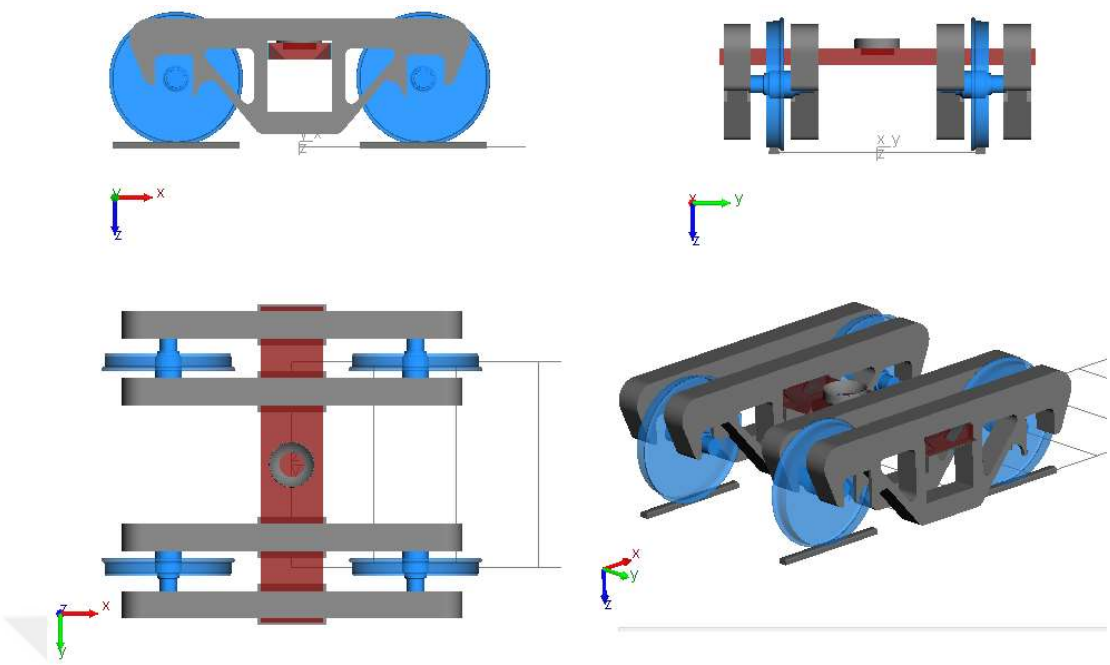

Figure 4.12 : Three-Dimensional View of Modeled Three-Piece Bogie

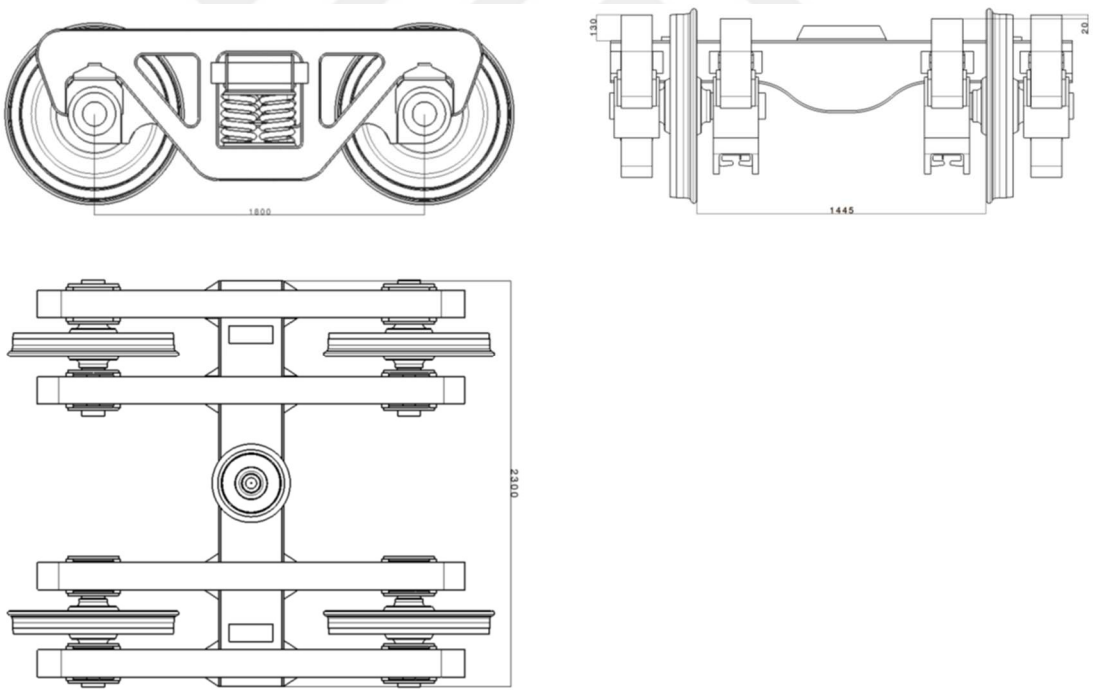

Figure 4.13 : Bogie technical drawing (on 1520 mm track gauge) [7].

In conclusion, the general characteristics of the variable gauge freight bogie are as in Table 4.4.

Table 4.4 : Modeled Variable Gauge Bogie Properties.

Characteristics	Value	Unit
Wheel Diameter	920	mm
Track Gauge (Variable)	1435 or 1520	mm
Wheel Base	1800	mm
Side Bearers' Distance to Pivot	635	mm
Max Axle-Load (Per Pair of Right and Left Concentric Axles)	22500	kg
Total Weight	4286	kg
Max Speed	100	km/h

4.2.1 Primary suspension for variable gauge bogie

There are no changes in the structures (stiffness, damping and clearance values) of the force elements which are related to primary suspension. There have been changes in the numbers and preloads only as the number of points where the axles are supported has increased. It is shown in Figure 4.14.

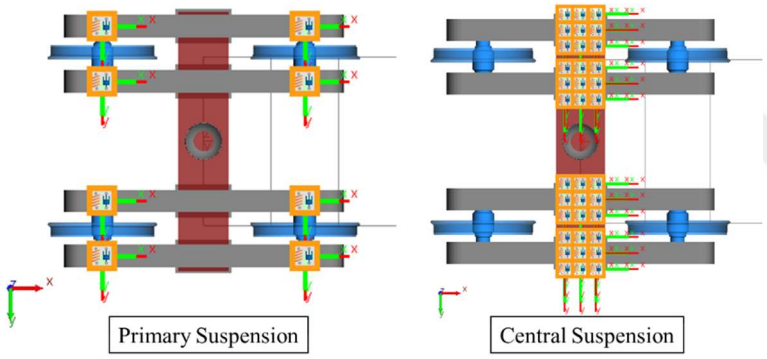

Figure 4.14 : Primary and Central Suspension Force Elements.

4.2.2 Central suspension for variable gauge bogie

As with the primary suspension, the central suspension element characteristics remained unchanged compared to the three-piece bogie model, but the number of friction wedges and spring sets which are related to central suspension has doubled (See Figure 4.14).

In summary, the side frames added to inside provided support to the bolster, exactly like the side frames on the outside. The number of springs and friction damping elements has increased accordingly.

4.2.3 Side bearers for variable gauge bogie

The side bearers are completely identical to the three-piece bogie, with no change in number and position.

5. TESTS AND RESULTS

Final tests were carried out by defining certain characteristics of vehicles and tracks. Hunting analysis was done by creating tangent track geometry. To provide the yaw angle required for bogie rotation tests, curved track geometry was created to provide it. The railway line sections used for dynamic behaviour tests are defined according to EN 14363 “Railway applications - Testing for the acceptance of running characteristics of railway vehicles – Testing of behaviour and stationary tests” standard.

5.1 Hunting Analysis

This analysis, which is important for dynamic stability measurements of bogies, has been carried out on tangent tracks. The velocities of the wagons are increased with constant acceleration on the track. There is a maximum velocity value at which the vibrations cannot be fully-damped and the hunting oscillation starts to appear for certain wagon configurations for most of the railway vehicles. It can be defined as the critical speed and is referred to as such in this thesis.

Modelled conventional three-piece bogie with 1435 mm axle distance and variable gauge bogie in 1435 mm and 1520 mm gauges are going to be compared in terms of instability characteristics. Bogies are attached to identical freight wagons. Firstly, the analysis is performed without any track excitation. Then, an examination was carried out by adding track irregularities. A constant acceleration to a speed of 140 km/h in 100 seconds is intended, which corresponds to 0.389 m/s^2. A track with a length that can be reached at the intended velocities from velocity of 0.00 m/s is defined and track is with no curvature and superelevation (Figure 5.1 and Figure 5.2).

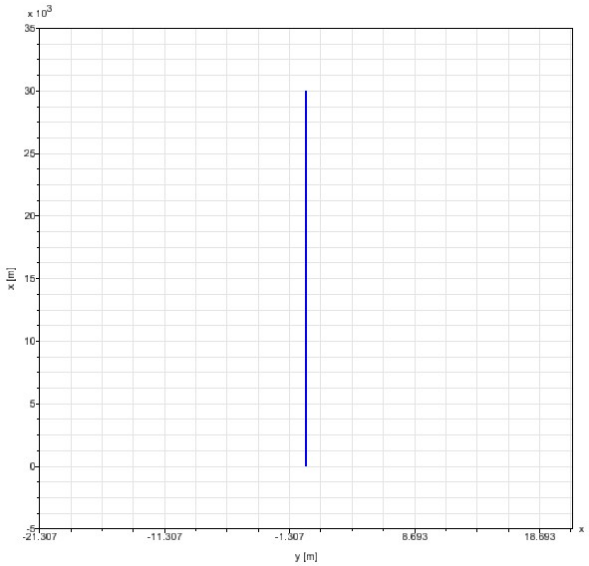

Figure 5.1 : Straight track layout top view.

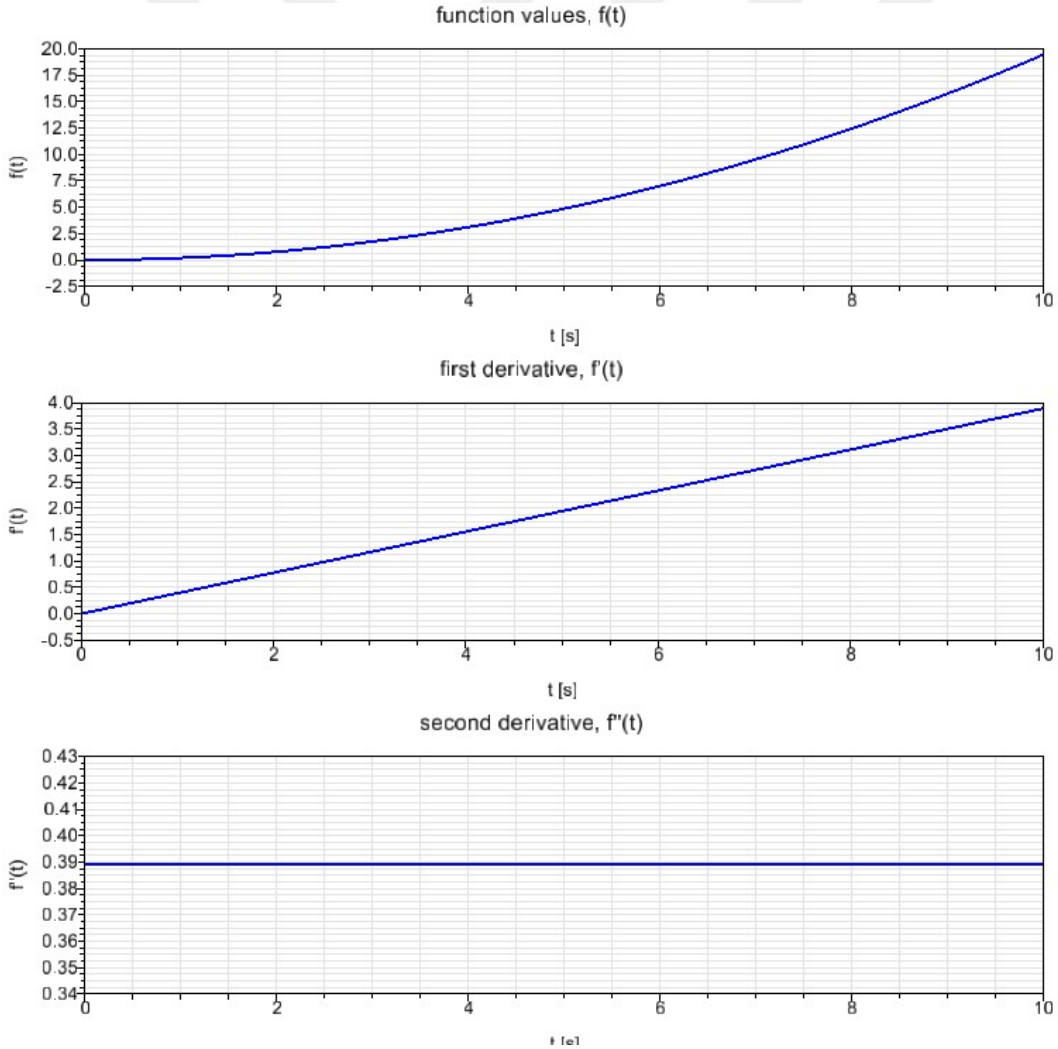

Figure 5.2 : Location, velocity and acceleration definition for test wagons.

5.1.1 Results of hunting tests

There are values where stability is lost at increasing speeds for most of the wagons. One of the main disadvantages of the three-piece bogie is this low stability characteristics. According to the results in the tangent test track with no excitations, the three-piece bogie reaches the critical level at velocity of approximately 43 m/s. Front axle of the wagon oscillates about ± 6 mm laterally after this velocity. (see Figure 5.3).

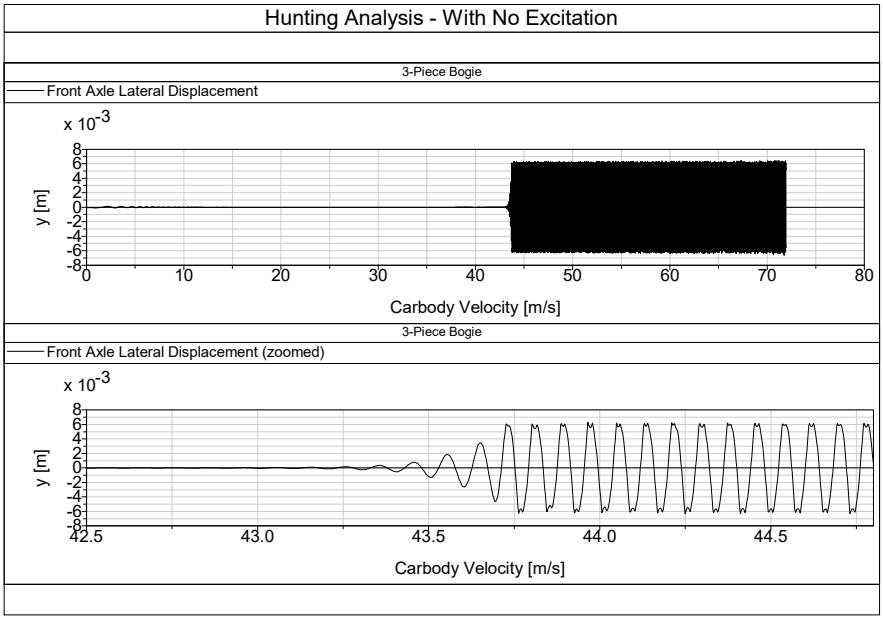

Figure 5.3 : Three Piece Bogie Lateral Displacement-Velocity Diagram.

The same analysis was also carried out on the specific bogie, whose axle gauge is variable. The average displacement of the two concentric axes is taken. The results of for two different gauges are as follows in Figure 5.4. This special designed bogie does not show an oscillation in the lateral displacement change at these velocity ranges. This bogie design did not tend to orient itself to the track center axis, unlike those involving a standard monobloc railway axle. Moreover, lateral displacements that can be considered high as like the conventional three-piece bogie are observed. The maximum lateral displacement is decreased for lower acceleration value (Figure 5.5). However, oscillation in the lateral axis on the straight path was not seen for both acceleration values.

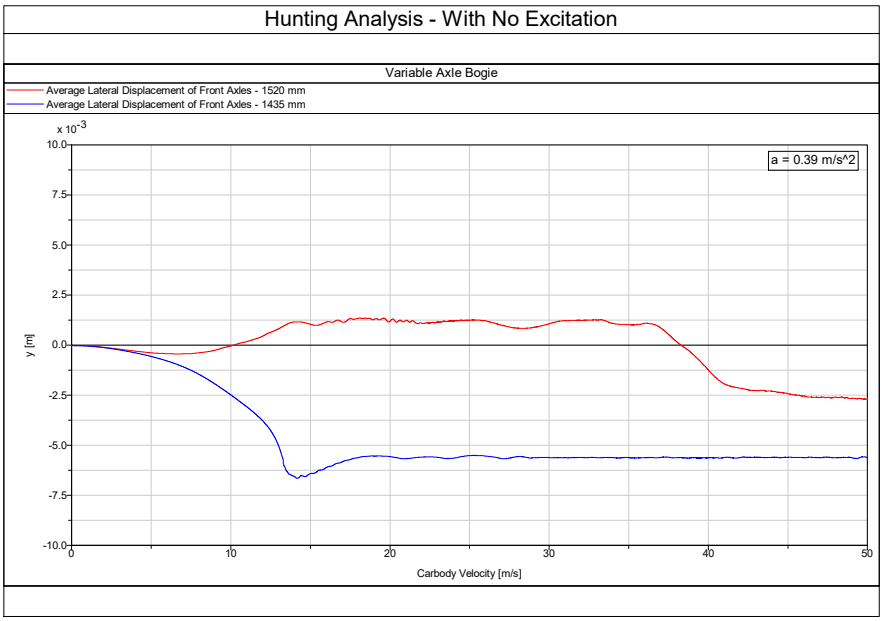

Figure 5.4 : Average Lateral Displacement of Left and Right Front Axles.

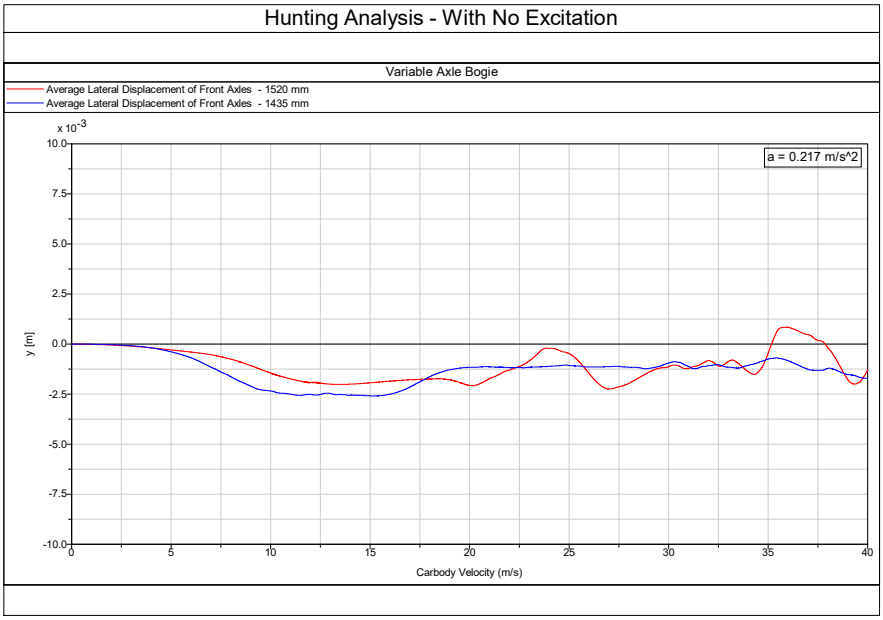

Figure 5.5 : Average Lateral Displacement, reduced acceleration.

5.1.2 Results of hunting tests with added track excitations

In order to examine the effect of track irregularities on stability, excitation to the straight track with the same characteristics has been defined. The maximum amplitude of the track excitations are about 3 mm. The critical velocity is determined as 17 m/s for the three-piece bogie while ± 6 mm lateral displacements seen which is the same with hunting test on zero track excitations (see Figure 5.6). Random track irregularities

had a negative impact on stability characteristics. Running behaviour without oscillation are seen when track excitation is added for variable gauge bogie design (Figure 5.7).

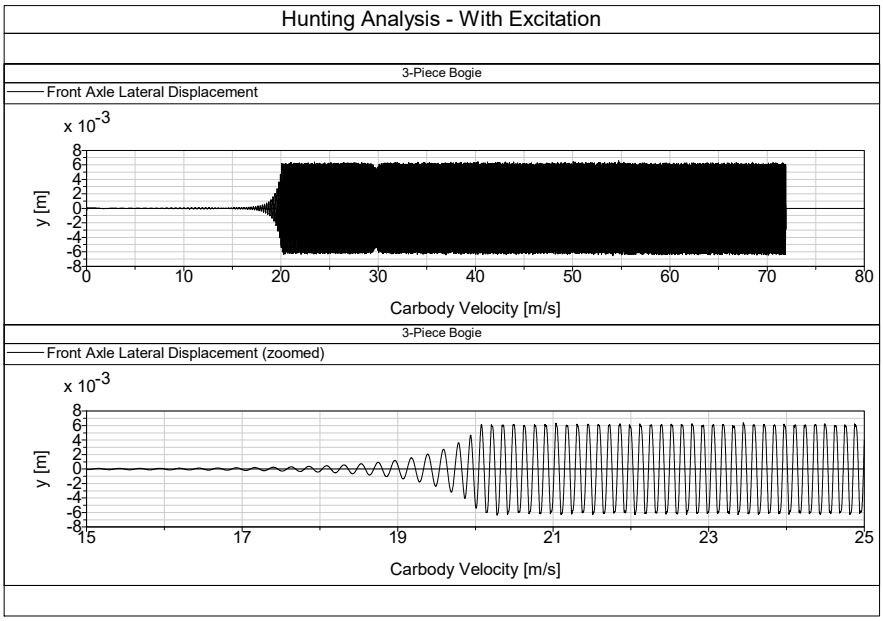

Figure 5.6 : Three-Piece Bogie Hunting Characteristics With Track Excitations.

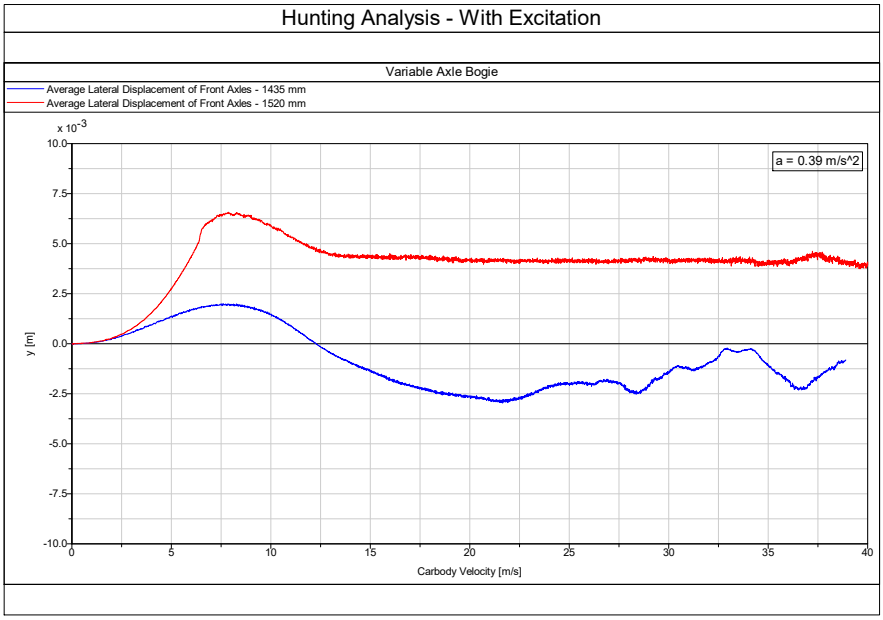

Figure 5.7 : Average Lateral Displacement With Track Excitation.

5.2 Twisted Track Tests

Railway vehicles move on curves under the influence of lateral forces between wheel and the rails. These lateral forces increase as the curve radius decreases. The flange contact that occurs during curving is the main reason that causes the wheel to climb on the rail.

Running safety of the railway vehicles is examined by a criterion such as the ratio of the lateral force to the vertical force (Y/Q) at the wheel. This ratio was first suggested by Nadal in 1908. Derailment occurs if the sum of the vertical components of the normal and tangential forces is sufficient to support the vertical force on the wheel.

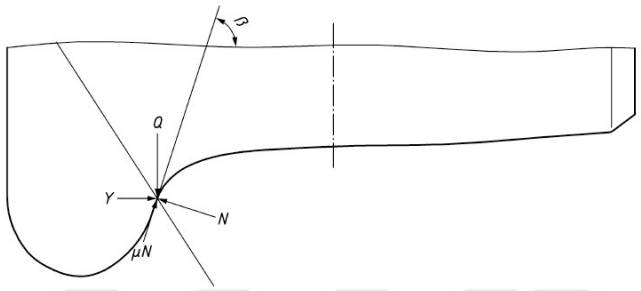

Figure 5.8 : Flange Forces [26].

The contact in flange and rail are expressed as in Figure 5.8. Nadal assumes that there is downward sliding on a flange contact point. Furthermore it is assumed that the tangential force across the flange is equal to the coefficient of friction on the flange μ multiplied by the normal force on the flange N [26]. Flange angle is expressed as β. Forces in the lateral and vertical directions give the (5.1) and (5.2).

$$Y = N\sin\beta - \mu N\cos\beta \tag{5.1}$$

$$Q = N\cos\beta - \mu N\sin\beta \tag{5.2}$$

As a result, Nadal formula for limiting (Y/Q) is shown in (5.3).

$$\frac{Y}{Q} = \frac{\tan\beta - \mu}{1 + \mu\tan\beta} \tag{5.3}$$

The twisted track analysis was carried out in order to simulate the conditions where the (Y/Q) ratio may be the highest in the operationg conditions of the railway vehicle. Bogies and the carbody were forced into a twist caused by the curved track and cant. The relevant test track geometry is defined in accordance with the EN 14363 "Railway applications - Testing and Simulation for the acceptance of running characteristics of railway vehicles - Running Behaviour and stationary tests." standard. It is ensured that the front bogie and the rear bogie have a superelevation difference up top 90 mm. Track layout views are given in Figure 5.9.

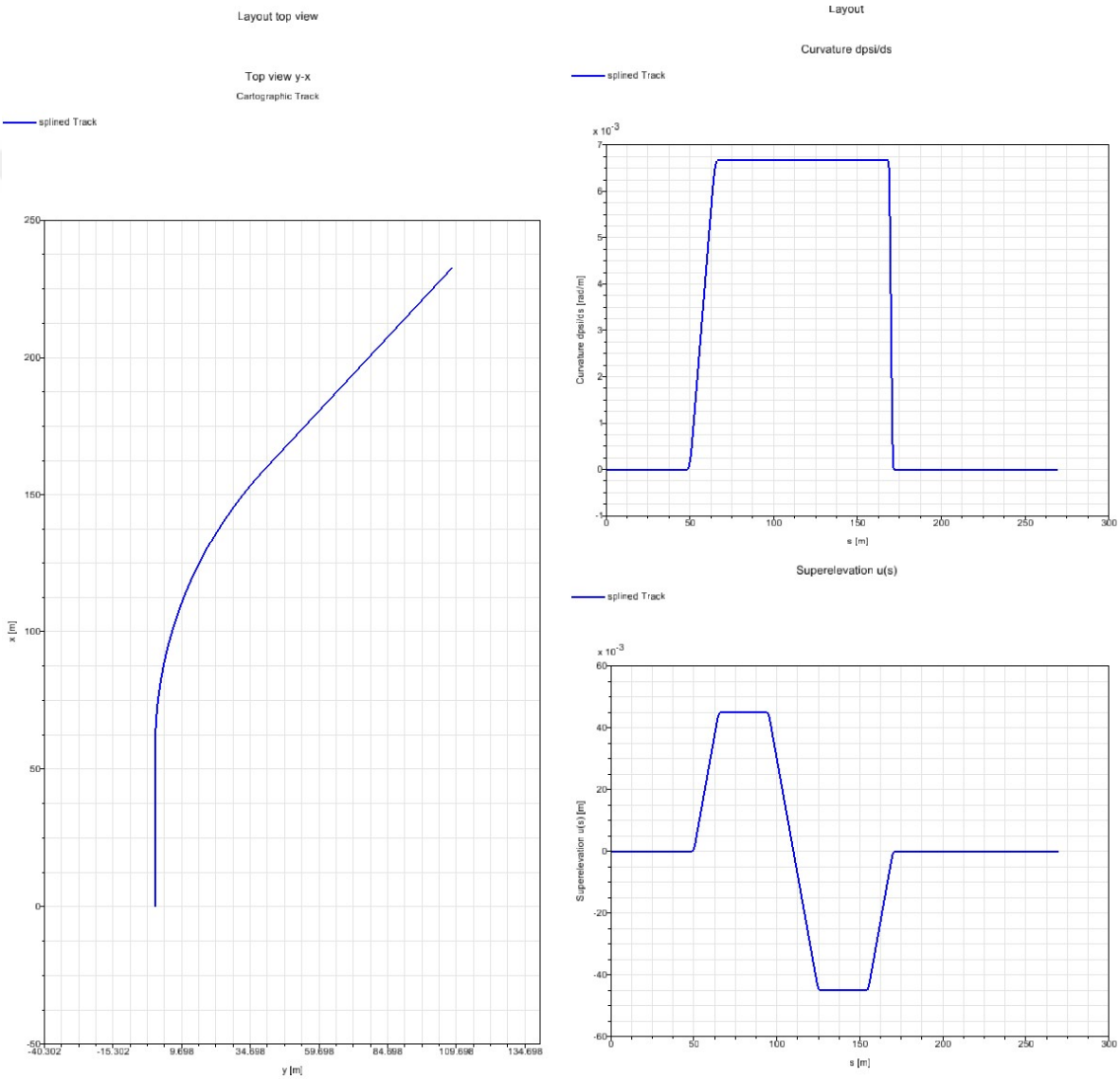

Figure 5.9 : Twisted Track Layout according to EN 14363 [26].

The tests were carried out in two different types of wagons, short and long. Bogie distance of the short wagon is 7 m and short wagon length is 11.3 m while long wagon has 13 m bogie distance and 17.3 m wagon length (Figure 5.10). Total vehicle mass is

set for 16 tonnes. The speed of the vehicle shall be constant and not exceed 10 km/h according to EN 14363 standard. Vehicle constant velocity is set for 2.5 m/s. The criteria of (Y/Q) ratio less than 1.25 and wheel lift (Δz) less than 5 mm were examined at the end of the tests.

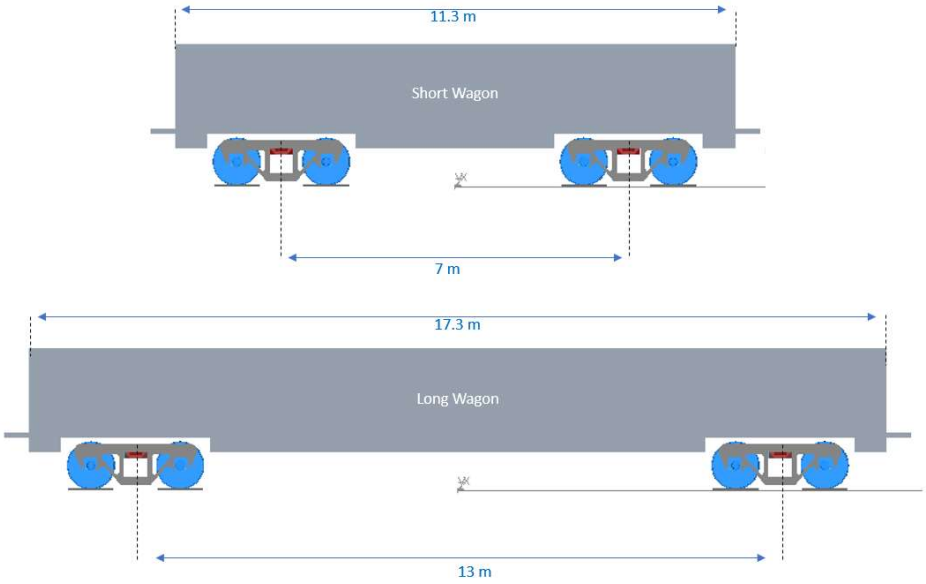

Figure 5.10 : Main dimensions for test wagons.

5.2.1 Results of twisted track tests

Three-piece bogie (Y/Q) diagram in both short wagon and long wagon configuration is given in Figure 5.11 and wheel lift diagram is given in Figure 5.12. Last mentioned output diagrams of variable gauge bogie in 1435 mm track gauge are given in Figure 5.13 and Figure 5.14. For track gauge 1520 mm, diagrams are given in Figure 5.15 and 5.16 respectively. It is seen that $(Y/Q) < 1.25$ and $(\Delta z) < 5$ mm limits provided for all wheels.

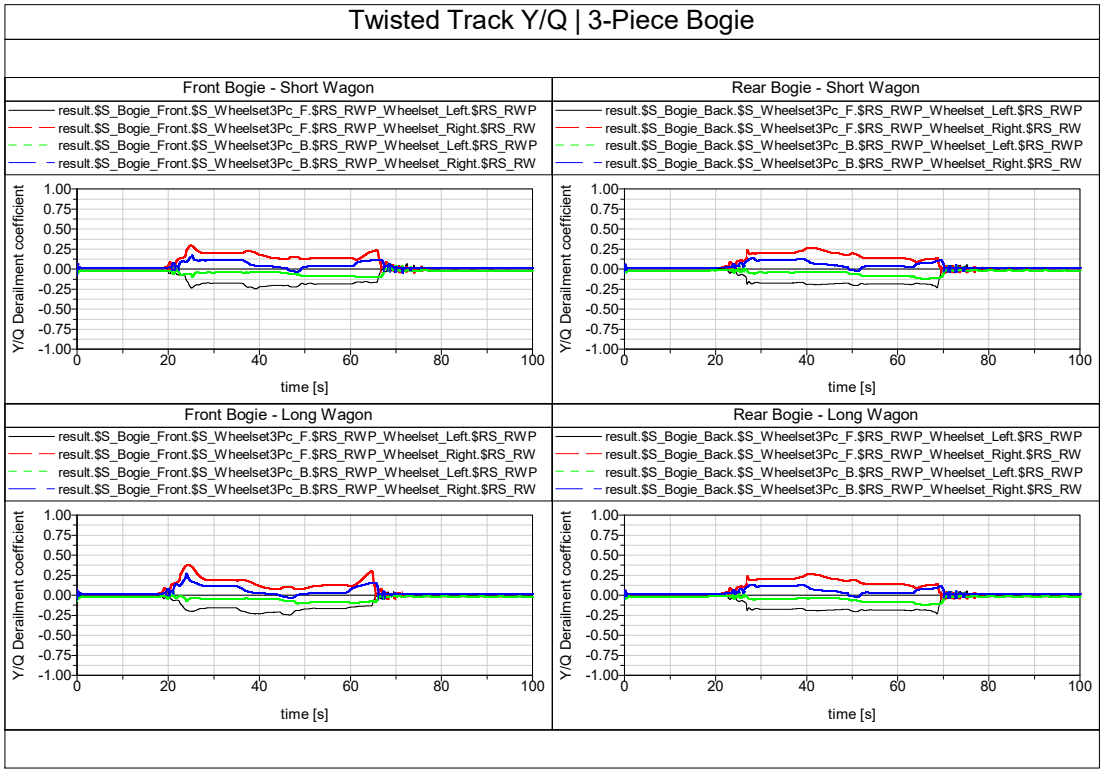

Figure 5.11 : Three-Piece Bogie Twisted Track Y/Q Results.

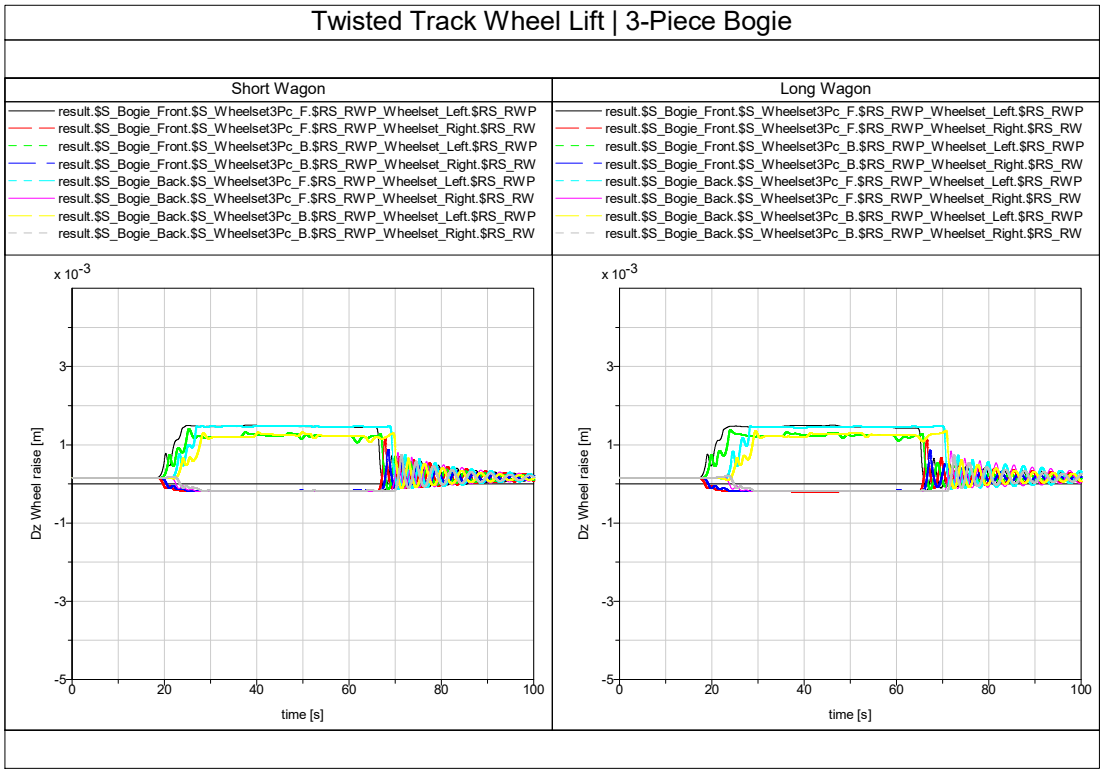

Figure 5.12 : Three-Piece Bogie Twisted Track Wheel Lift Results.

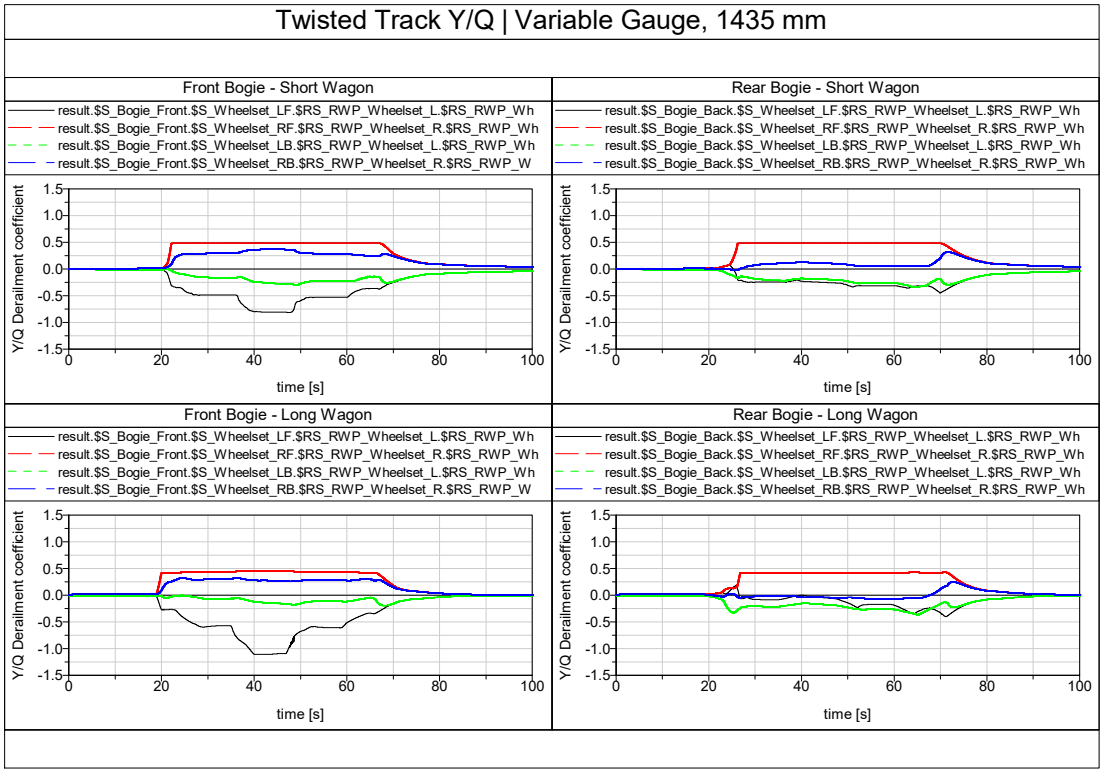

Figure 5.13 : Variable Gauge Bogie Twisted Track Y/Q, adjusted for 1435 mm.

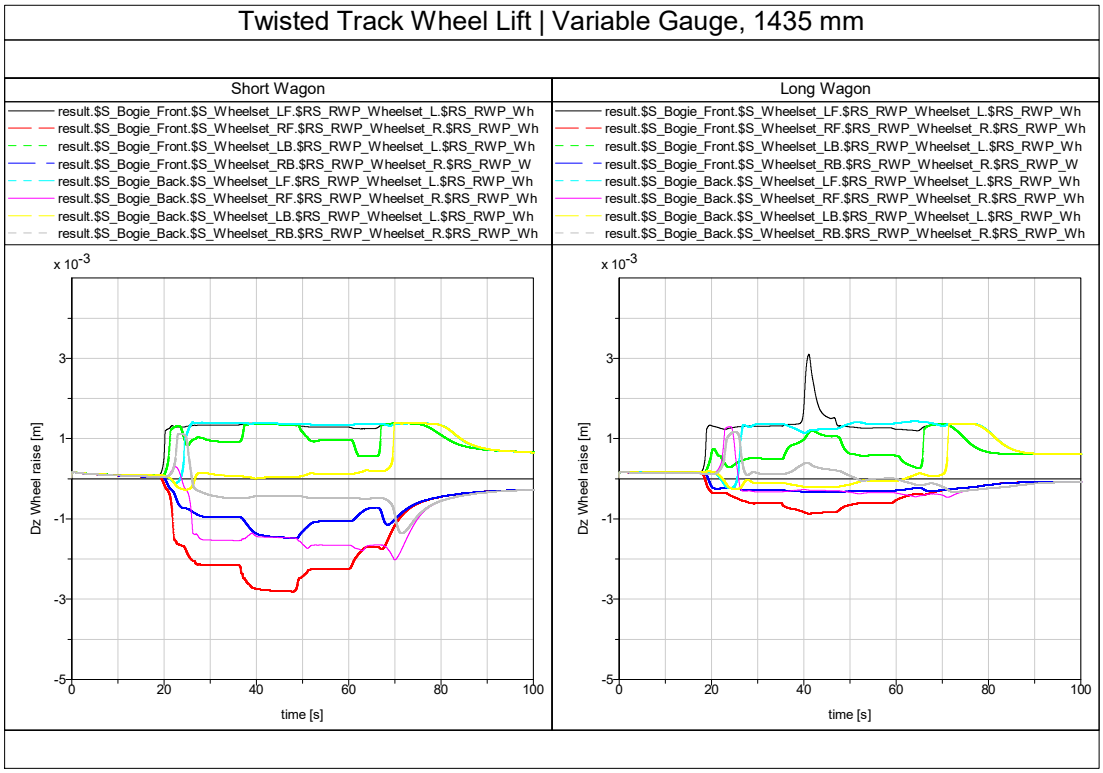

Figure 5.14 : Variable Gauge Bogie Wheel Lift on Twisted Track (1435 mm).

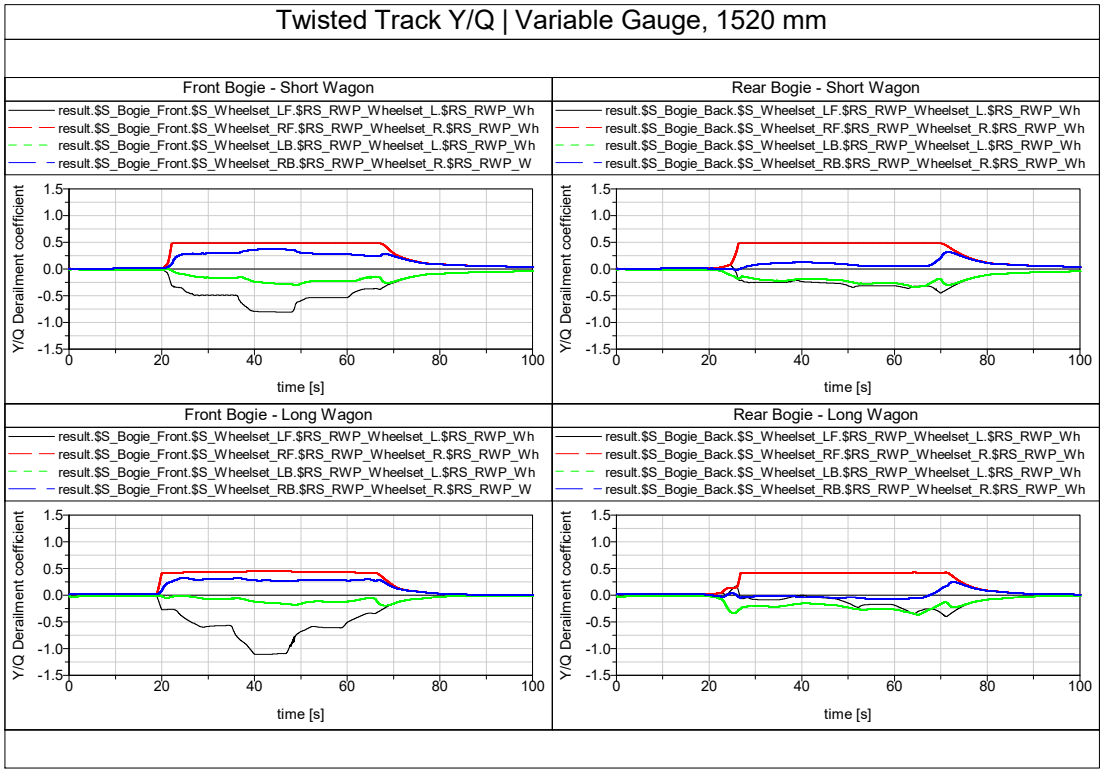

Figure 5.15 : Variable Gauge Bogie Twisted Track Y/Q, adjusted for 1520 mm.

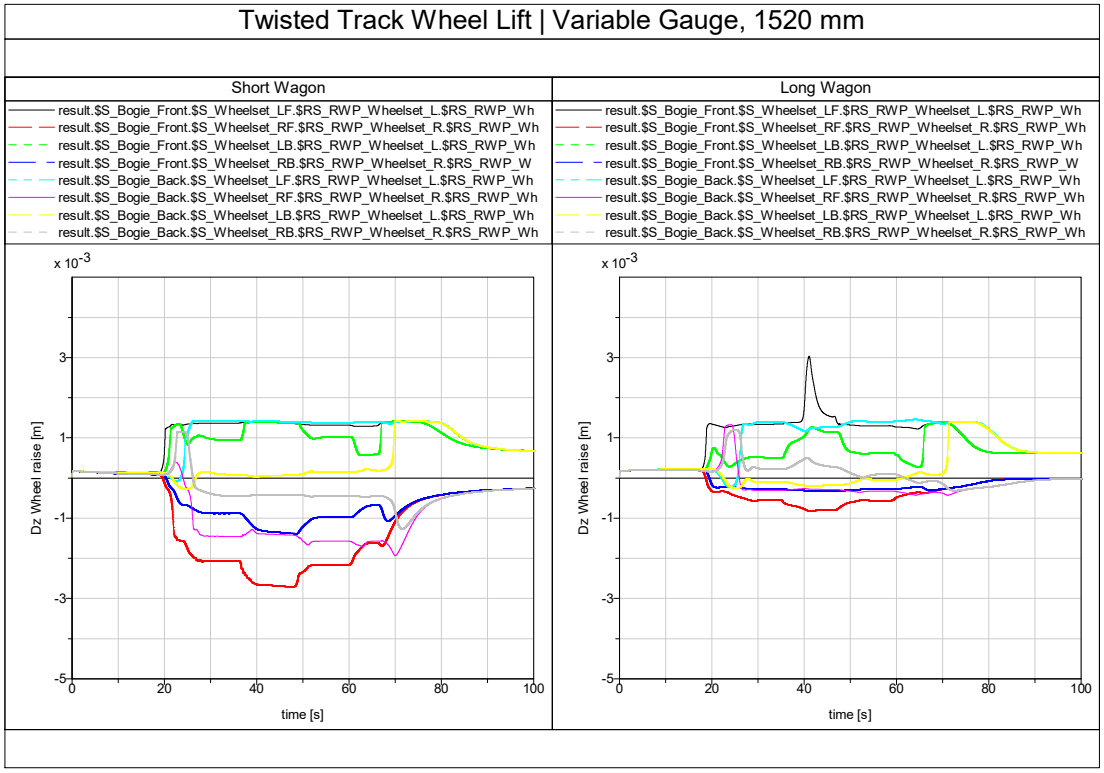

Figure 5.16 : Variable Gauge Bogie Wheel Lift on Twisted Track (1520 mm).

The maximum values in the results of the twisted track analysis are in Table 5.1. It is seen that the maximum value for Y/Q increases as the wagon length increases. In addition, there is a slight decrease in the increase in gauge for Y/Q values. The modeled variable gauge bogie reaches higher values than the three-piece bogie.

Table 5.1 : Maximum Y/Q and Wheel Lift Values for Twisted Track Tests.

	Three-Piece Bogie		Variable Gauge 1435 mm		Variable Gauge 1520 mm	
	Short	Long	Short	Long	Short	Long
Max Y/Q	0.295	0.378	0.809	1.109	0.805	1.109
Max Wheel Lift [mm]	1.5	1.5	2.8	3.1	2.7	3.0

5.3 Bogie Rotation Tests

The center pivot of the bogie is defined by adding the frictional force due to the angular relative displacement with respect to the reference point on the wagon and the force from the weight of the vehicle. The yaw torque magnitude generated here must not exceed the limits specified in EN 16235 standard. Yaw hysteresis magnitude of a standardized tare wagon (total mass 20 t) should be in (10 ± 4) kNm limits. Additionally, it must be less than 45 kNm for a loaded wagon of 22,5 t axle load (90t total mass) [27].

A special track is defined to obtain this angular displacement and the resulting moment (Figure 5.17). Approximately 5 degrees of relative displacement is achieved at the joint between the center pivot of the bogie and the wagon thanks to the sequential right and left curves of 50 m radii. Each turn is defined to be 10 meters long. The test vehicles used this road at a velocity of 2 km/h.

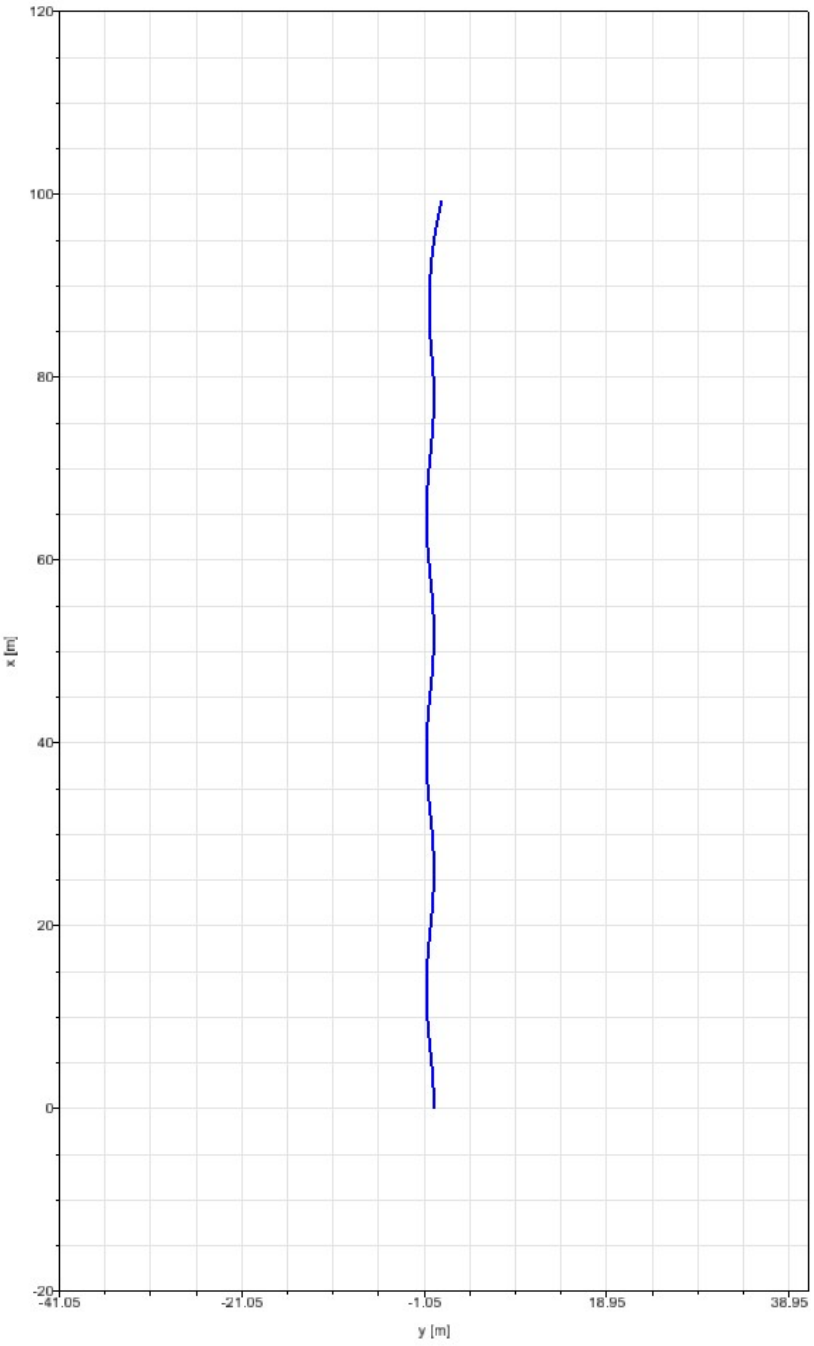

Figure 5.17 : Bogie Yaw Torque Measurement Track Section.

The corresponding diagrams of the three-piece bogie and the bogie with variable gauge are as follows in Figure 5.18 and 5.19. Modeled bogies meet the main criteria established in the relevant standard.

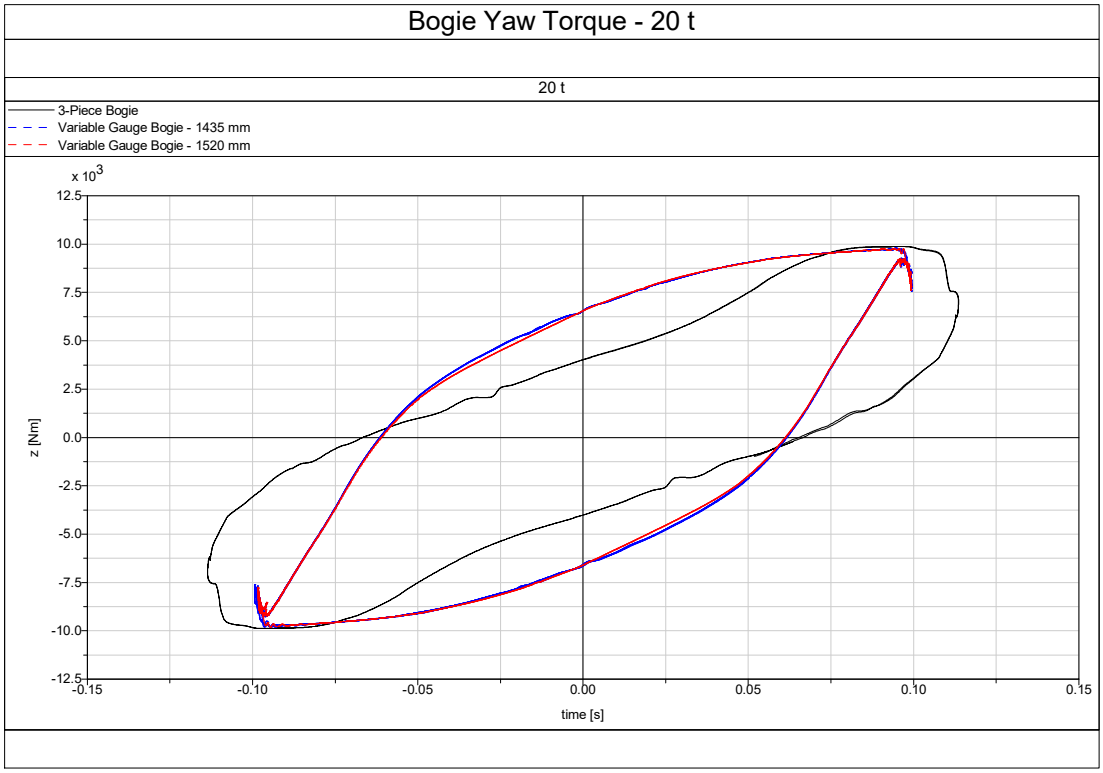

Figure 5.18 : Bogie Yaw Hysteresis for 20 t Loaded Wagons.

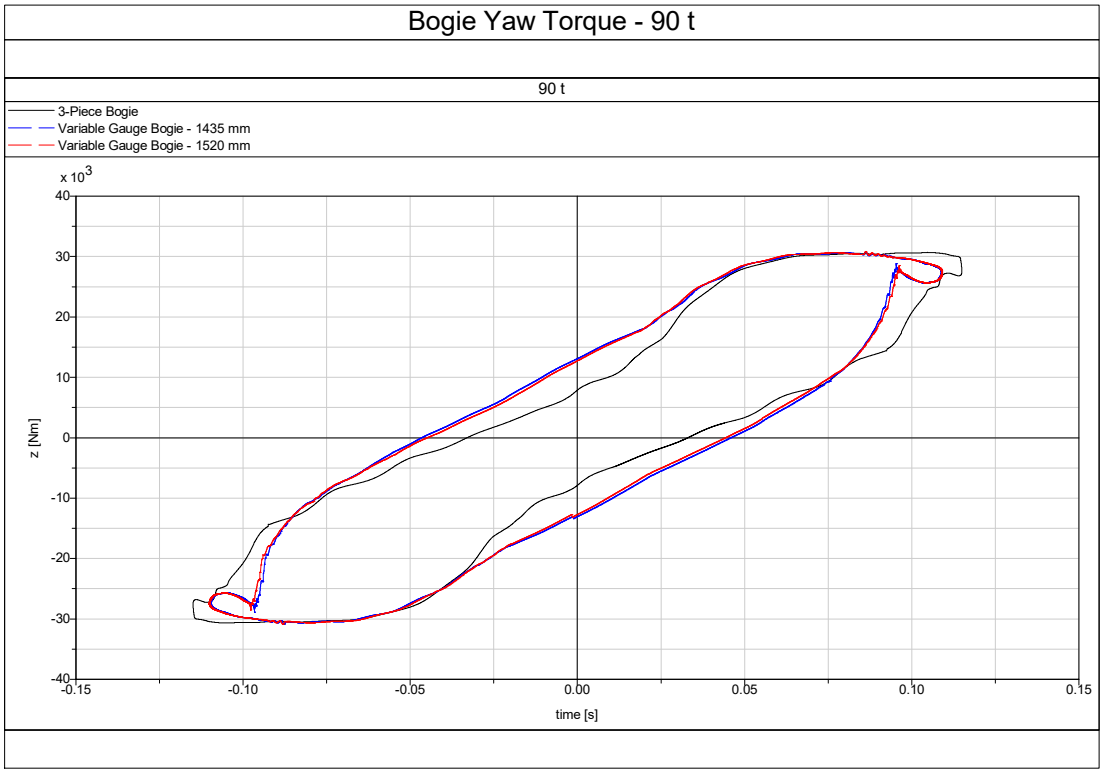

Figure 5.19 : Bogie Yaw Hysteresis for 90 t Loaded Wagons.

5.4 On-Track Tests for Variable Gauge Bogie

The three-piece American type bogie which was modeled and special designed variable gauge bogie have been compared in terms of stability and running safety with hunting mode analyzes, twisted track analyzes and bogie-yaw torque reviews. These models met the requirements in the relevant standards in general. On-track tests of the designed bogie that this thesis has examined in particular have been examined in this section.

On-track tests have been carried out as specified in EN 14363 standard and ERA technical document 2013-01-INT [28] under the various conditions of the load of the wagon (tare or laden), length of the wagon (long or short), the geometry of the track and various speed configurations.

This mentioned on-track tests examine all general characteristics i.e. risks of instability, wheel vertical/lateral forces and wheel climb. The tracks where the on-track tests will be carred out are examined in four seperate groups (zones) according to their geometry:

- Zone 1: Tangent track
- Zone 2: Large radius curves (1000 m curve radius was chosen for analysis.)
- Zone 3: Small radius curves (500 m curve radius was chosen for analysis.)
- Zone 4: Very small radius curves (250 m radius was chosen for analysis.)

In all of these zones, what should be known about the lateral geometry of the railway track is related to slope or level difference between two load-bearing rails. There is an ideal cant value to provide balance by taking into account centripetal accelerations in circular motions of rolling stock. According to the relevant standard EN 14363, the cant deficiency value can reach a maximum value of 130 mm for standardized designs. The calculation of cant deficiency is shown in (5.4) [29].

$$Cant\ Deficiency = \frac{gauge_{se}}{\left(1 + \frac{R^2 g^2}{v_{act}^4}\right)^{\frac{1}{2}}} - superelevation \tag{5.4}$$

$gauge_{se}$ denotes the rail gauge (from axis to axis, i.e. not 1435mm but 1500mm for European tracks), R denotes the curve radius, g denotes gravity and v_{act} denotes the actual velocity. Actual superelevations are zero in all scenarios because track sections

are modeled as flat. In other words, the level difference between two load-carrying rails is always zero. In this way, the maximum possible speeds were determined for 130 mm admissible cant deficiency which is the maximum value. The maximum admissible speed for designed bogie was 100 km/h and at this value, it can turn zone 2 curve at its maximum speed in both 1435 mm and 1520 mm gauges. All relevant calculations made by considering equation 5.4 are explained in Table 5.2.

Table 5.2 : Speed adjustments for all on-track test scenarios.

Track Zone	Gauge [mm]	Radius [m]	Velocity [m/s]	Velocity [km/h]	Cant Deficiency [mm]
Zone 1	1435	-	27.77	100	-
Zone 2	1435	1000	27.77	100	112.57
Zone 3	1435	500	21.11	76.00	129.97
Zone 4	1435	250	14.92	53.70	129.85
Zone 1	1520	-	27.77	100	-
Zone 2	1520	1000	27.77	100	119.24
Zone 3	1520	500	20.50	73.80	129.89
Zone 4	1520	250	14.50	52.20	129.96

The velocity values which found for these limit cant deficiency values were used as constant velocity in the zones.

The track definition method started with a straight track segment for balancing the vehicle at the begginig for each zone. This straight track is determined as 50 meters in all sections. Then the transition to the curve zones was defined by a 40 meters clothoid track segment. After a 50 meters fixed radius curve turn, a 40 meters clothoid transition to the straight track is defined. Finally, each zone is defined by the straight line segment. Section geometry with 250 m radius is in Figure 5.20 i.e. Rail inclination was used as1:40 in all track sections.

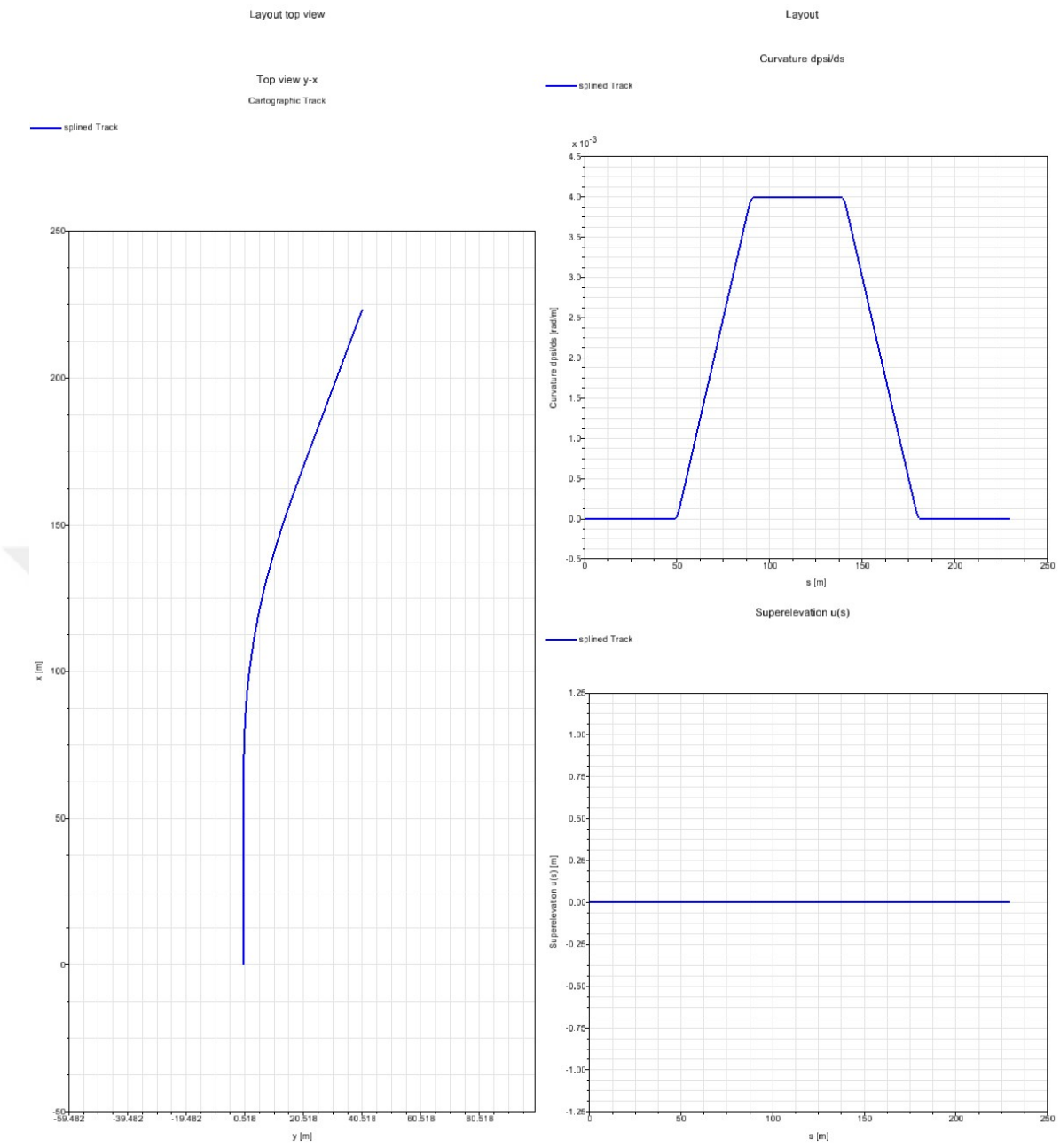

Figure 5.20 : 250 meters Curved Zone 4 Geometric Track Definition.

The tare weight of the carbody is 16 tons including the bogies. The laden weight is 90 tons, including the bogies. Another two different combinations for carbody are available for length other than weight. Short test wagon has 7 meters distance between two bogie centres while long test wagon has 13 meters distance between two bogie centres.

In summary, there are 16 different scenarios for a single axle gauge with two different loading conditions, two different lenghts and four different track geometries (Table 5.3).

Table 5.3 : On-track test scenarios.

Scenario ID	Track Gauge	Track Zone	Vehicle Load	Vehicle Length
001	1435 mm	Zone 1	Tare	Short
002	1435 mm	Zone 2	Tare	Short
003	1435 mm	Zone 3	Tare	Short
004	1435 mm	Zone 4	Tare	Short
005	1435 mm	Zone 1	Laden	Short
006	1435 mm	Zone 2	Laden	Short
007	1435 mm	Zone 3	Laden	Short
008	1435 mm	Zone 4	Laden	Short
009	1435 mm	Zone 1	Tare	Long
010	1435 mm	Zone 2	Tare	Long
011	1435 mm	Zone 3	Tare	Long
012	1435 mm	Zone 4	Tare	Long
013	1435 mm	Zone 1	Laden	Long
014	1435 mm	Zone 2	Laden	Long
015	1435 mm	Zone 3	Laden	Long
016	1435 mm	Zone 4	Laden	Long
017	1520 mm	Zone 1	Tare	Short
018	1520 mm	Zone 2	Tare	Short
019	1520 mm	Zone 3	Tare	Short
020	1520 mm	Zone 4	Tare	Short
021	1520 mm	Zone 1	Laden	Short
022	1520 mm	Zone 2	Laden	Short
023	1520 mm	Zone 3	Laden	Short
024	1520 mm	Zone 4	Laden	Short
025	1520 mm	Zone 1	Tare	Long
026	1520 mm	Zone 2	Tare	Long
027	1520 mm	Zone 3	Tare	Long
028	1520 mm	Zone 4	Tare	Long
029	1520 mm	Zone 1	Laden	Long
030	1520 mm	Zone 2	Laden	Long
031	1520 mm	Zone 3	Laden	Long
032	1520 mm	Zone 4	Laden	Long

5.4.1 Results of on-track tests

When the new design bogie analyzes were started, it was observed that this bogie was derailed by the wheel near the center of the turning radius without being able to take

turns properly. The fact that concentric wheels were not connected to each other with high rigidity, caused the inside wheel move to the central axis of the rails without a flange stop from the other wheel (Figure 5.21).

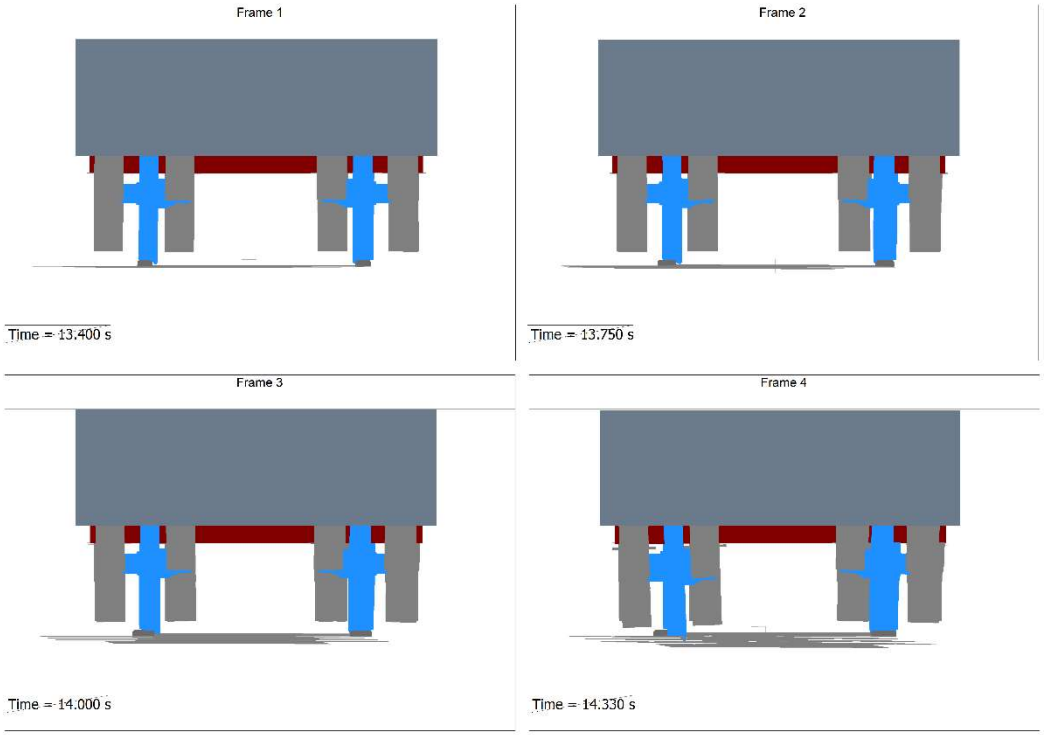

Figure 5.21 : Derailment in the case of unconnected concentric wheels.

A common axle beam can be used in such bogie designs. However, a connection running on the lateral axis between the inner axle boxes also provided the necessary solution within the scope of this study. (Figure 5.22).

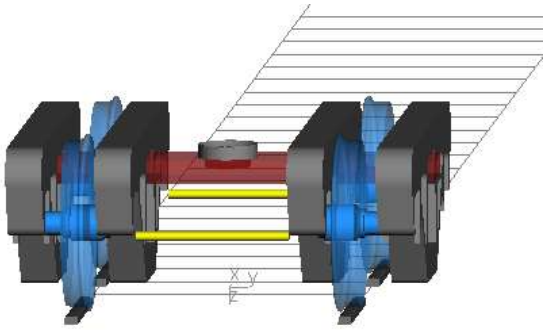

Figure 5.22 : Support link between inner axleboxes. (shown in yellow).

On-track tests and the tests mentioned in previous topics of the thesis were completed without any derailment after this arrangement.

This section summarizes the maximum Y/Q wheel climb ratios observed in each scenario in on-track tests. Considering the Y/Q ratios from the analysis results, the relevant models met this safety criterion according to the standards.

Vertical and lateral wheel-rail forces, wheel lifts and graph of forces on suspension springs related to the on-track tests are given in the appendix. The maximum Y/Q wheel climb rate seen in eact test case and which wheel it was observed are given in the Table 5.4.

Table 5.4 : Maximum Y/Q and Locations for On-track Tests.

ID	Max. Y/Q Value	Bogie Location	Wheel Location	ID	Max. Y/Q Value	Bogie Location	Wheel Location
001	0.02	Rear	Rear, Left	017	0.04	Front	Front, Left
002	0.54	Front	Front, Left	018	0.54	Front	Front, Left
003	0.59	Front	Front, Left	019	0.58	Front	Front, Left
004	0.66	Front	Front, Left	020	0.65	Front	Front, Left
005	0.02	Rear	Rear, Left	021	0.03	Front	Rear, Right
006	0.38	Front	Front, Left	022	0.37	Front	Front, Left
007	0.45	Front	Front, Left	023	0.44	Front	Front, Left
008	0.48	Front	Front, Left	024	0.48	Front	Front, Left
009	0.02	Rear	Rear, Left	025	0.04	Front	Front, Left
010	0.54	Front	Front, Left	026	0.54	Front	Front, Left
011	0.63	Front	Front, Left	027	0.62	Front	Front, Left
012	0.76	Front	Front, Left	028	0.76	Front	Front, Left
013	0.02	Rear	Rear, Left	029	0.03	Front	Rear, Right
014	0.37	Front	Front, Left	030	0.35	Front	Front, Left
015	0.43	Front	Front, Left	031	0.43	Front	Front, Left
016	0.48	Front	Front, Left	032	0.48	Front	Front, Left

As can seen in the Table 5.4, the maximum Y/Q ratio was realized at the leading outer wheel on all tracks with curve radius. It is seen that Y/Q is very close to zero in tangent tracks. The locations written in the table for these near-zero values are relative to the value calculated by the solver. All eight wheels have Y/Q ratios very close to zero.

6. CONCLUSION

In accordance with the purpose of the thesis, the modeling and tests of a bogie, whose concept design has been made before, in order to examine the running behaviour have been successfully completed.

After a literature review was made at the beginning, a central suspension system was proposed for the variable gauge bogie, considering the suspension types of freight wagon bogies and their characteristics. Friction wedges became parts that provide damping in this system.

The built of a conventional three-piece bogie MBS model was not only used as a reference model, but was used for comparisons based on the new design variable gauge bogie.

For the variable gauge bogie, in addition to concept design, the system using the suspension with friction wedges in the center was proposed at the beginning of this study. In addition, a revision has been made that connects the inner side frames with fixed connections to each other in order to reset the risk of derailment occuring during curves.

The stability analysis, twisted track analysis and bogie yaw resistance analysis of the conventional three-piece bogie and the newly designed variable gauge bogie were made for comparison purposes and both designs met the examined standards EN 14363 and EN 16235 with the parts examined in the thesis study.

Finally, the special designed bogie was analyzed in the on-track sections for the tests specified in EN 14363. Various loading and length situations of test wagons are taken into account. The bogie with variable gauge has been used with two track gauges, 1435 mm and 1520 mm. The wheel and axle boxes on the bogie are also positioned according to this opening and mounted accordingly. The tests were carried out and the safety coefficients were determined according to the Y/Q wheel climbing ratio. Safe running behaviour is ensured by staying below the maximum values specified in the standard.

The freight wagon bogie with variable gauge wheels exhibits similar characteristics on the tracks as 1435 mm gauge and 1520 mm gauge. No very different Y/Q values were observed for line spans at different track gauges.

This thesis study succeeded in setting an example in terms of making suggestions for vehicle designs without experimental tests by utilizing computer aided MBS tests. After evaluations in the manufacturing process, more accurate design can be made.

Vehicles operating in three-piece bogie logic contain a very high level of non-linearity. However, this study was able to provide basic knowledge and ideas about what can change with the varying degrees of freedom and body numbers in two different bogie designs.

In the new design, since the number of force elements changed compared to the conventional design, the equivalent stiffness of the system has been adjusted. In the central suspension, the number of springs has doubled.. Here the optimization of this spring system must be carried out.

There are other circumstances on this topic may need to be examined. Analysis for the running dynamics in gauge station region is required. The systems of this mechanism need validation with bogie or rolling stock level tests. It is also necessary to examine the integration of the brake system and the behaviour of the brake system, accordingly.

REFERENCES

[1] **Url-1** <*https://commons.wikimedia.org/wiki/File:Gauge_EN.svg*>, date retrieved 03.06.2021

[2] **Url-2** <*https://commons.wikimedia.org/wiki/File:Rail_gauge_world.png*>, date retrieved 03.06.2021

[3] **Url-3** <*https://en.wikipedia.org/wiki/Bogie*>, date retrieved 08.06.2021

[4] **Iwnicki, S** (2006). *Handbook of railway vehicle dynamics,* CRC Press.

[5] **Iwnicki, S., Grassie, S. and Kik, W.** (1999). Track Settlement Prediction Using Computer Simulation Tools, *Vehicle System Dynamics, **33***, 37-46.

[6] **Wu, Q., Cole, J., Spiryagin, M., Sun, Y.Q.** (2014). A Review of Dynamics Modelling of Friction Wedge Suspensions, *Vehicle System Dynamics, **52***, 1389-1415.

[7] **İgde, V.** (2018). *Concept and Construction Design of a Freight Wagon Bogie Frame With Variable Axle Distance* (M.Sc. Thesis). Istanbul Technical University, Department of Mechanical Engineering, ISTANBUL.

[8] **Url-4** <*https://www.elh.de/produkte/y25*>, date retrieved 19.12.2021

[9] **Stichel, S.** (1999). How to improve the running behavior of freight wagons with UIC-link suspension, *Vehicle System Dynamics, **33***, 394-405.

[10] **Jönsson, P-A., Stichel, S. and Persson, I.** (2009). New simulation model for freight wagons with UIC link suspension, *Vehicle System Dynamics, **46***, 695-704.

[11] **Eickhoff, B.M., Evans, J.R. and Minnis A.J.** (1995). A Review of Modelling Methods for Railway Vehicle Suspension Components, *Vehicle System Dynamics, **24***, 469-496.

[12] **Bosso, N., Gugliotta, A., Somá, A.** (2002). Multibody simulation of a freight bogie with friction dampers, *ASME/IEEE 2002 Joint Rail Conference,* pp. 47-56.

[13] **Shabana, A. A.** (2013). *Dynamics of multibody systems,* Cambridge University Press.

[14] **Shabana, A. A.** (2011). *Computational Dynamics,* Wiley.

[15] **Spicka, J., Hajzman, M., Bonkowski, T.** (2016). In-house Multibody Human Model Based on Euler Parameters for the Fast Impact Scenario Calculation, *ECCOMAS 2016.*

[16] **Yücel, E., Göloğlu, C.** (2013). Evaluation of Contact Models on Wheel Rail Pairs in Railways, *7th International Advanced Technologies Symposium,* İstanbul.

[17] **Johnson, K. L.** (1985). *Contact Mechanics*, Cambridge University Press.

[18] **Popov, V.L.** (2017). *Contact Mechanics and Friction*, Cambridge University Press.

[19] **Kalker, J.J.** (1990). *Three-Dimensional Elastic Bodies in Rolling Contact*, Springer Science & Business Media.

[20] **Shevtsov, I.Y.,** (2008). *Wheel/rail Interface Optimisation*, Technische Universiteit Delft.

[21] **Vollebregt, E.A.H.** (2020). *User Guide for CONTACT, Rolling and Sliding Contact With Friction*, VTECH CMCC. Available from: https://www.kalkersoftware.org/downloads/user-guide.pdf

[22] **Simpack** (2017). *Simpack Documentation,* Dassault Systemes Simulia Corp.

[23] **Piatkowski, T.** (2014). Dahl and LuGre dynamic friction models – The analysis of selected properties, *Mech. Mach. Theory, **73***, 91-100.

[24] **Taheri, M.** (2016). *Machine Learning from Computer Simulations with Applications in Rail Vehicle Dynamics and System Identification* (Doctoral Dissertation). Virginia Polytechnic Institute and State University, Department of Mechanical Engineering, Blacksburg, VA, USA.

[25] **Iwnicki, S., Stichel S., Orlova, A., Hecht M.** (2015). Dynamics of Railway Freight Vehicles, *Vehicle System Dynamics, **53***, 995-1033.

[26] **BS EN 14363** (2016), Railway applications - Testing and Simulation for the acceptance of running characteristics of railway vehicles - Running Behaviour and stationary tests. Retrieved from https://shop.bsigroup.com/products/railway-applications-testing-and-simulation-for-the-acceptance-of-running-characteristics-of-railway-vehicles-running-behaviour-and-statiounary-tests/standard

[27] **BS EN 16235** (2013), Railway application — Testing for the acceptance of running characteristics of railway vehicles — Freight wagons — Conditions for dispensation of freight wagons with defined characteristics from on-tracktests according to EN 14363. Retrieved from https://shop.bsigroup.com/products/railway-applications-testing-for-the-acceptance-of-running-characteristics-of-railway-vehicles-freight-wagons-conditions-for-dispensation-of-freight-wagons-with-defined-characteristics-from-on-track-tests-according-to-en-14363/standard

[28] **ERA (**2013), Specific Procedures for Running Dynamics, Technical document. Retrieved from https://www.era.europa.eu/sites/default/files/activities/docs/era_td_2013_01_int_en.pdf

[29] **Url-5** <*https://en.wikipedia.org/wiki/Cant_deficiency*>, date retrieved 19.12.2021

APPENDICES

APPENDIX A: Result diagrams for on-track testing.

APPENDIX A

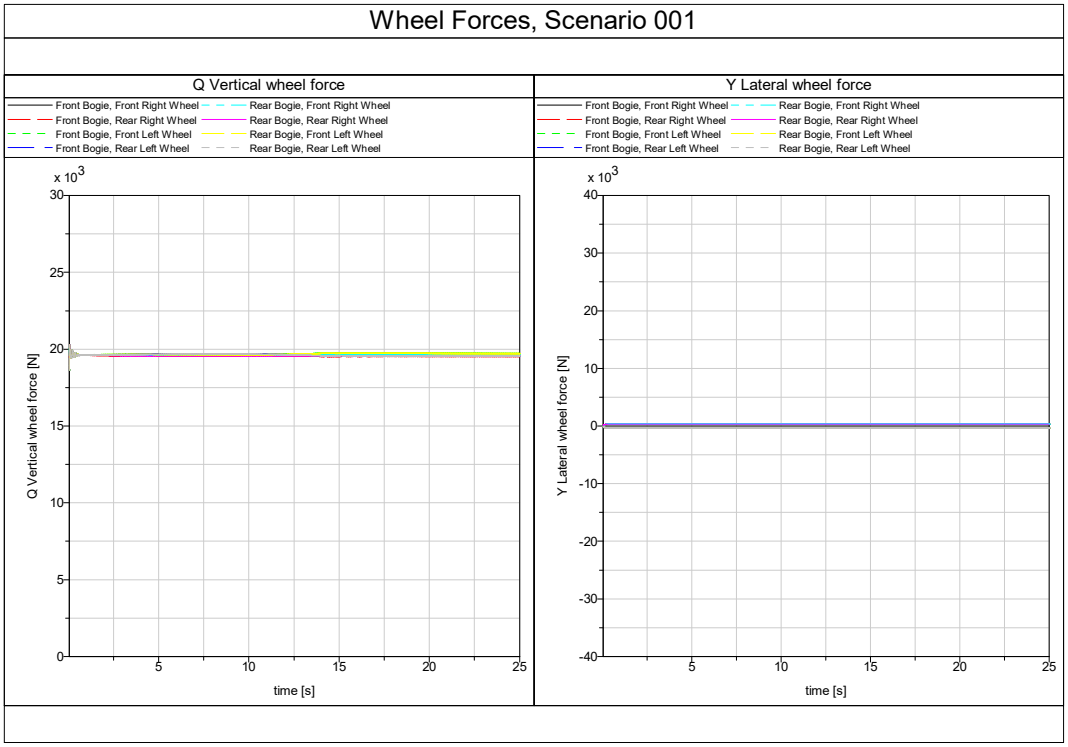

Figure A.1 : Wheel Forces of Scenario 001.

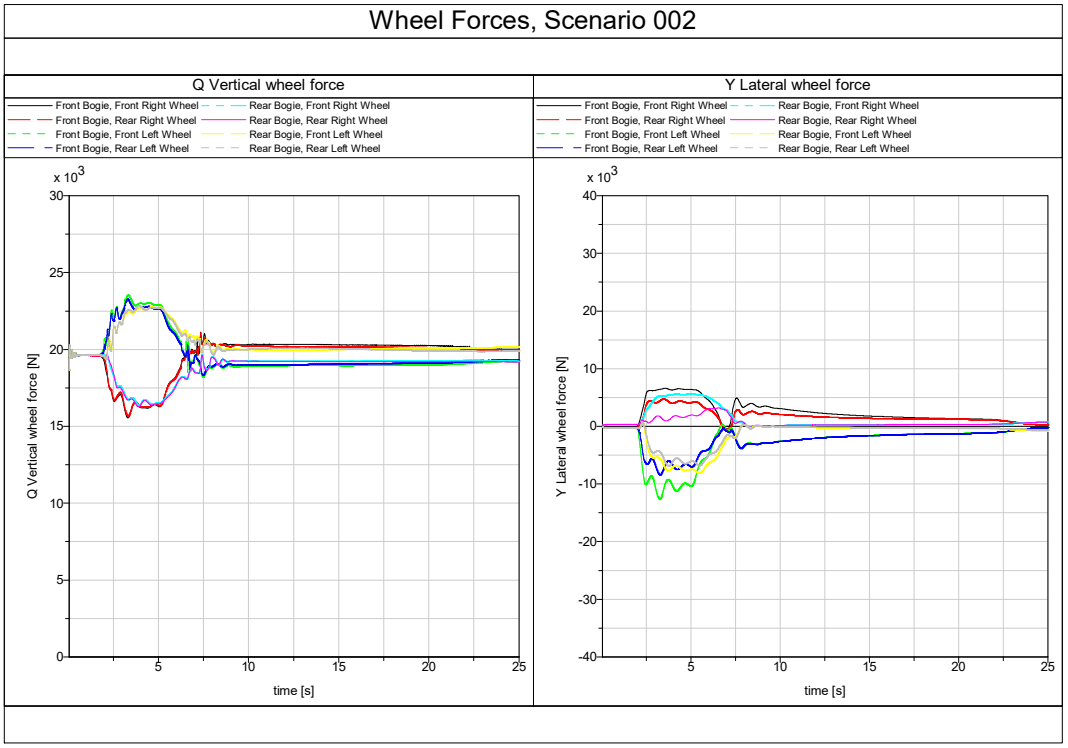

Figure A.2 : Wheel Forces of Scenario 002.

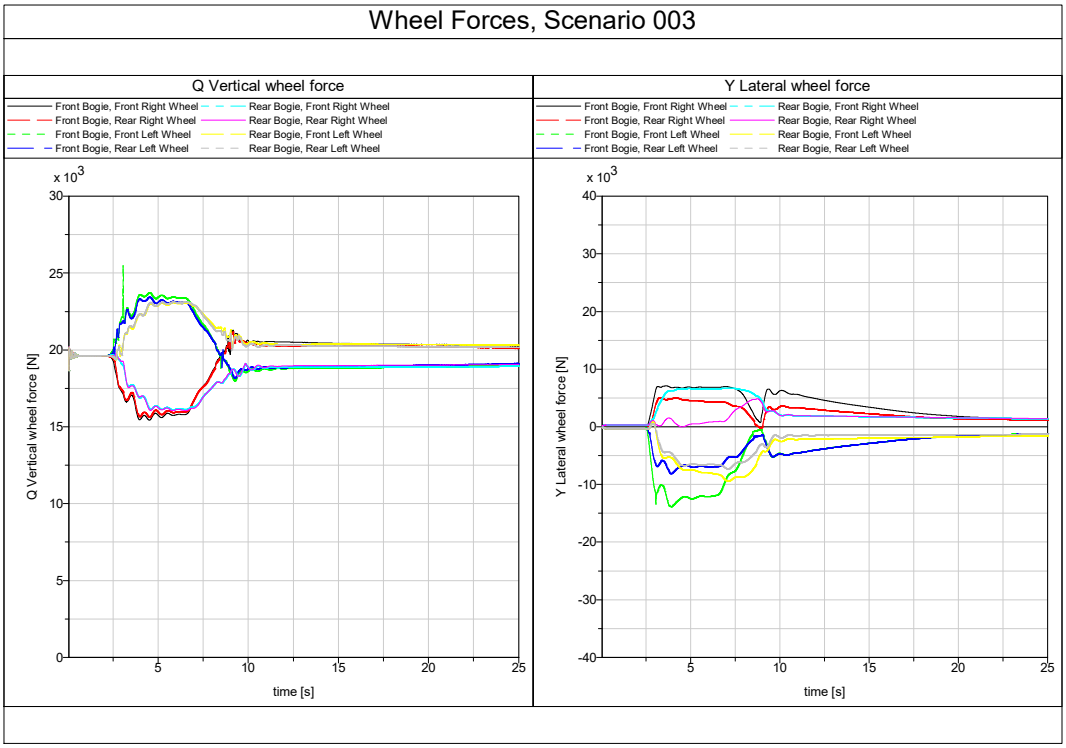

Figure A.3 : Wheel Forces of Scenario 003.

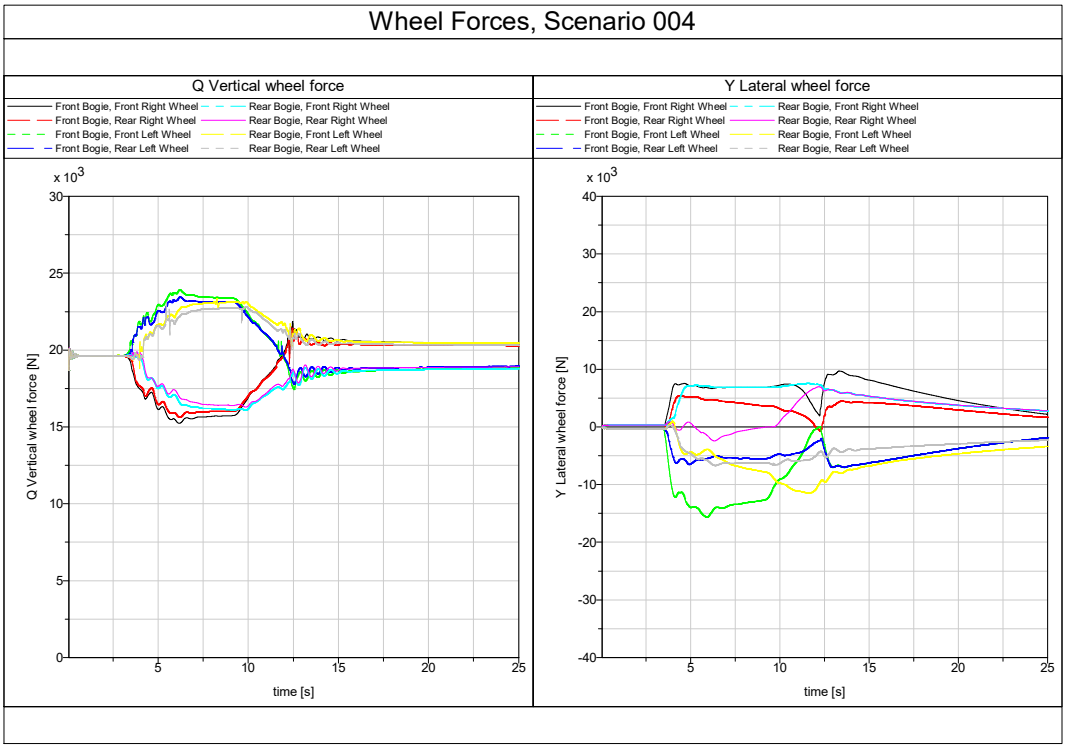

Figure A.4 : Wheel Forces of Scenario 004.

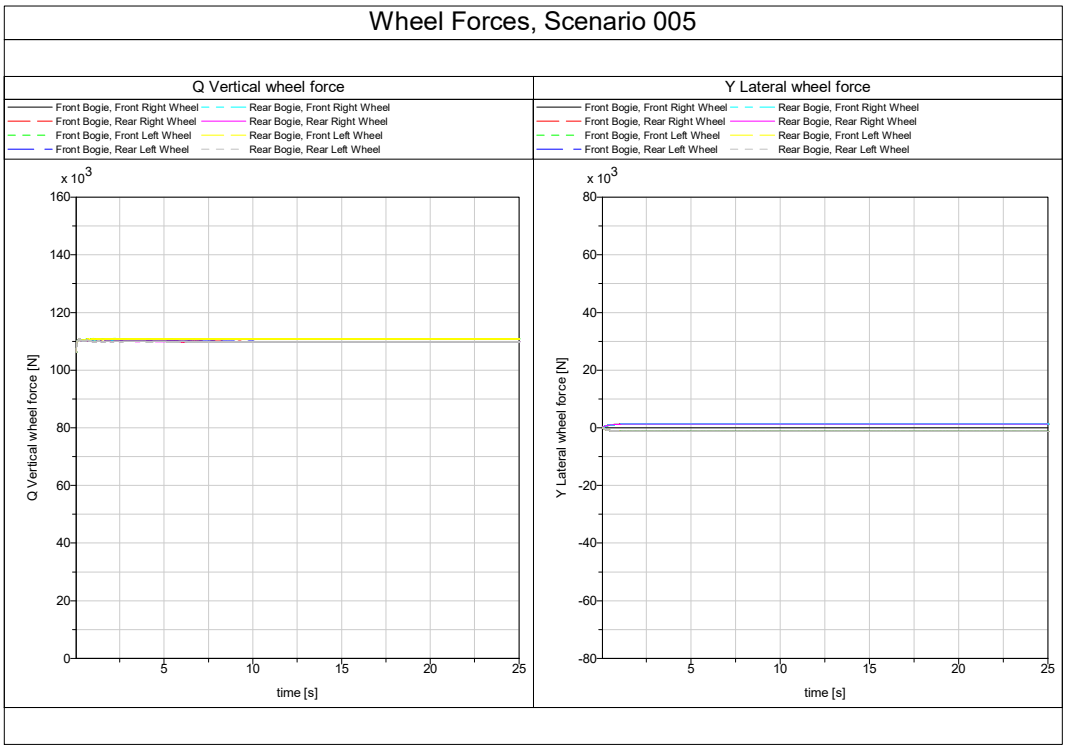

Figure A.5 : Wheel Forces of Scenario 005.

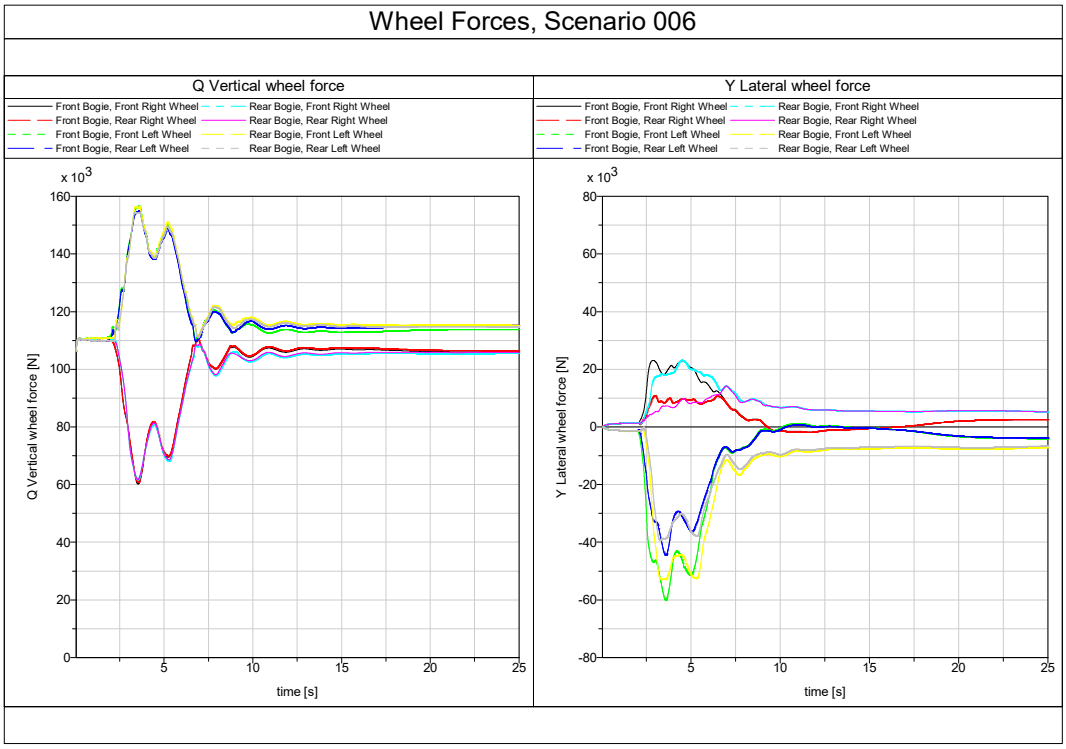

Figure A.6 : Wheel Forces of Scenario 006.

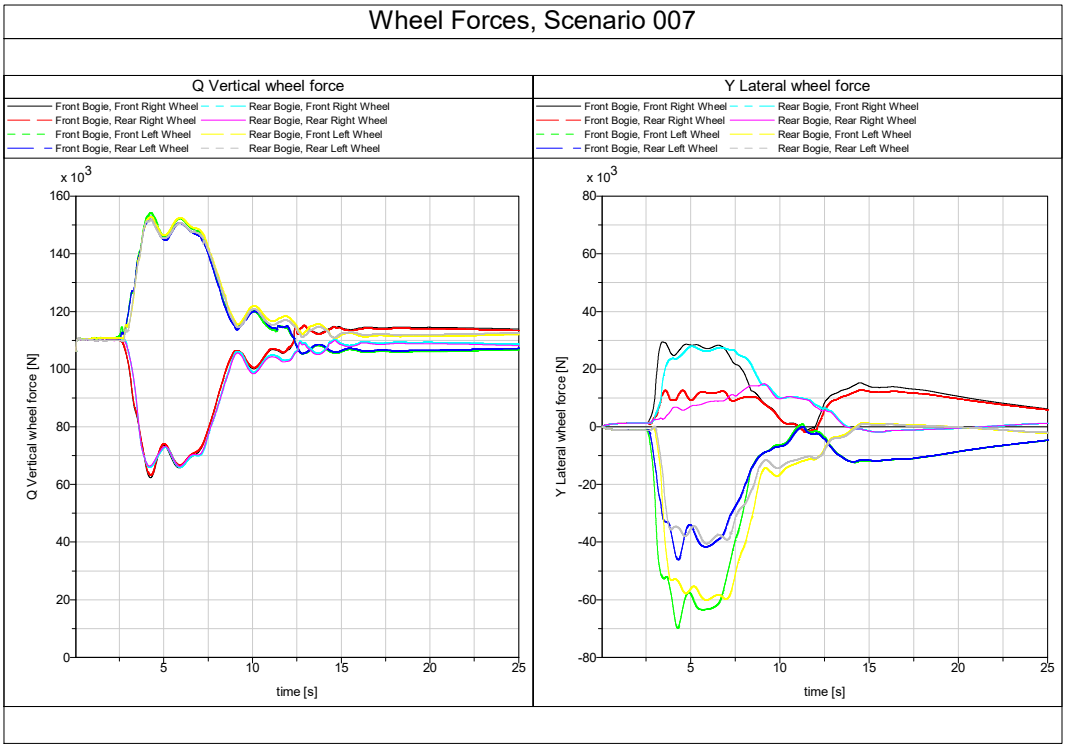

Figure A.7 : Wheel Forces of Scenario 007.

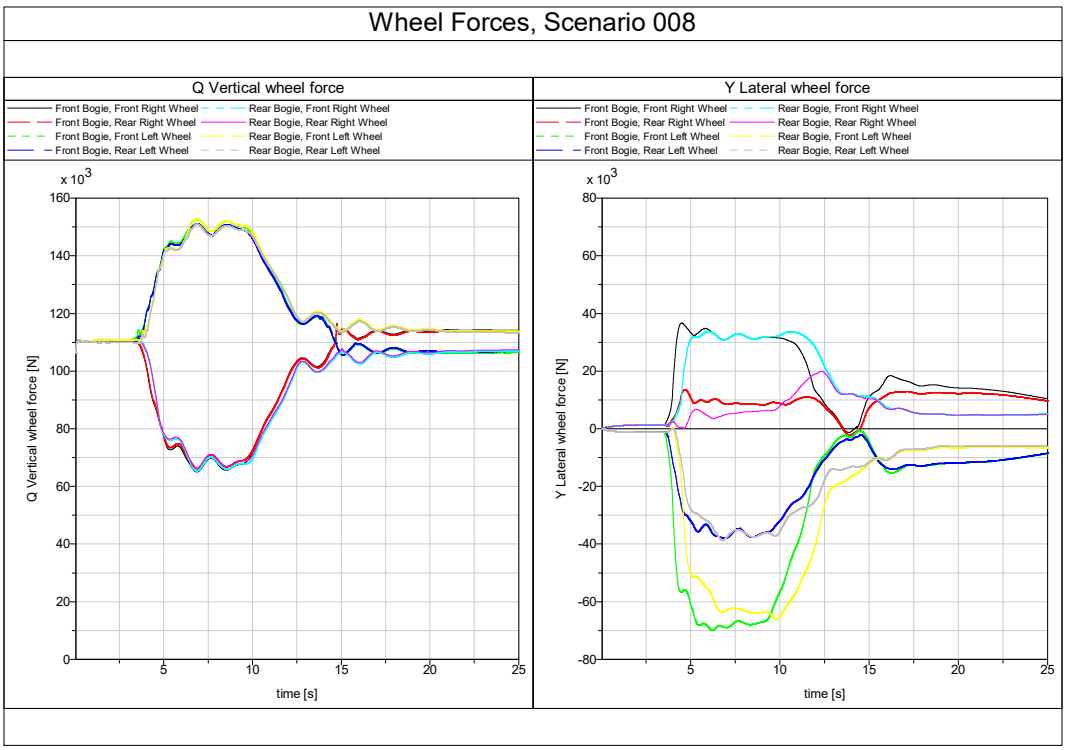

Figure A.8 : Wheel Forces of Scenario 008.

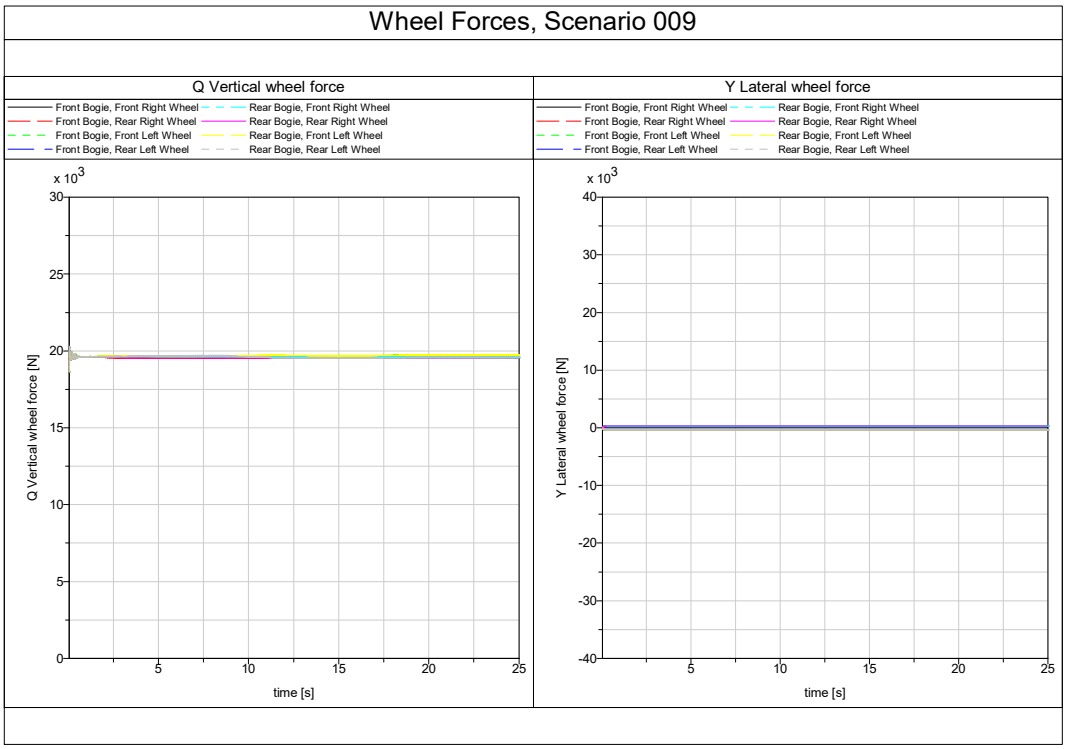

Figure A.9 : Wheel Forces of Scenario 009.

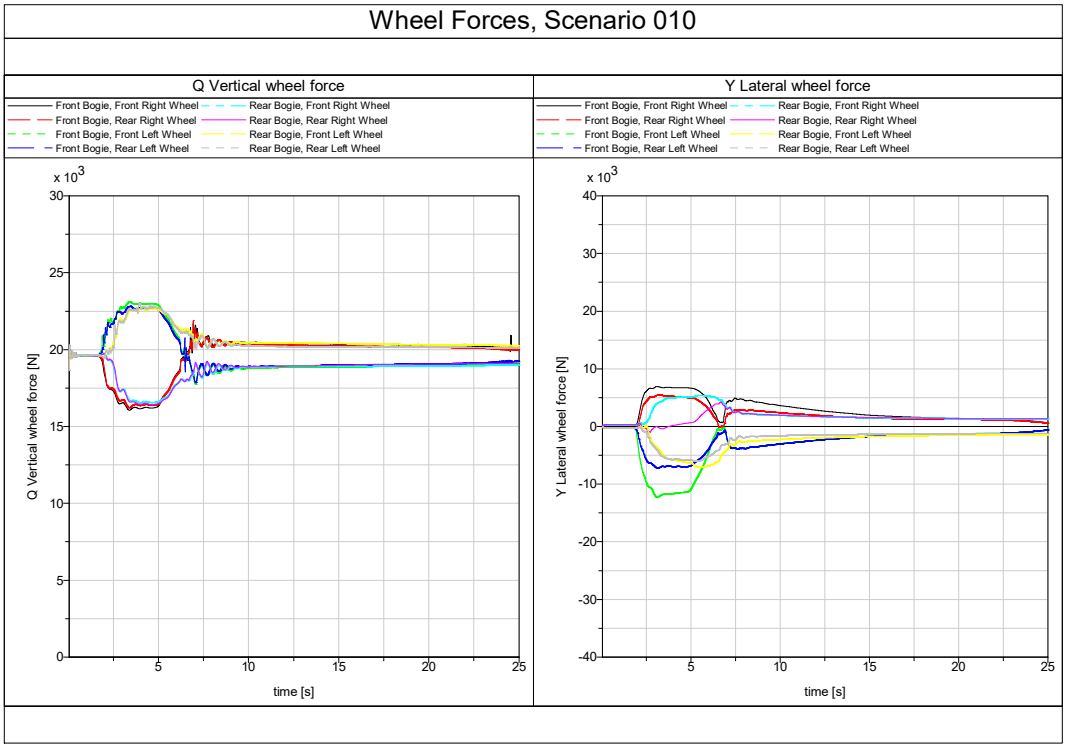

Figure A.10 : Wheel Forces of Scenario 010.

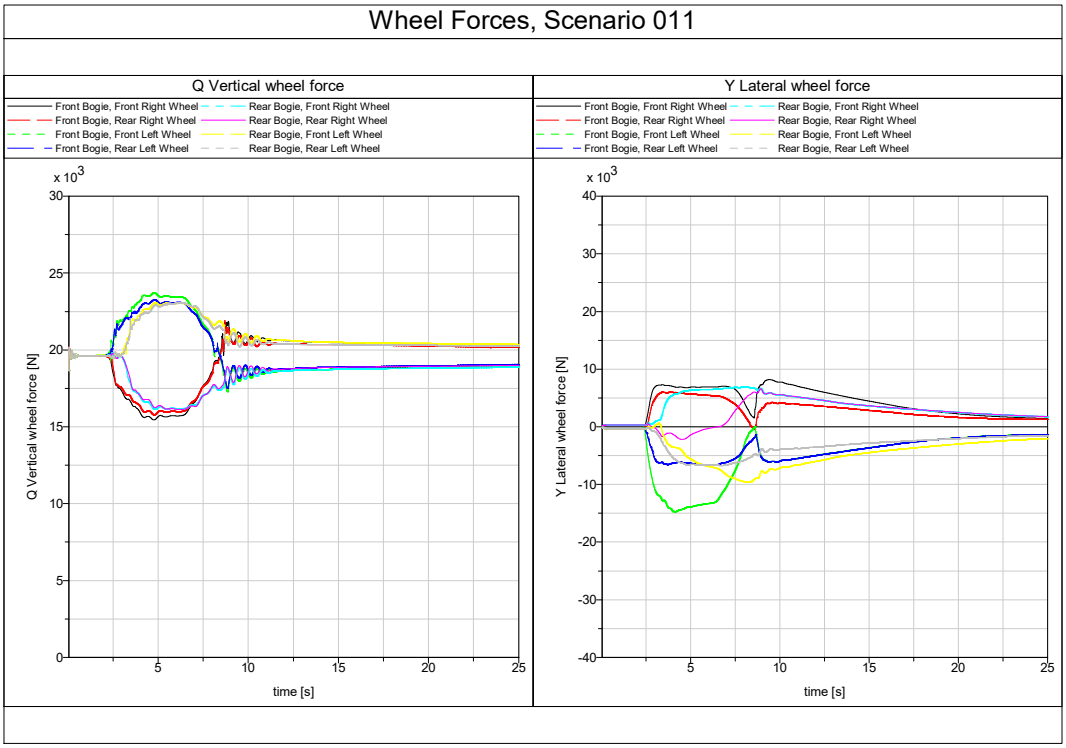

Figure A.11 : Wheel Forces of Scenario 011.

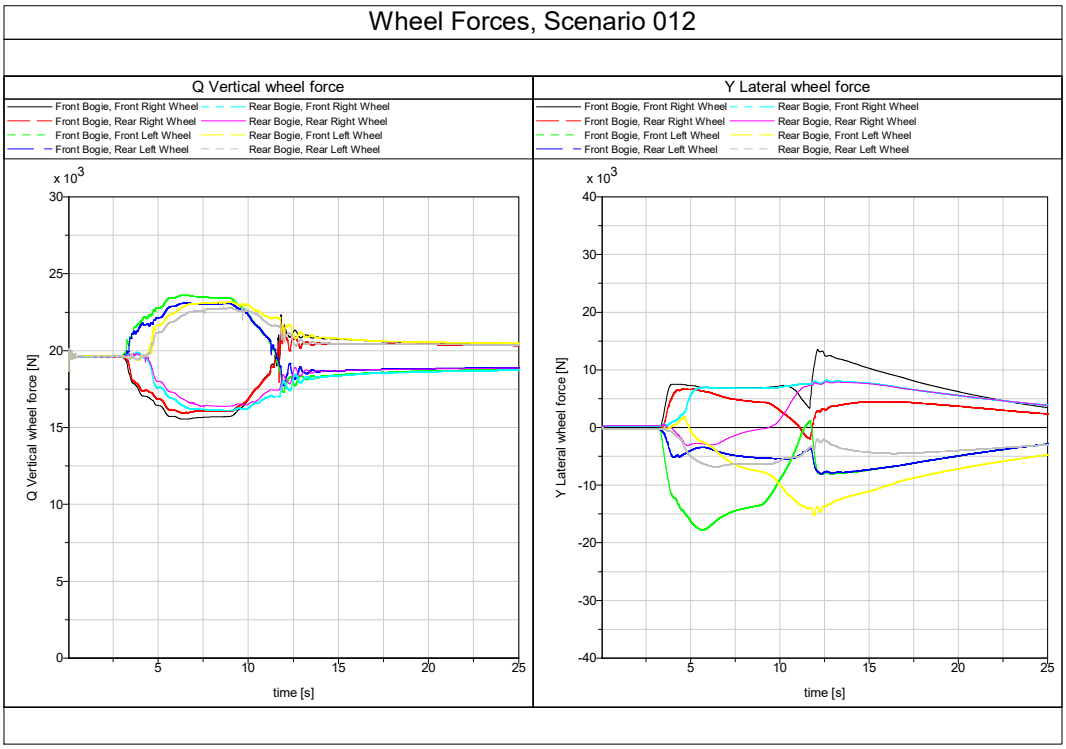

Figure A.12 : Wheel Forces of Scenario 012.

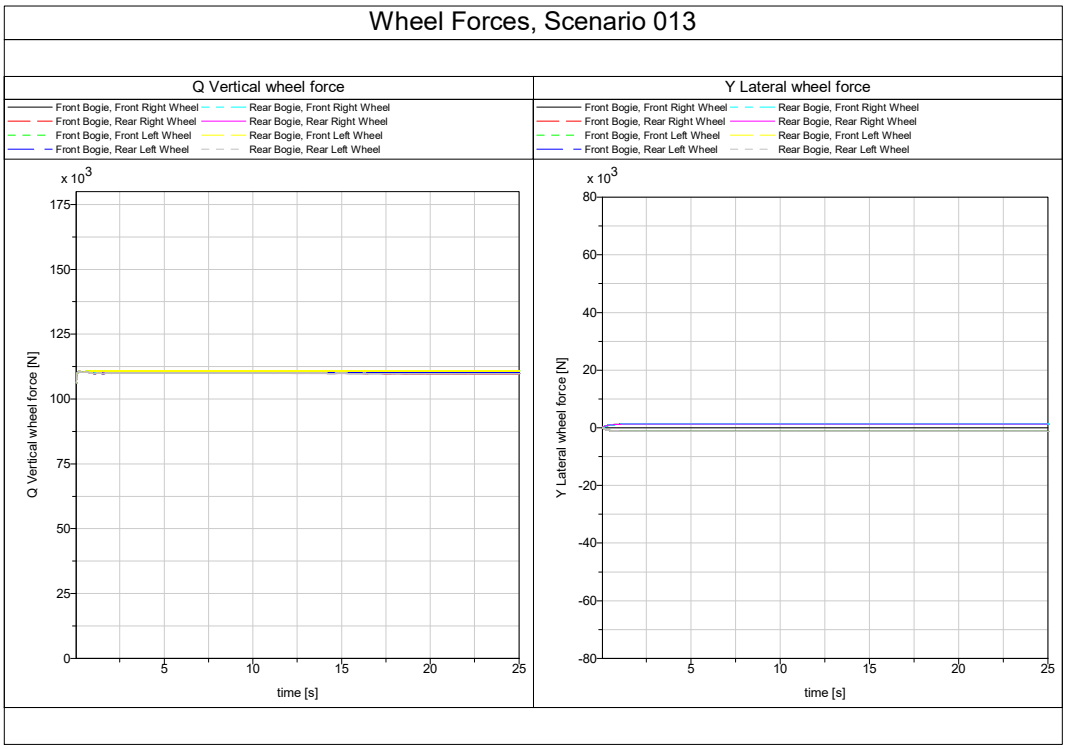

Figure A.13 : Wheel Forces of Scenario 013.

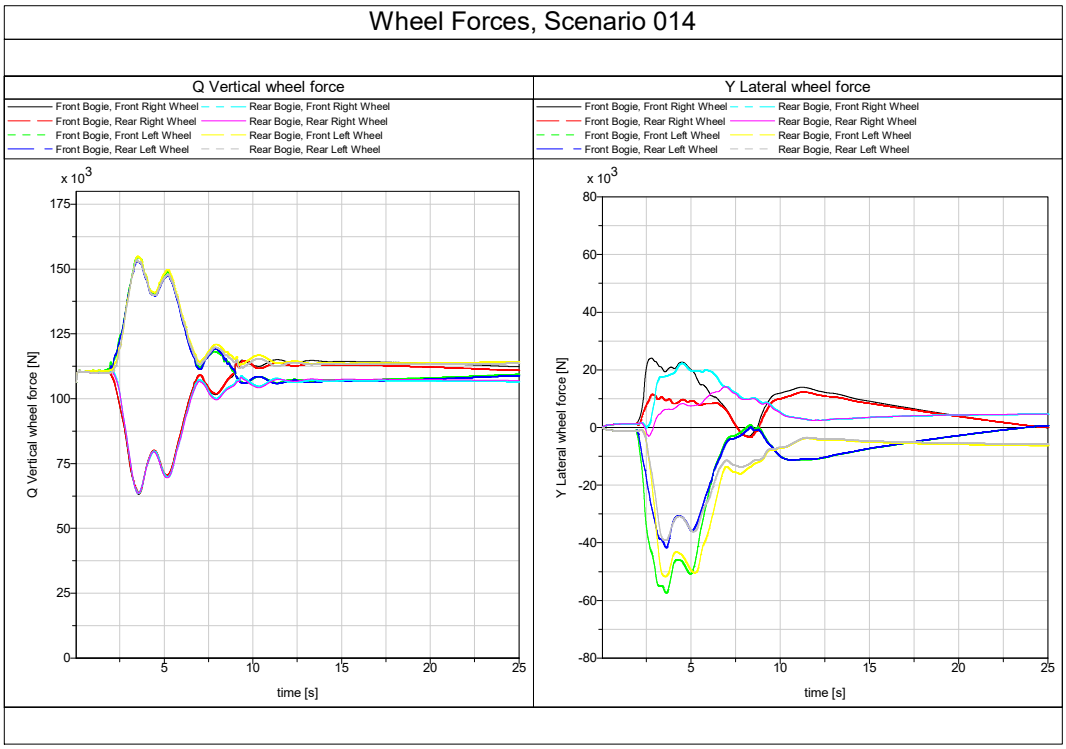

Figure A.14 : Wheel Forces of Scenario 014.

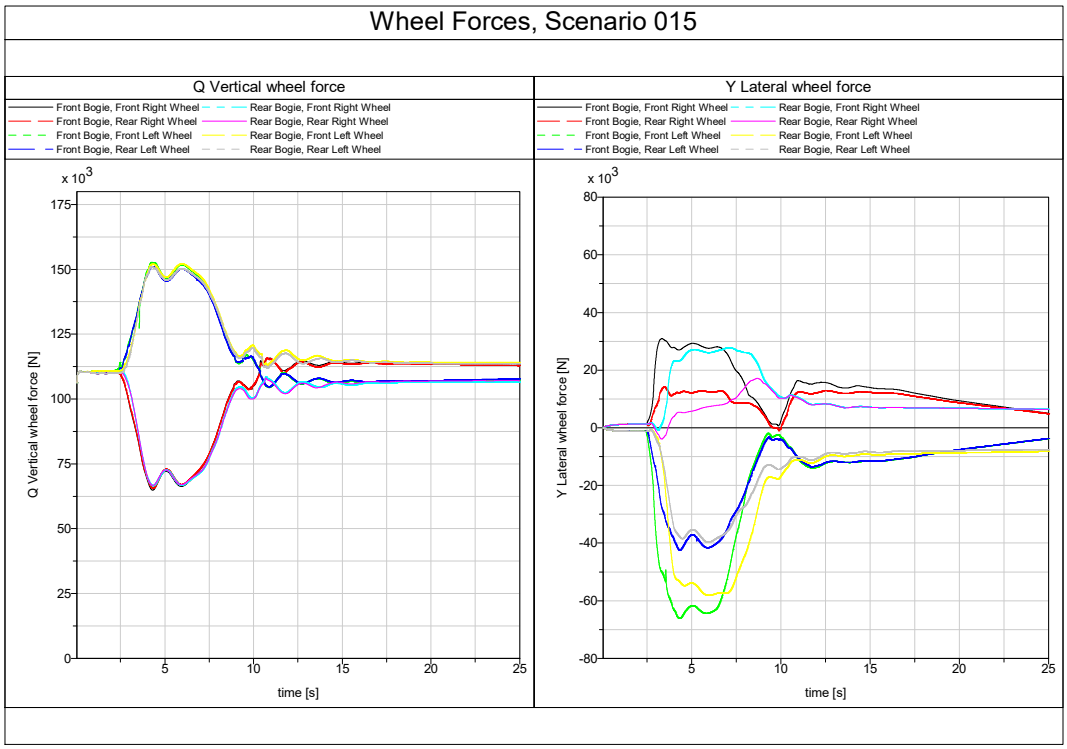

Figure A.15 : Wheel Forces of Scenario 015.

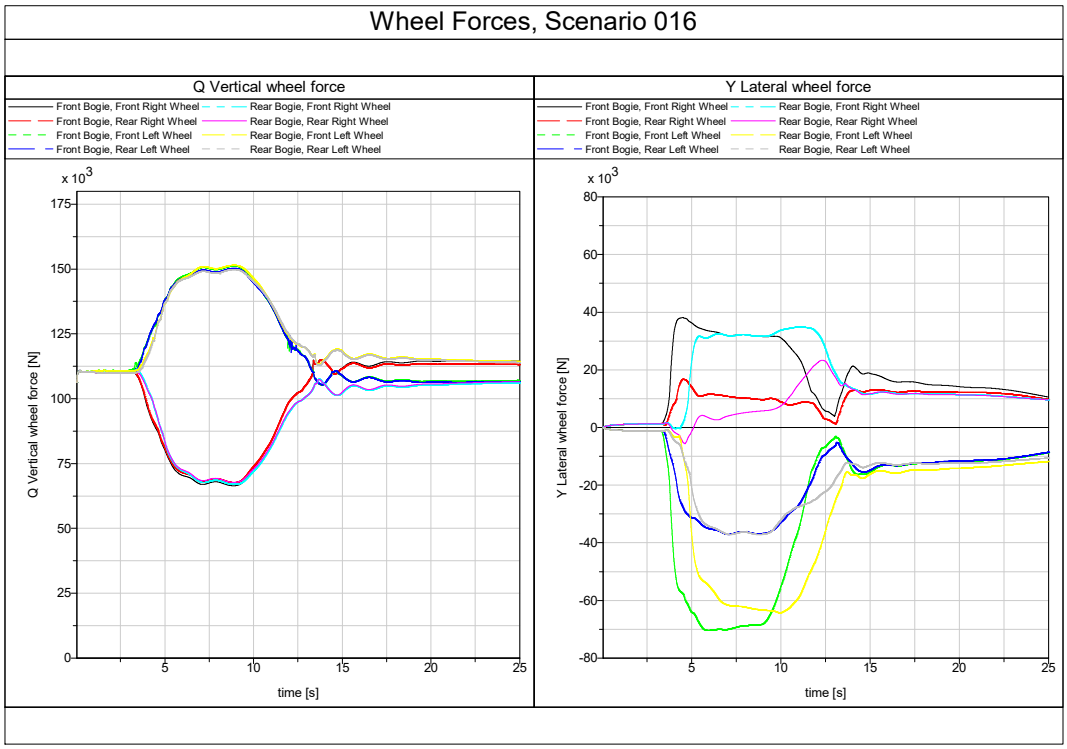

Figure A.16 : Wheel Forces of Scenario 016.

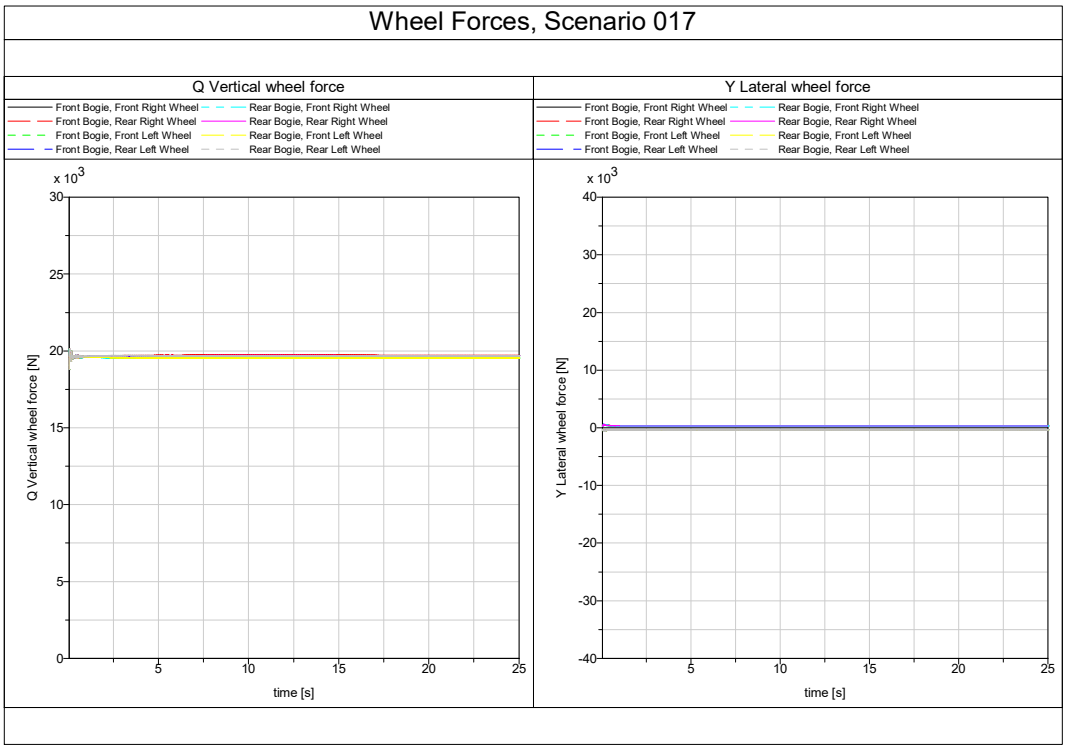

Figure A.17 : Wheel Forces of Scenario 017.

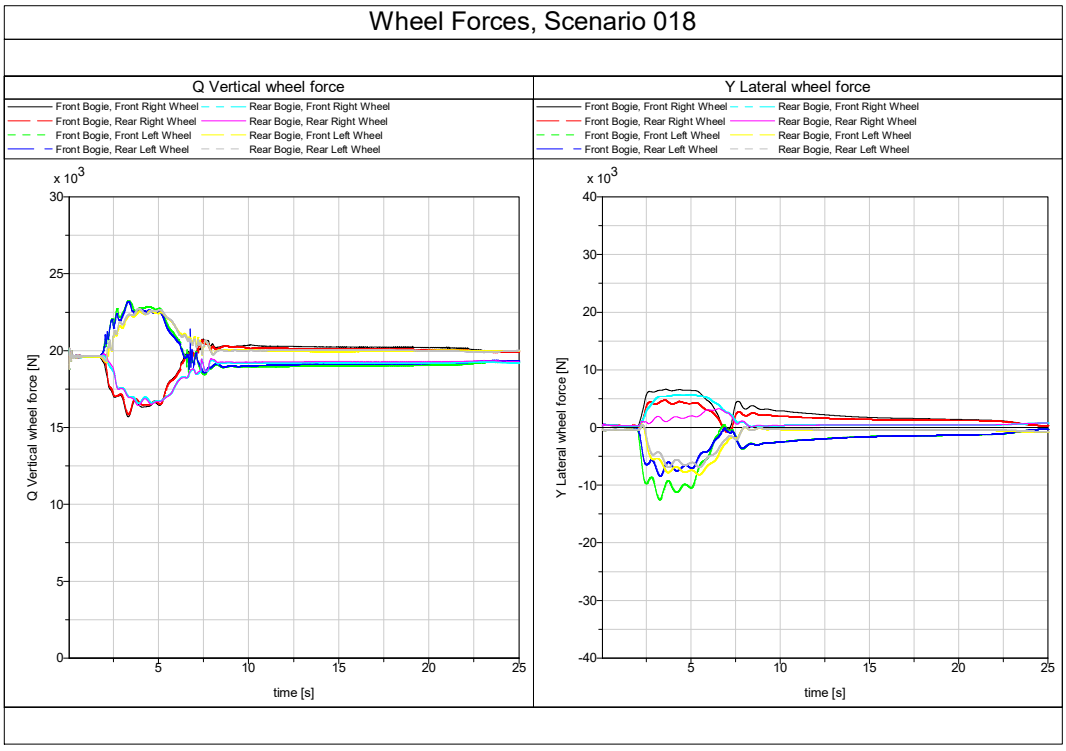

Figure A.18 : Wheel Forces of Scenario 018.

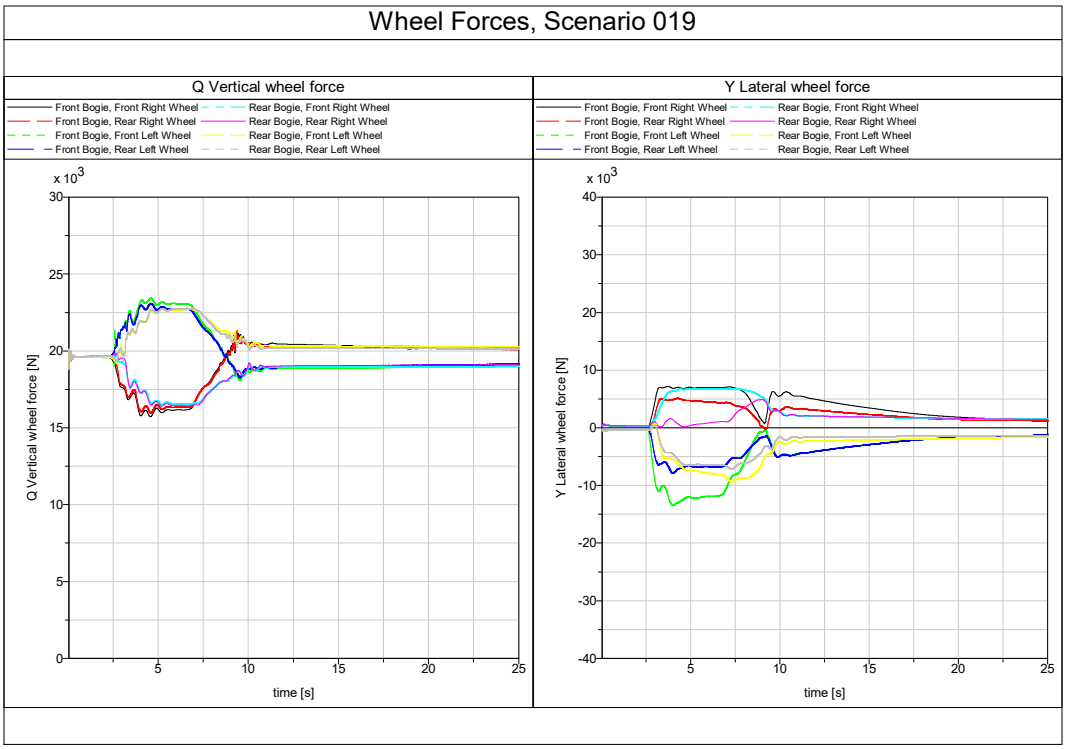

Figure A.19 : Wheel Forces of Scenario 019.

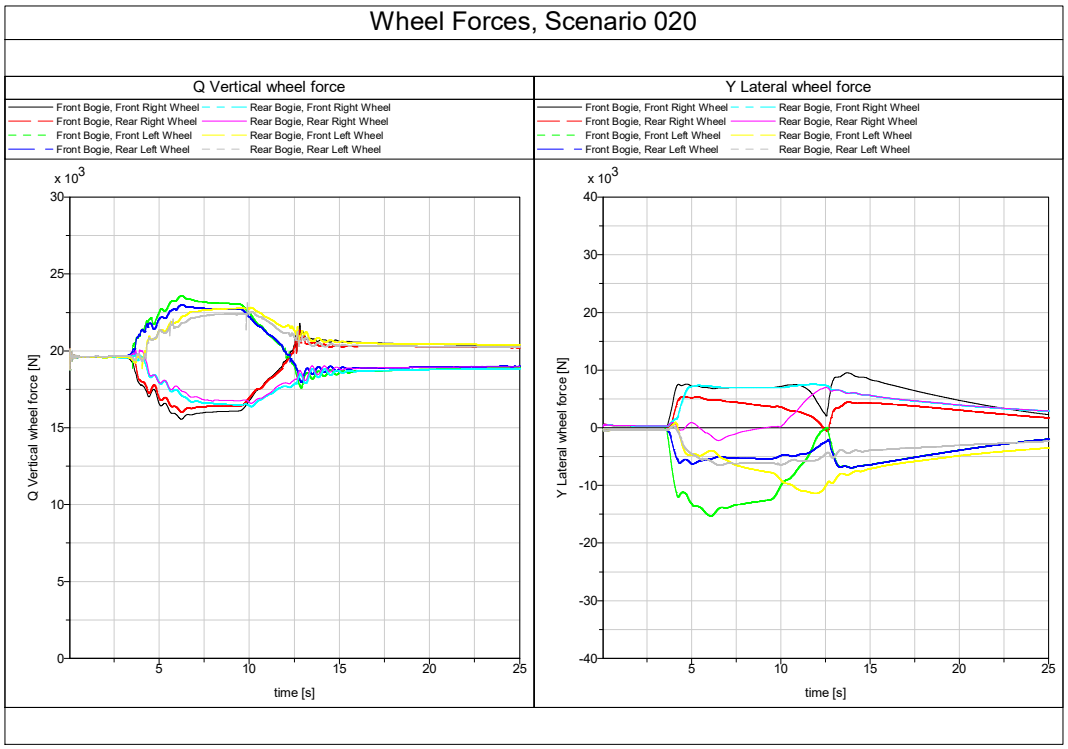

Figure A.20 : Wheel Forces of Scenario 020.

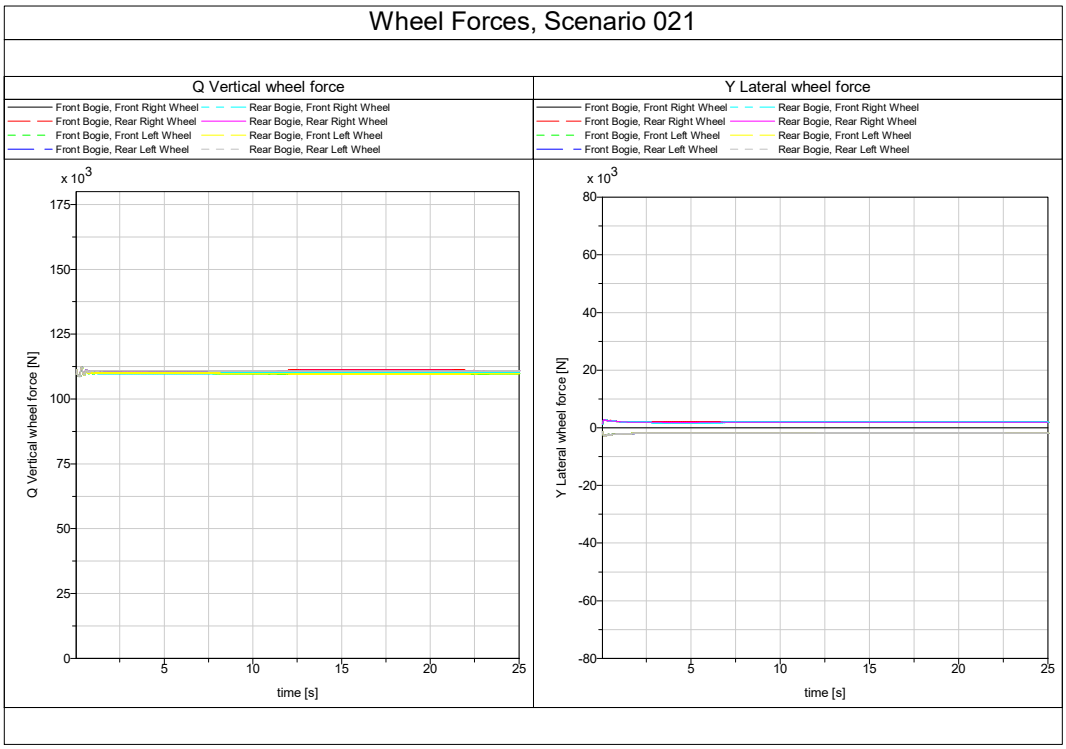

Figure A.21 : Wheel Forces of Scenario 021.

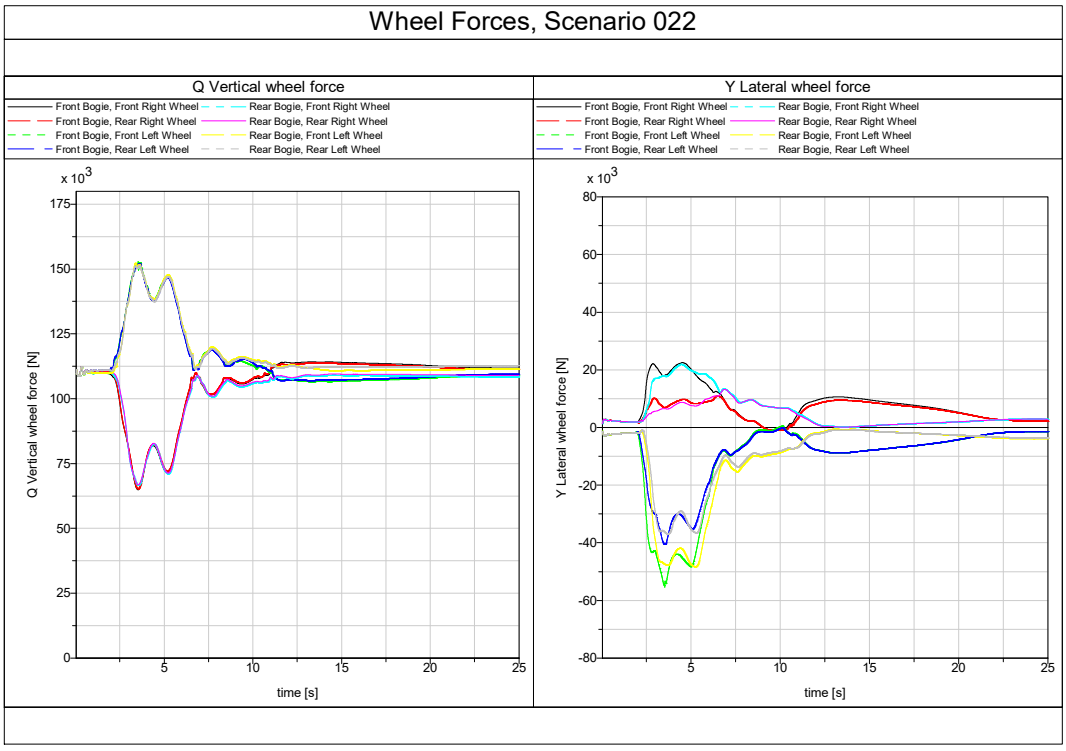

Figure A.22 : Wheel Forces of Scenario 022.

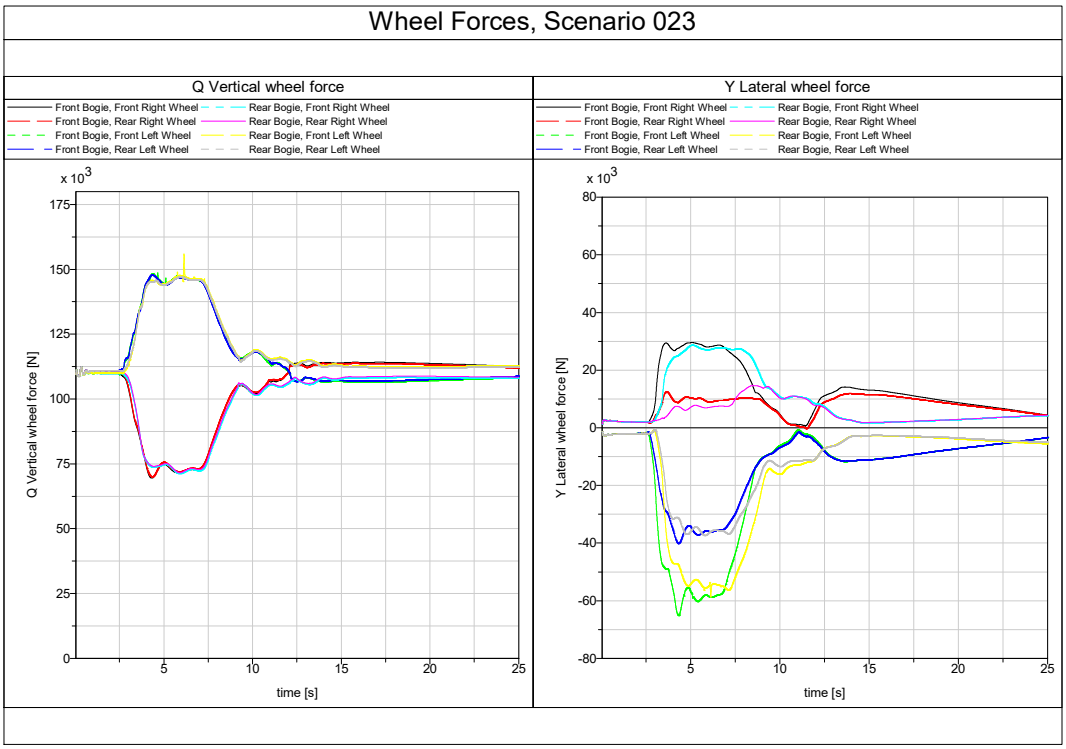

Figure A.23 : Wheel Forces of Scenario 023.

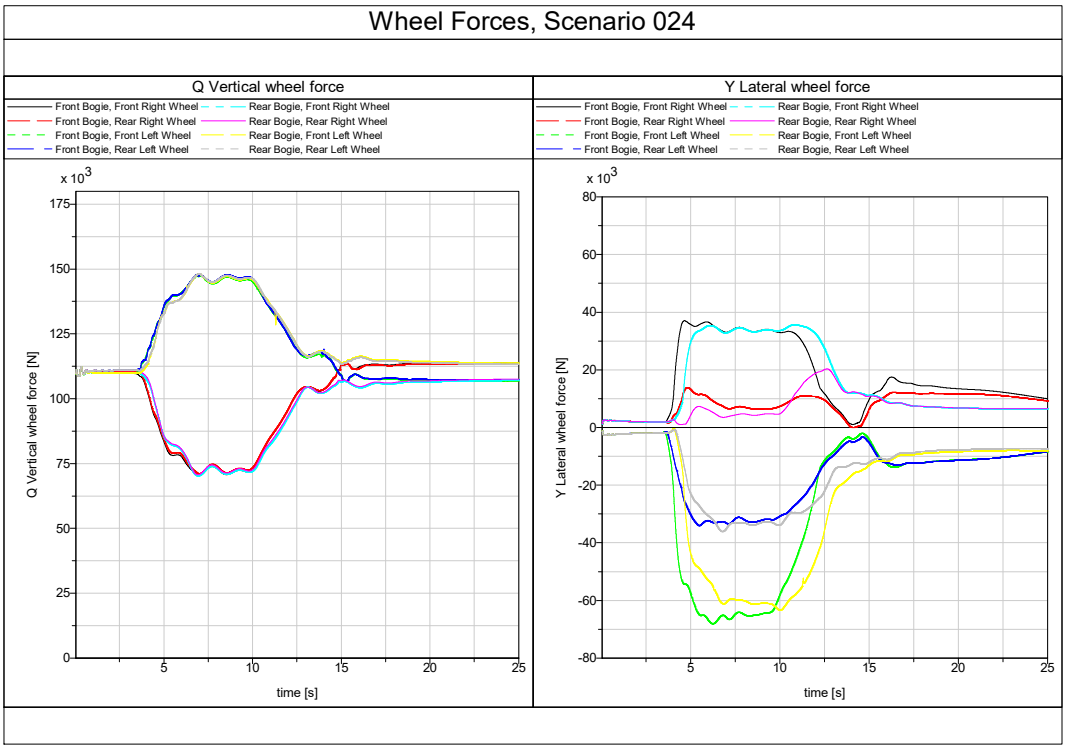

Figure A.24 : Wheel Forces of Scenario 024.

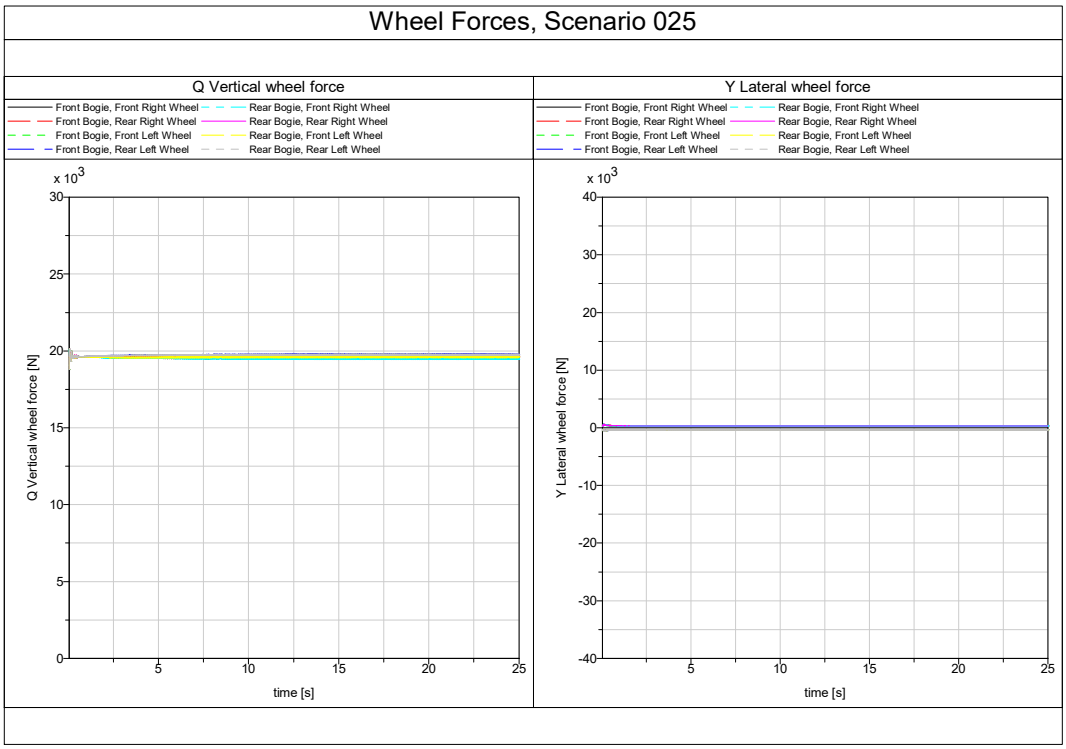

Figure A.25 : Wheel Forces of Scenario 025.

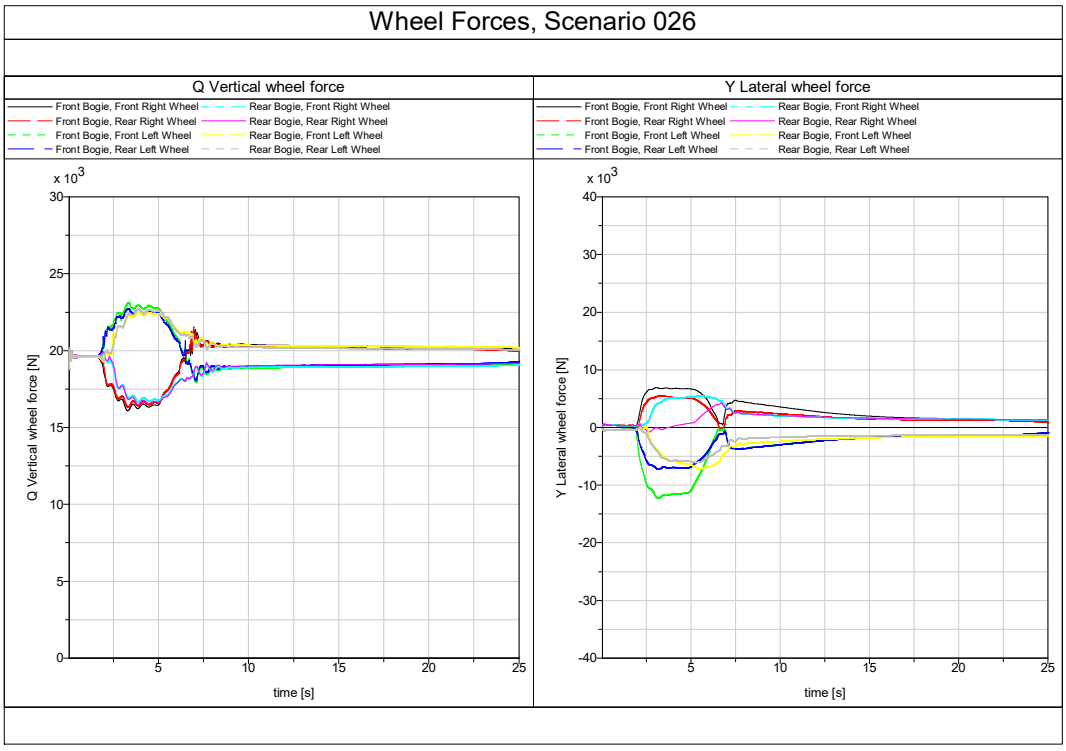

Figure A.26 : Wheel Forces of Scenario 026.

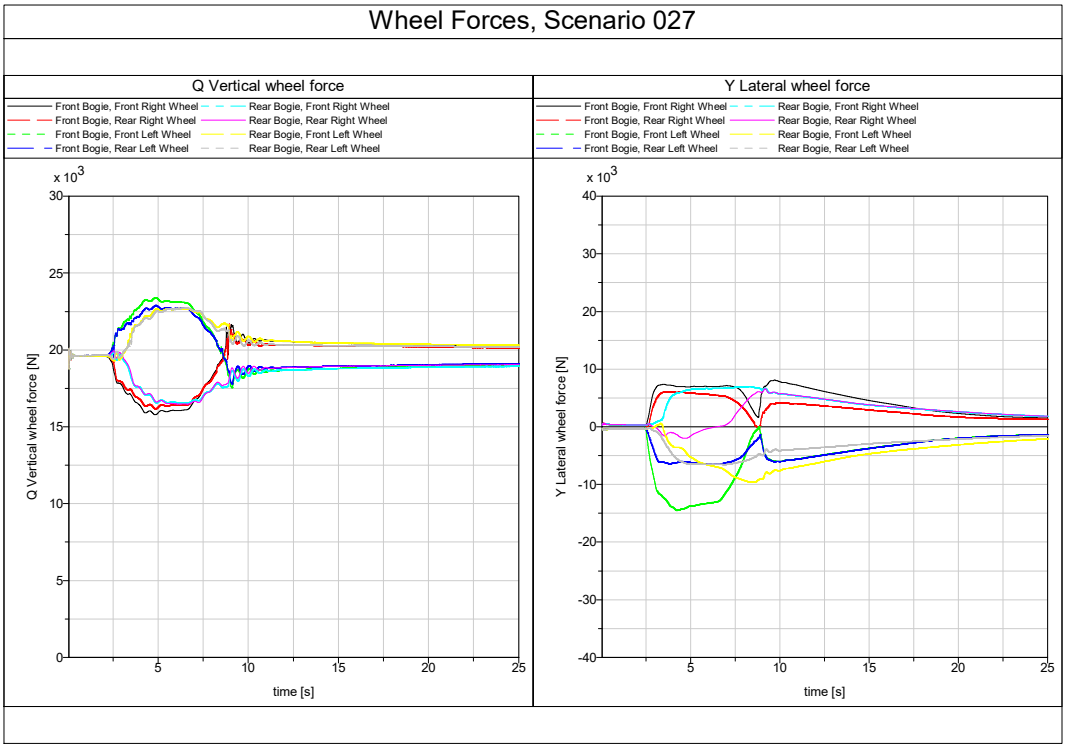

Figure A.27 : Wheel Forces of Scenario 027.

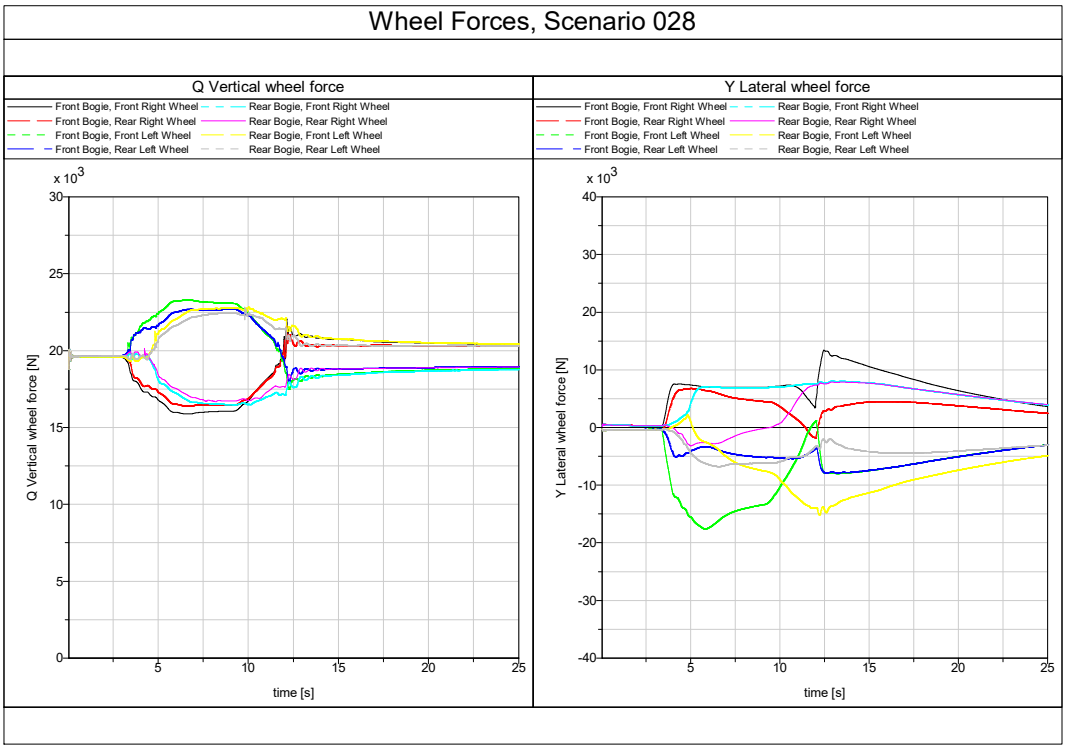

Figure A.28 : Wheel Forces of Scenario 028.

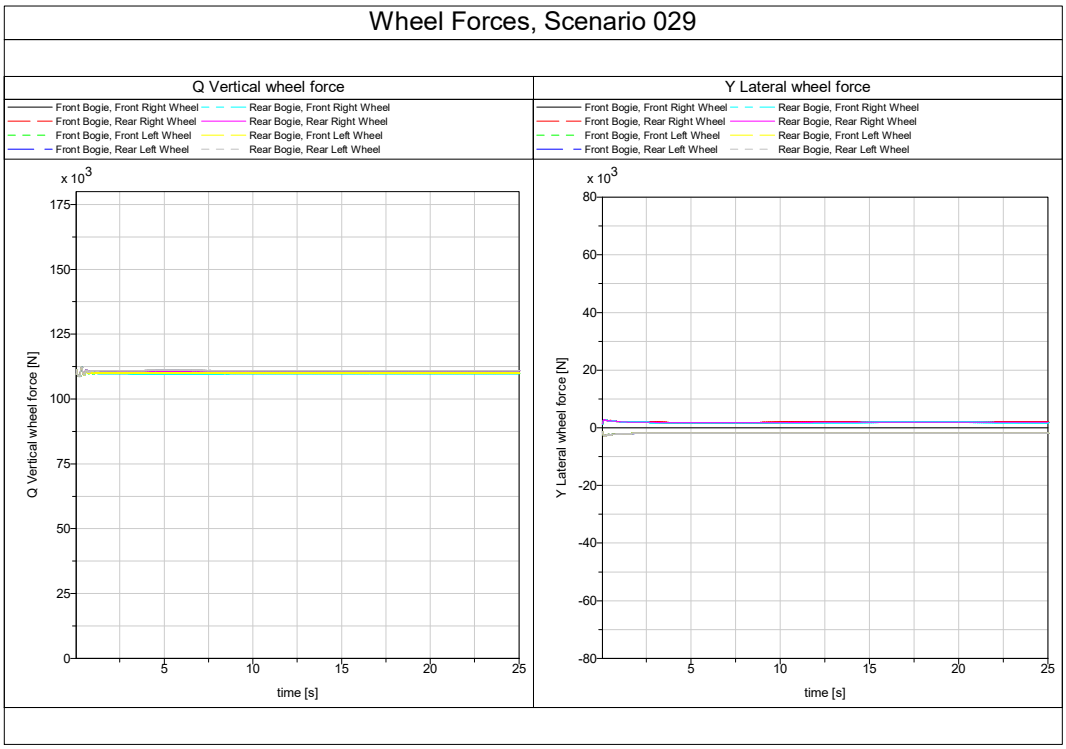

Figure A.29 : Wheel Forces of Scenario 029.

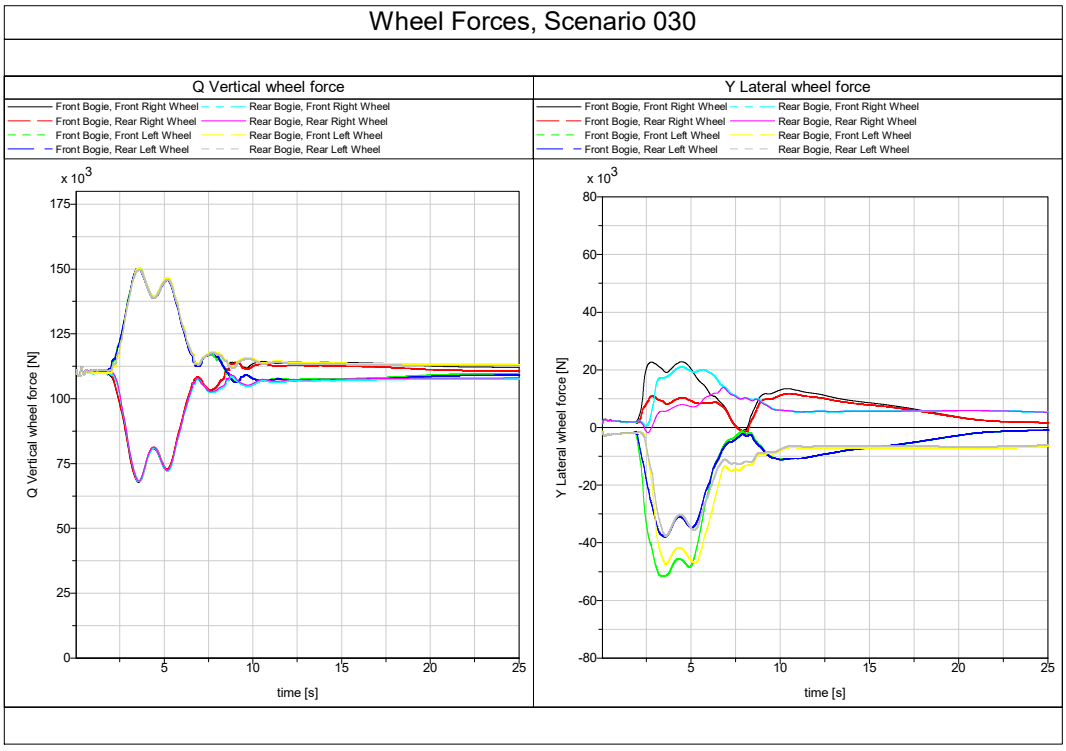

Figure A.30 : Wheel Forces of Scenario 030.

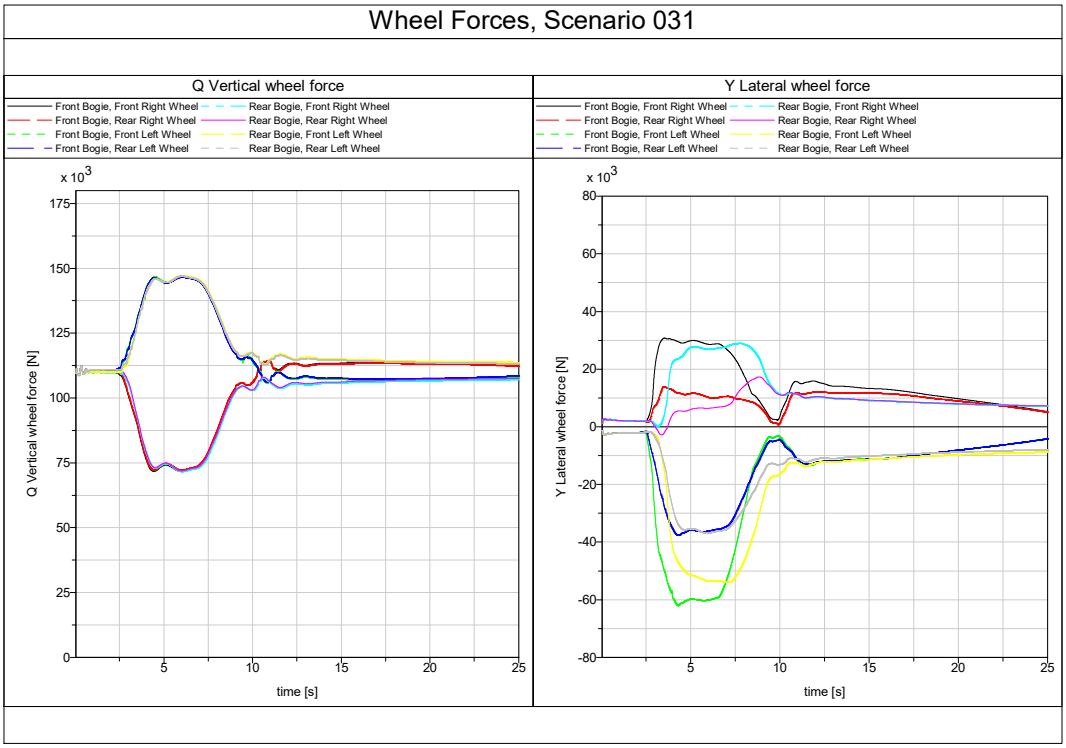

Figure A.31 : Wheel Forces of Scenario 031.

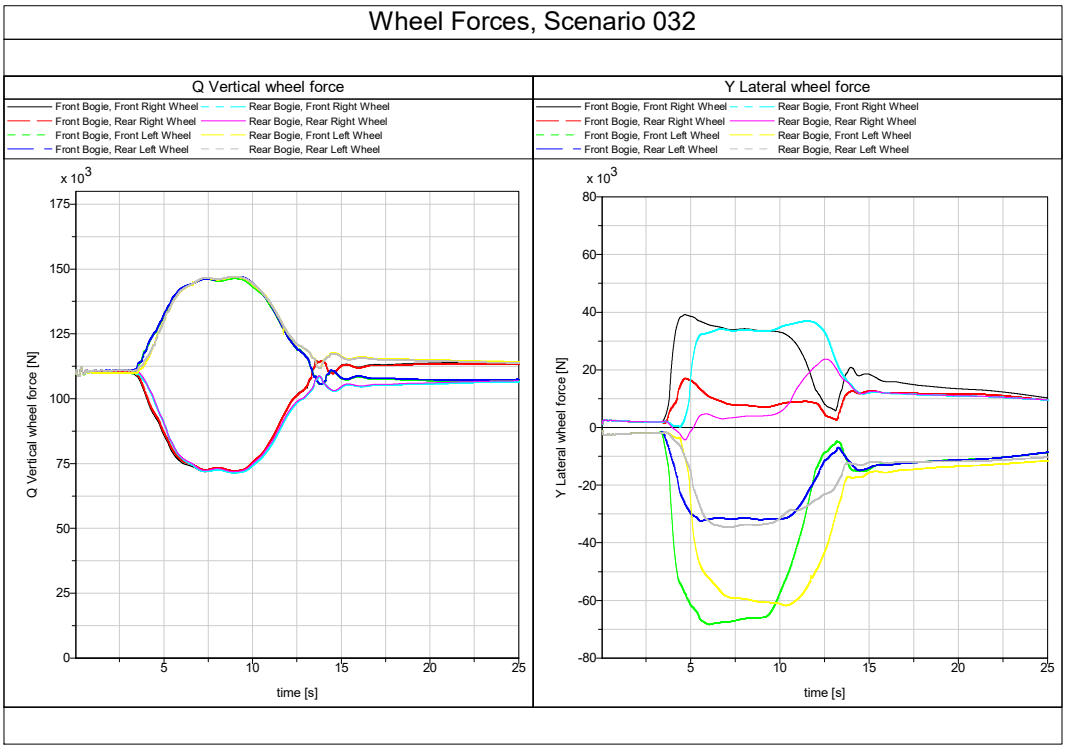

Figure A.32 : Wheel Forces of Scenario 032.

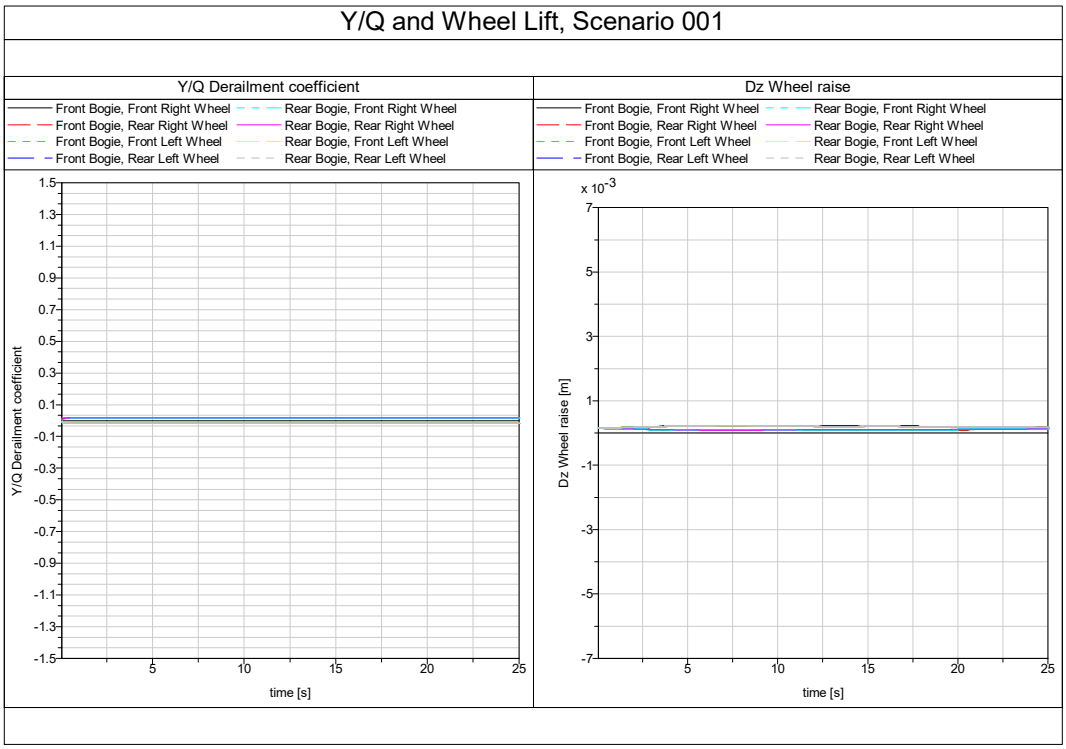

Figure A.33 : Y/Q and Wheel Lift for Scenario 001.

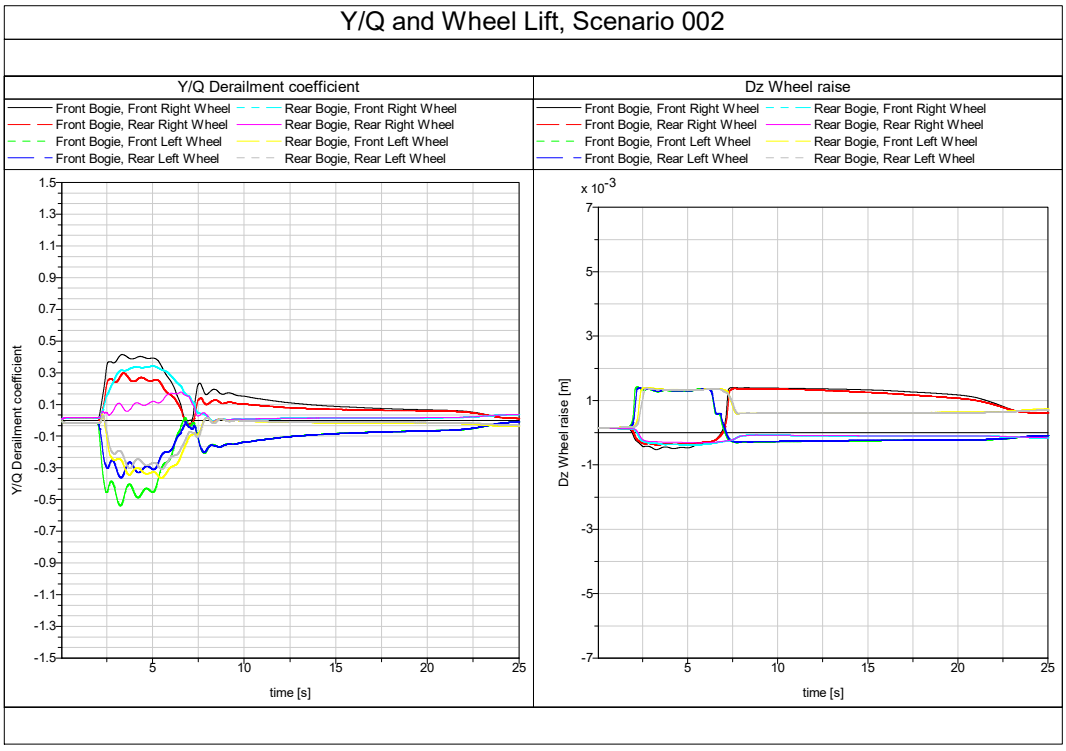

Figure A.34 : Y/Q and Wheel Lift for Scenario 002.

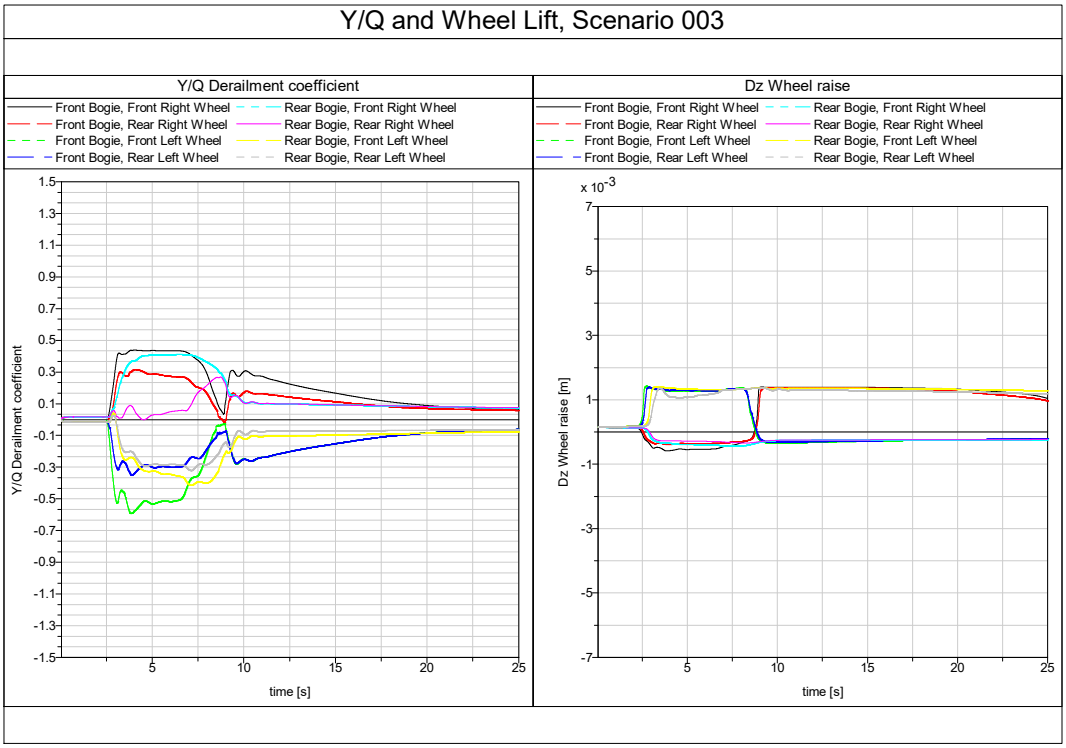

Figure A.35 : Y/Q and Wheel Lift for Scenario 003.

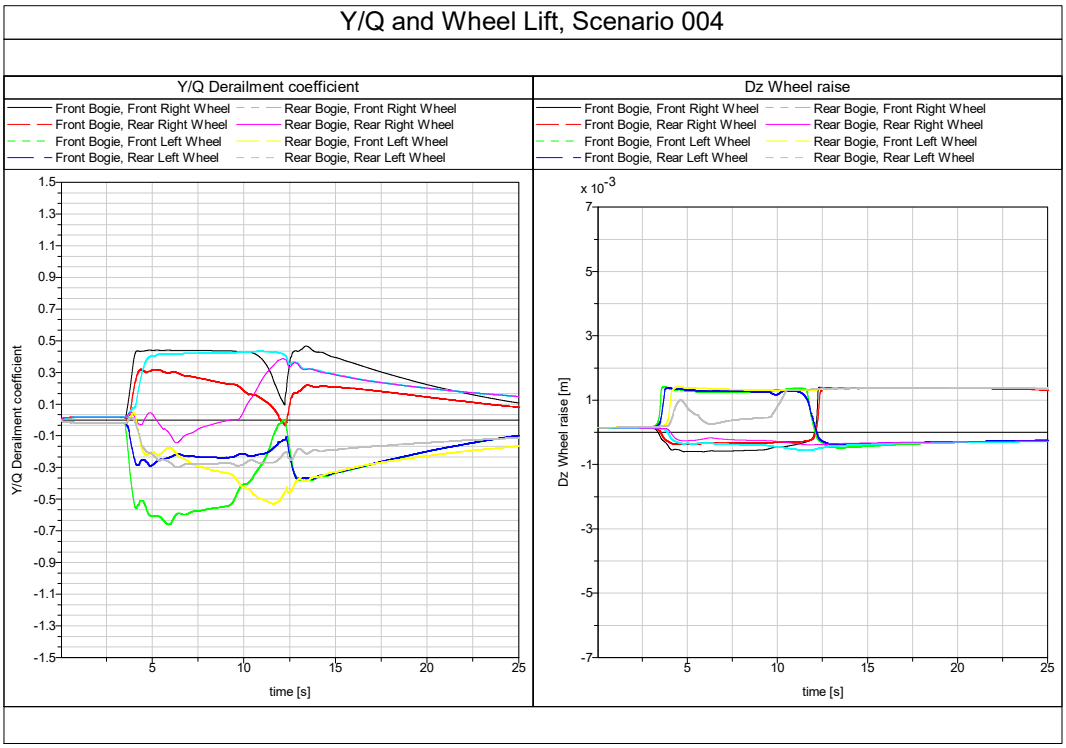

Figure A.36 : Y/Q and Wheel Lift for Scenario 004.

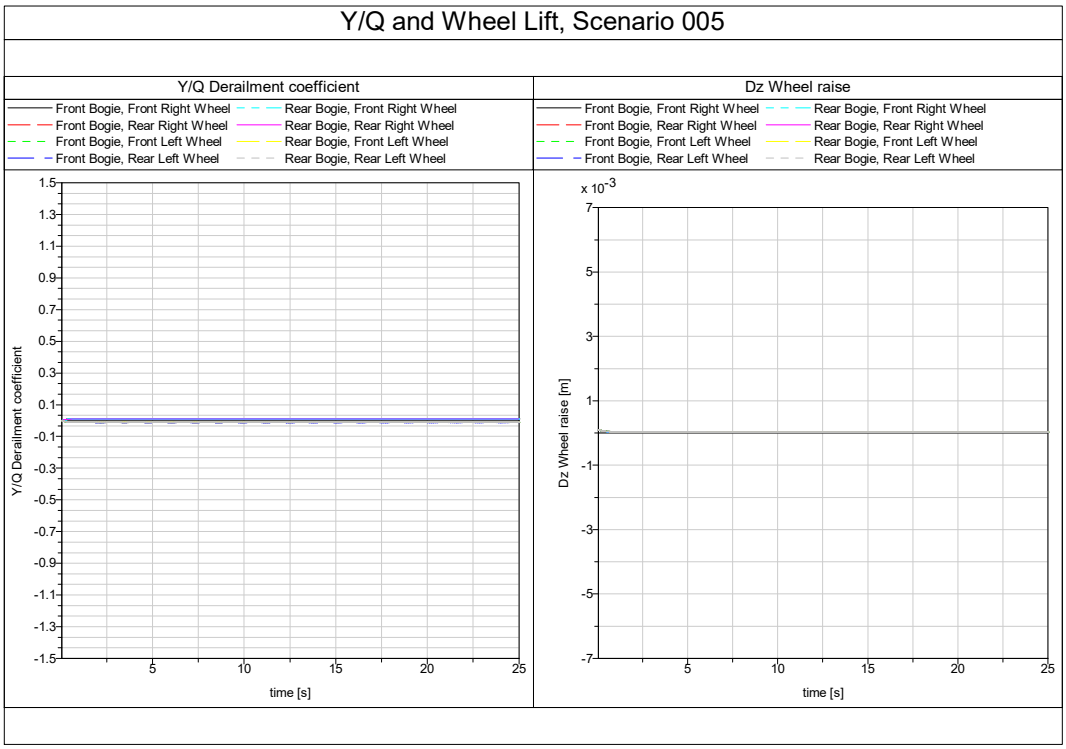

Figure A.37 : Y/Q and Wheel Lift for Scenario 005.

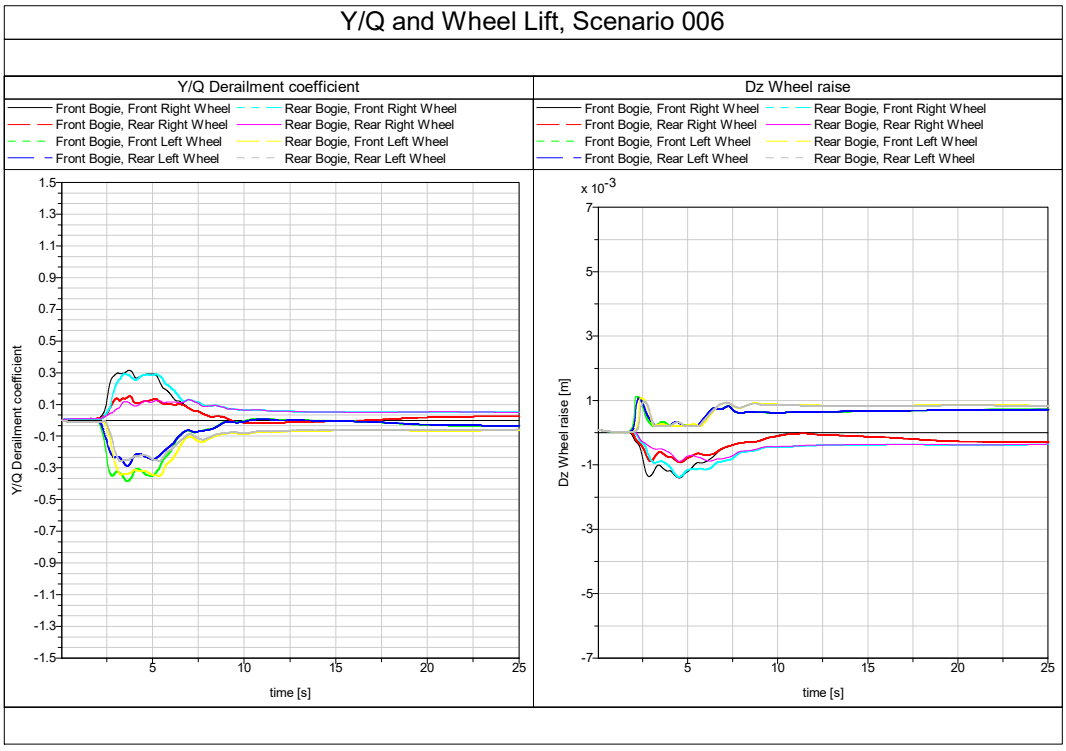

Figure A.38 : Y/Q and Wheel Lift for Scenario 006.

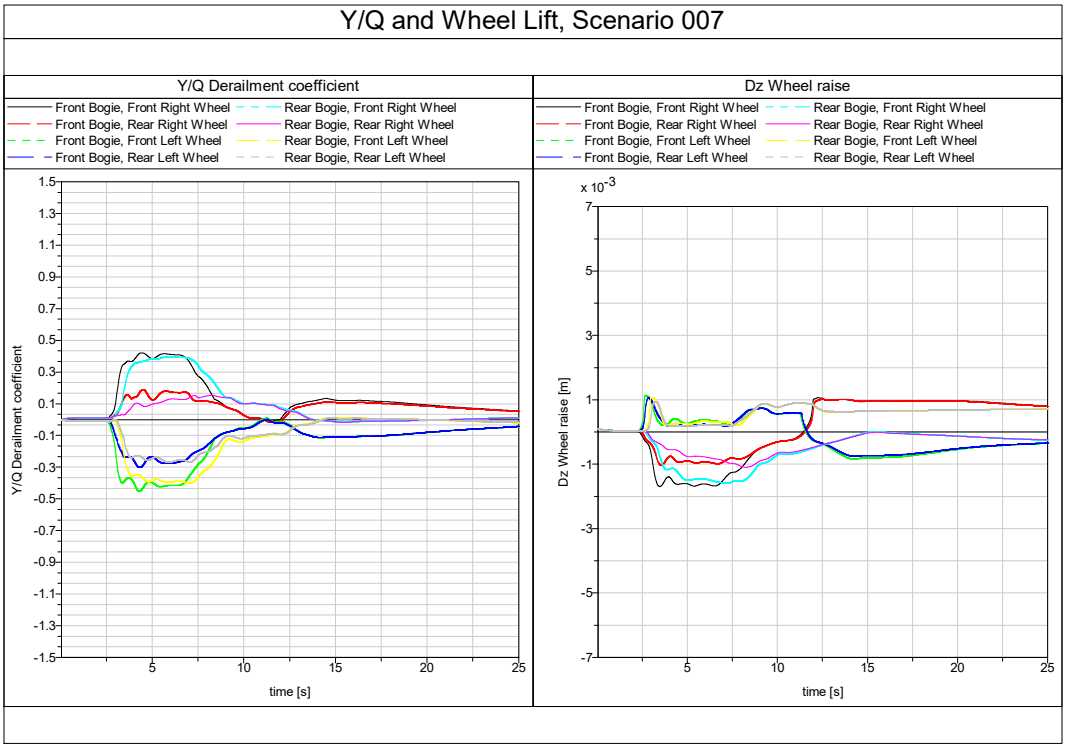

Figure A.39 : Y/Q and Wheel Lift for Scenario 007.

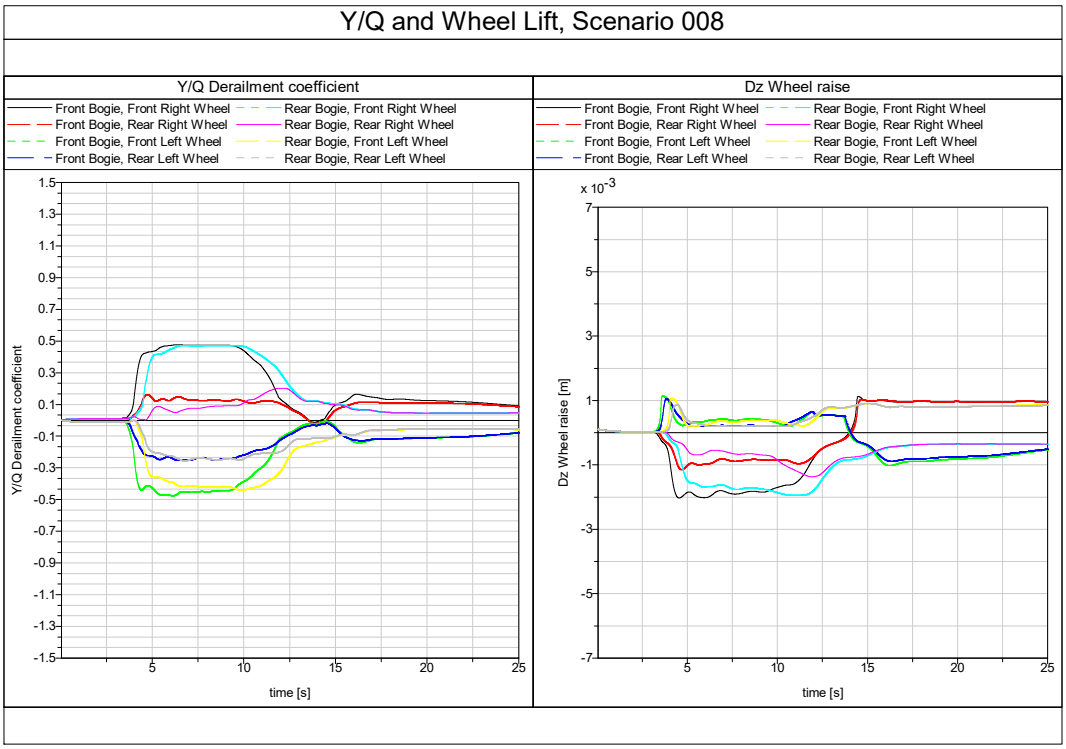

Figure A.40 : Y/Q and Wheel Lift for Scenario 008.

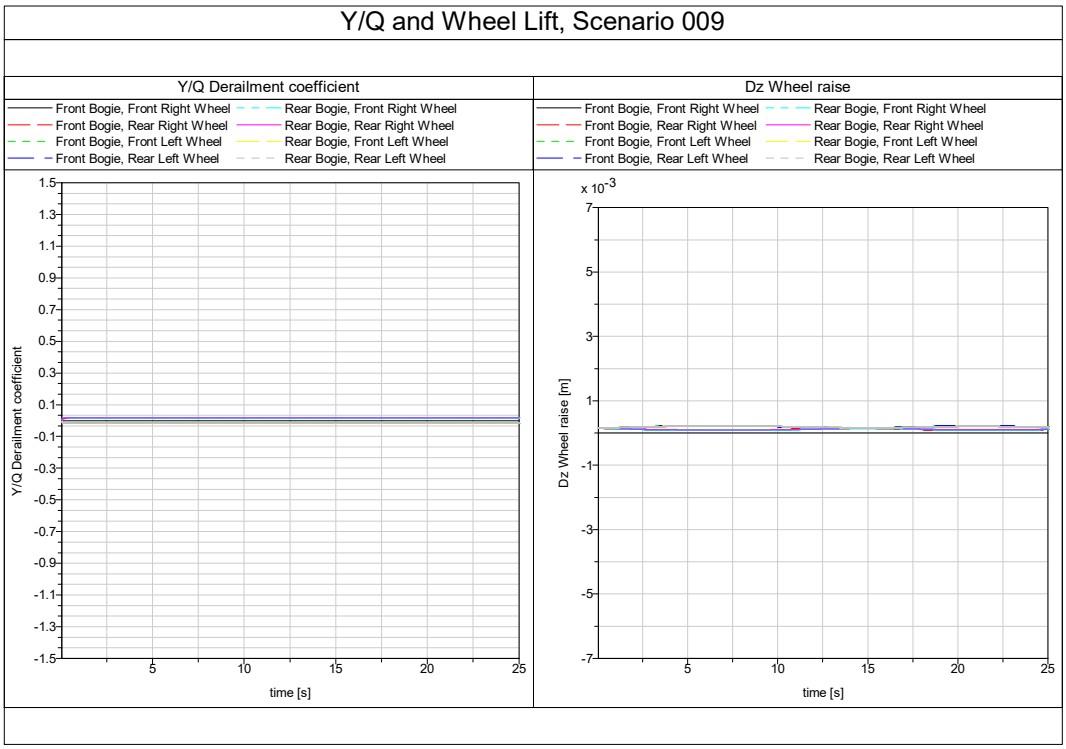

Figure A.41 : Y/Q and Wheel Lift for Scenario 009.

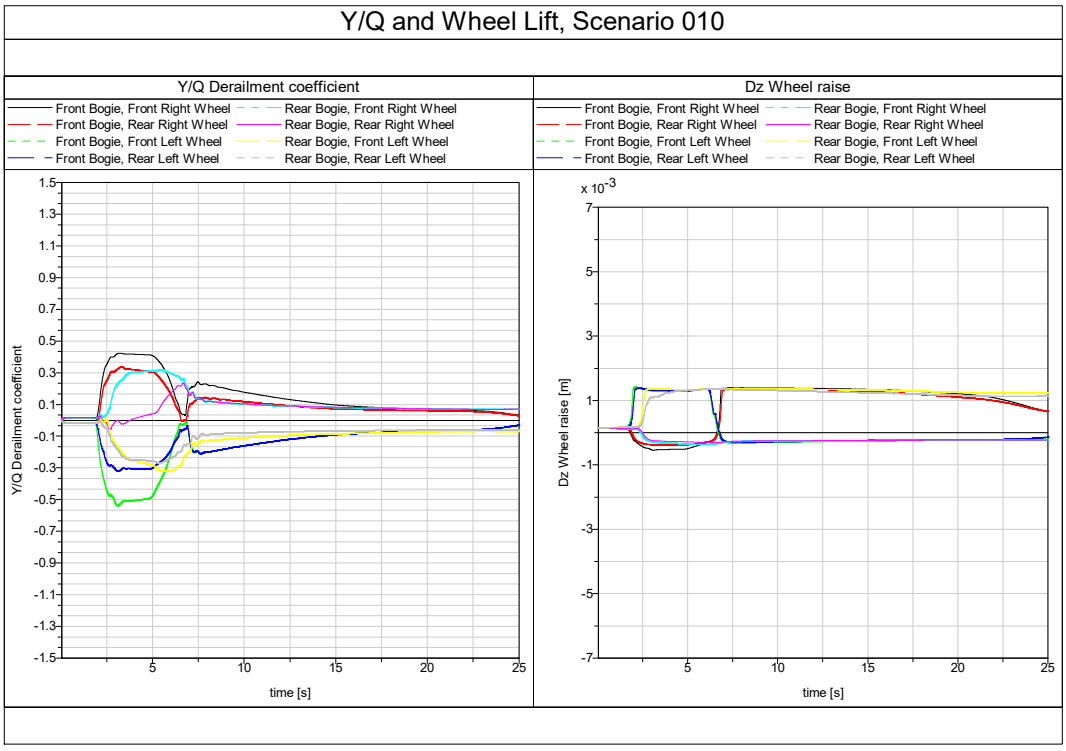

Figure A.42 : Y/Q and Wheel Lift for Scenario 010.

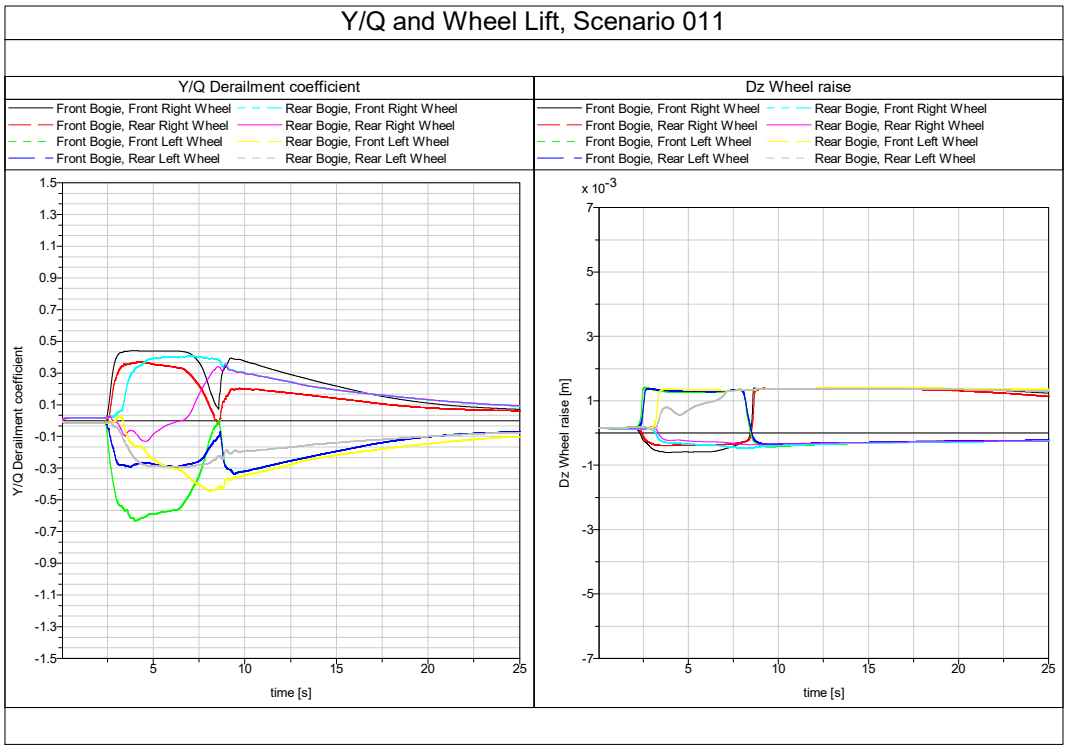

Figure A.43 : Y/Q and Wheel Lift for Scenario 011.

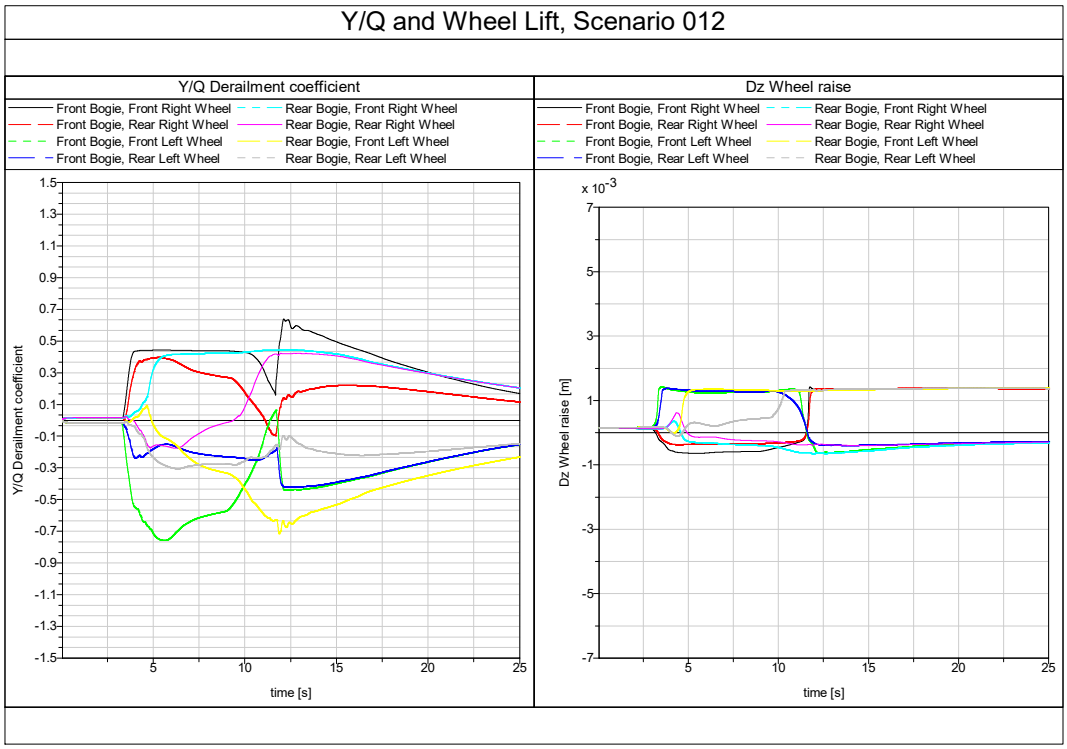

Figure A.44 : Y/Q and Wheel Lift for Scenario 012.

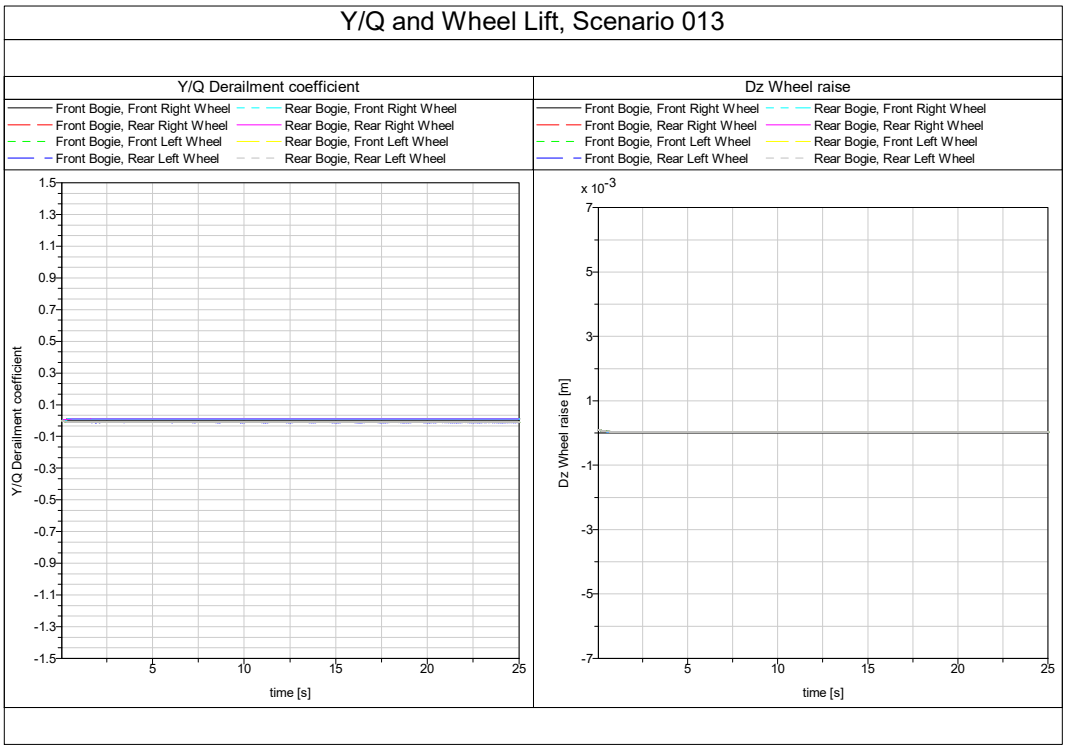

Figure A.45 : Y/Q and Wheel Lift for Scenario 013.

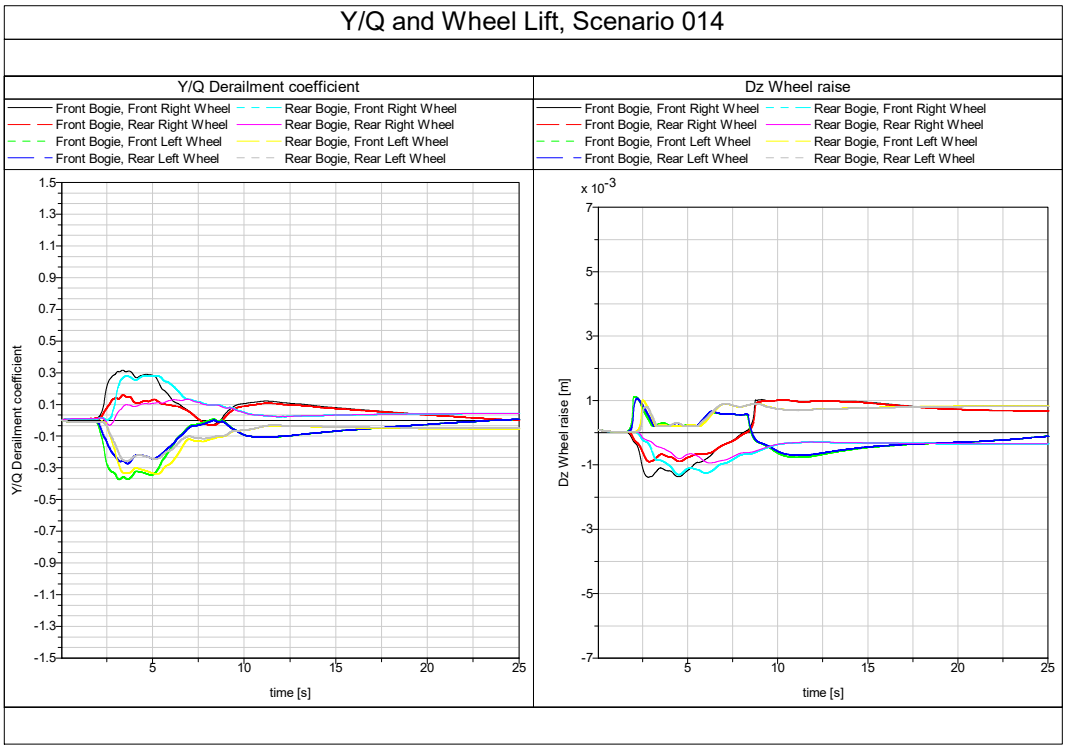

Figure A.46 : Y/Q and Wheel Lift for Scenario 014.

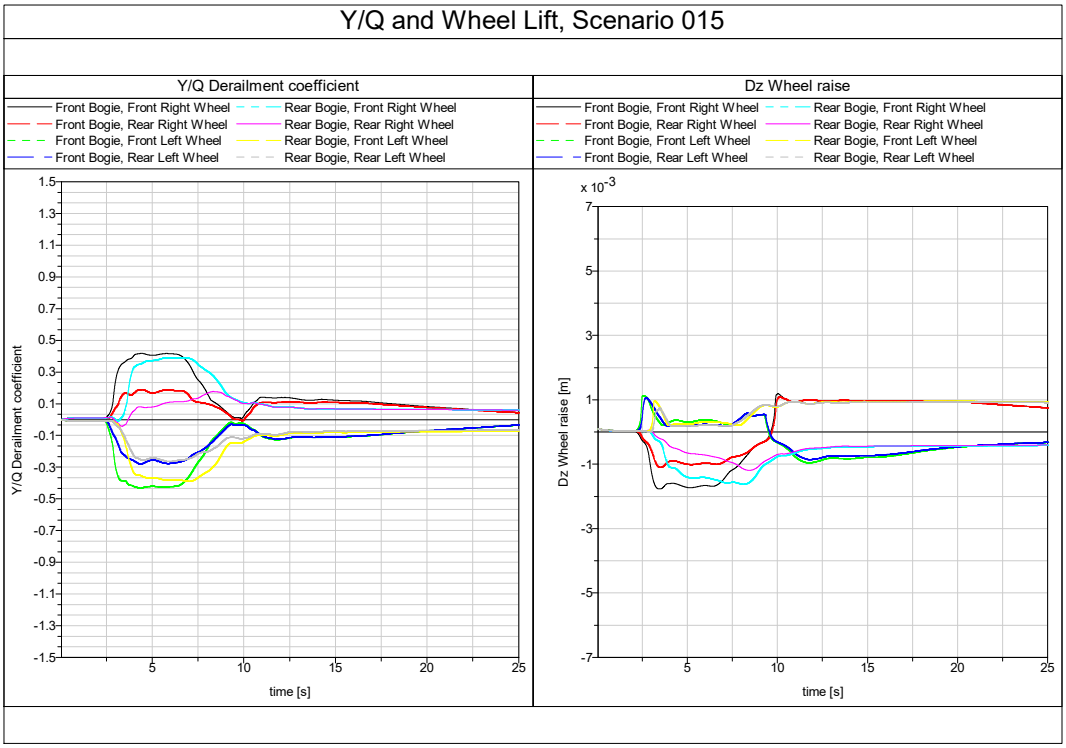

Figure A.47 : Y/Q and Wheel Lift for Scenario 015.

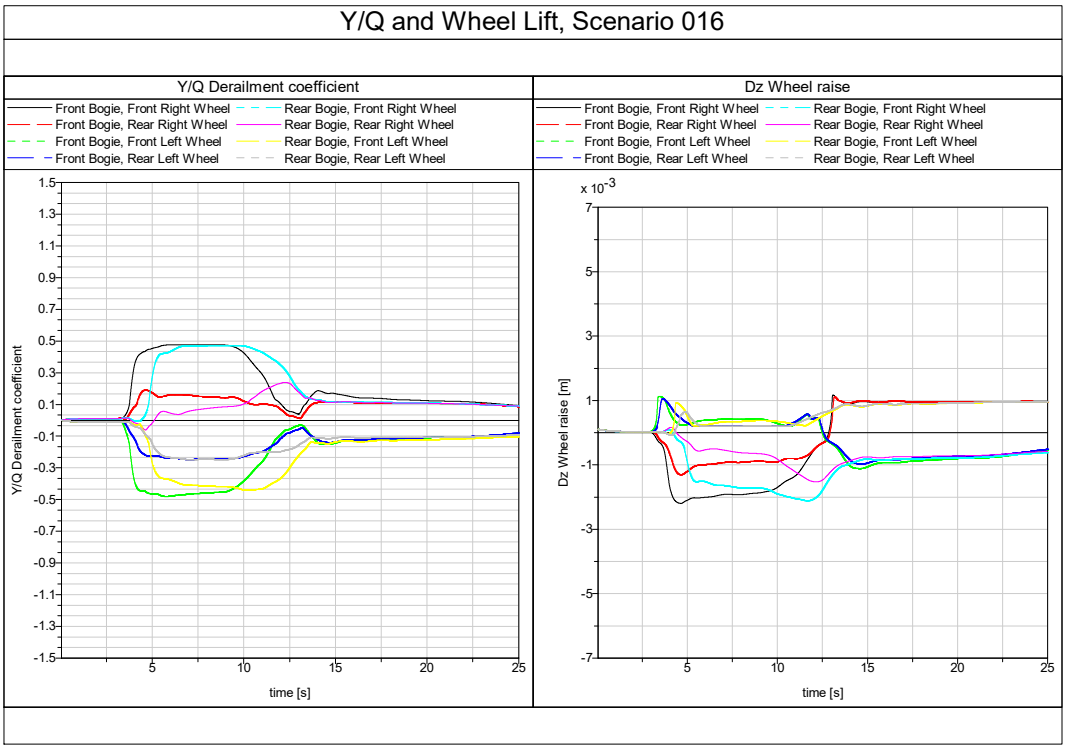

Figure A.48 : Y/Q and Wheel Lift for Scenario 016.

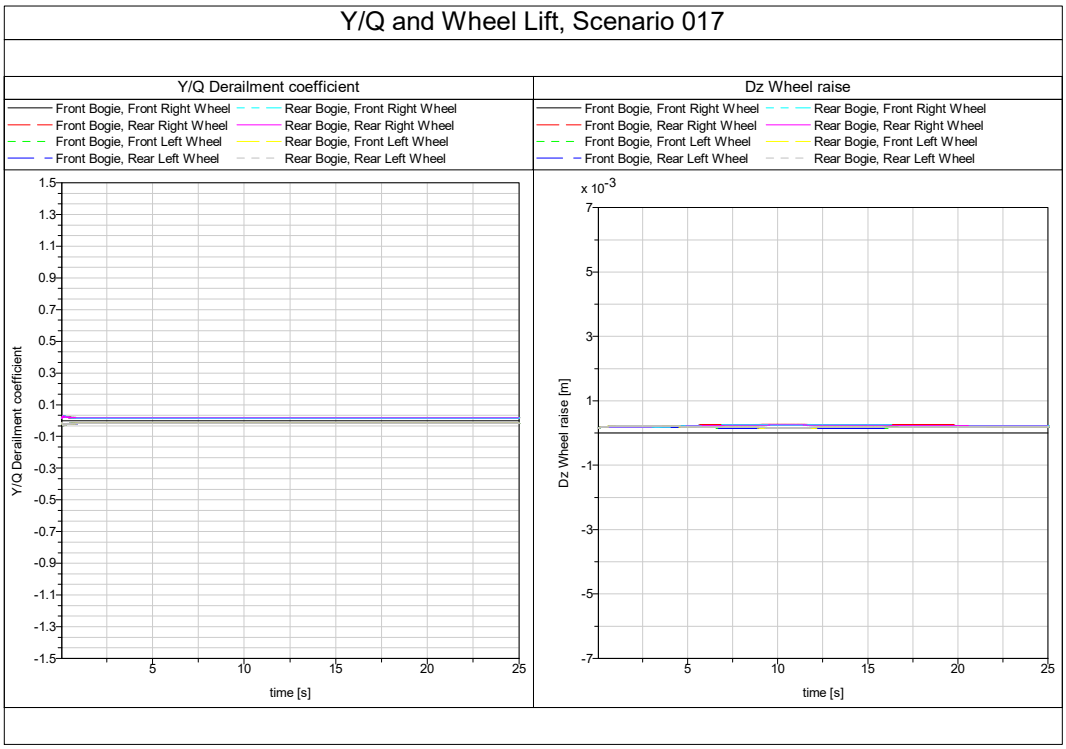

Figure A.49 : Y/Q and Wheel Lift for Scenario 017.

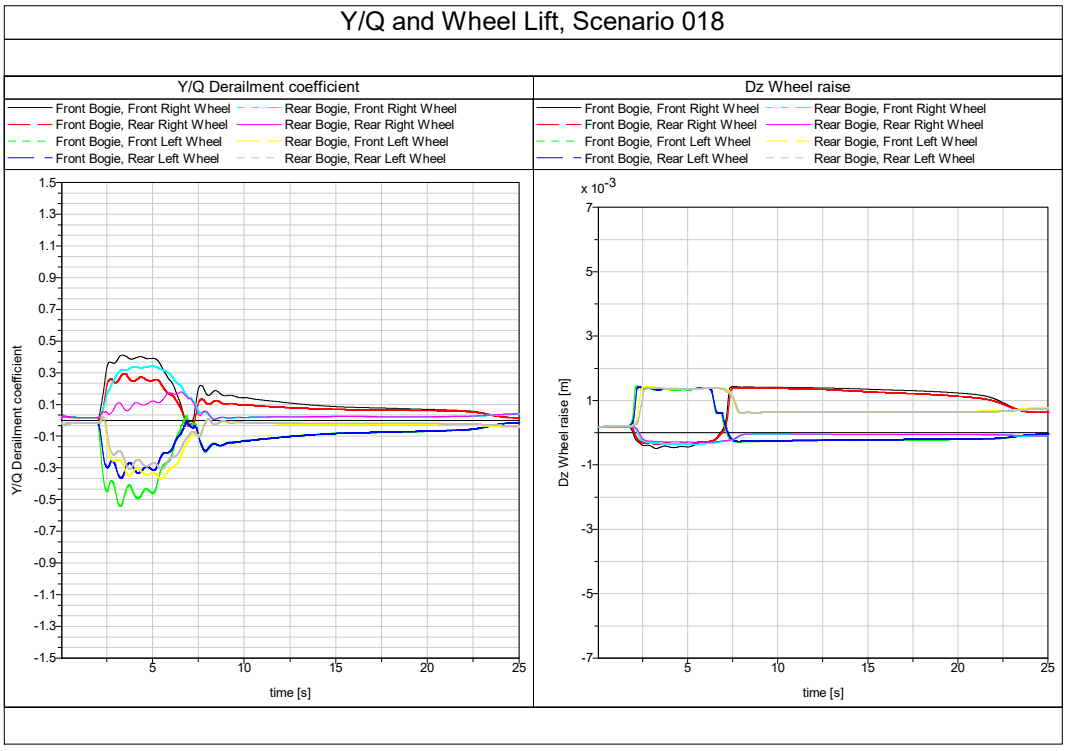

Figure A.50 : Y/Q and Wheel Lift for Scenario 018.

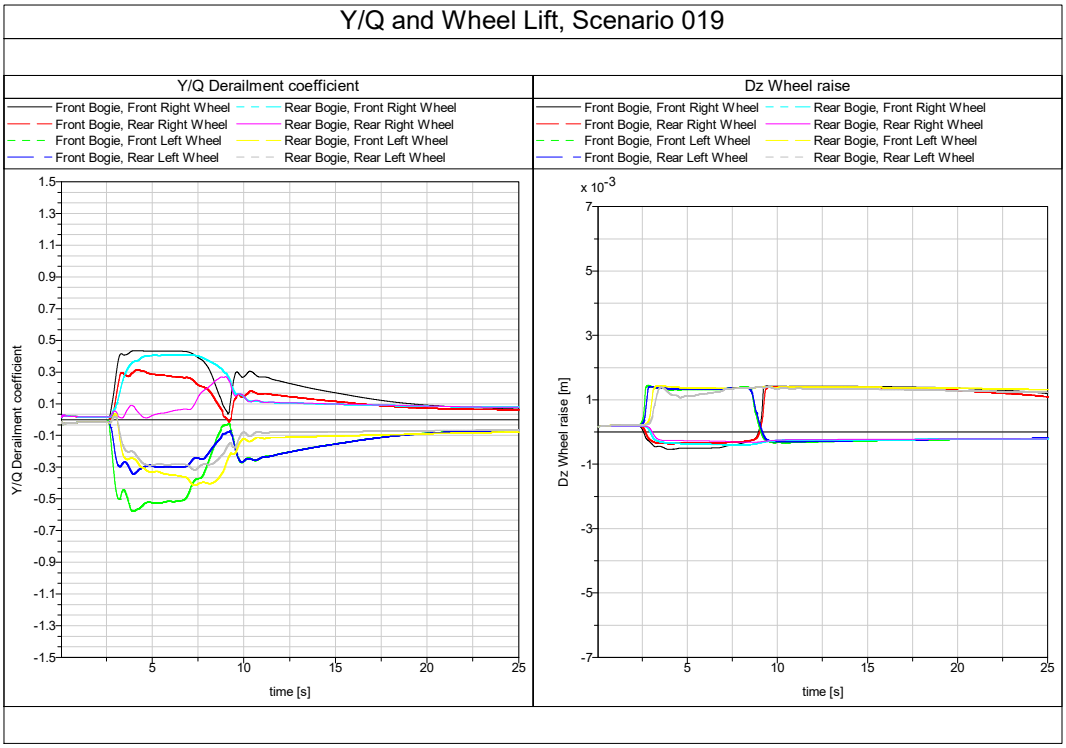

Figure A.51 : Y/Q and Wheel Lift for Scenario 019.

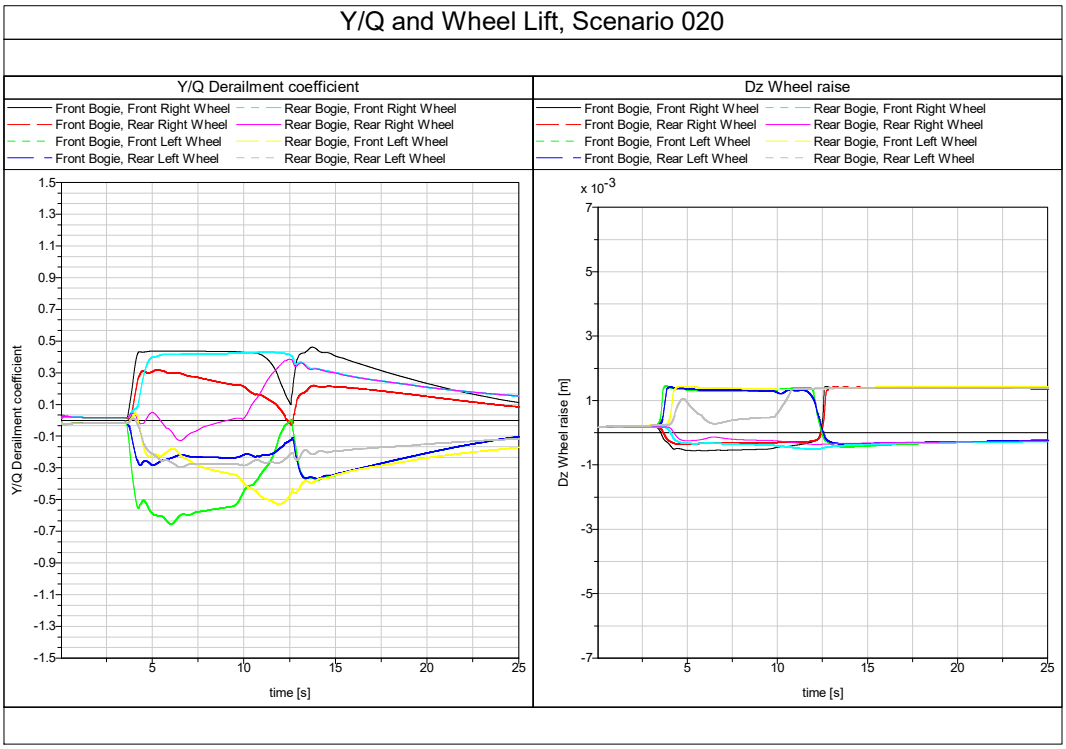

Figure A.52 : Y/Q and Wheel Lift for Scenario 020.

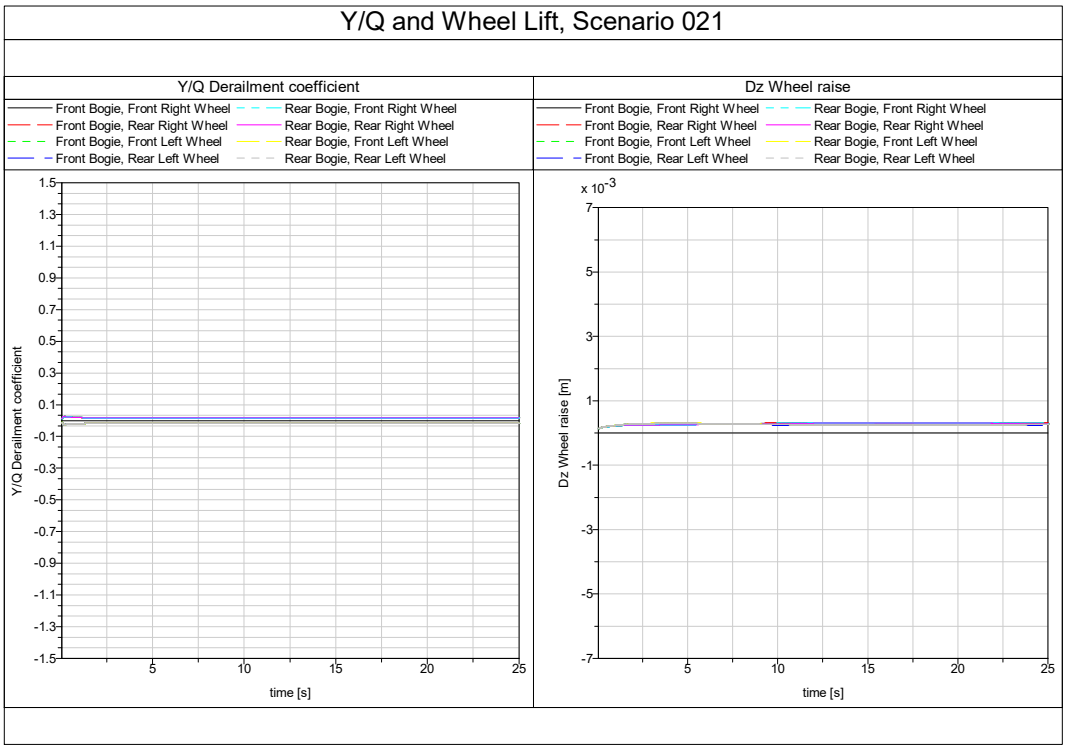

Figure A.53 : Y/Q and Wheel Lift for Scenario 021.

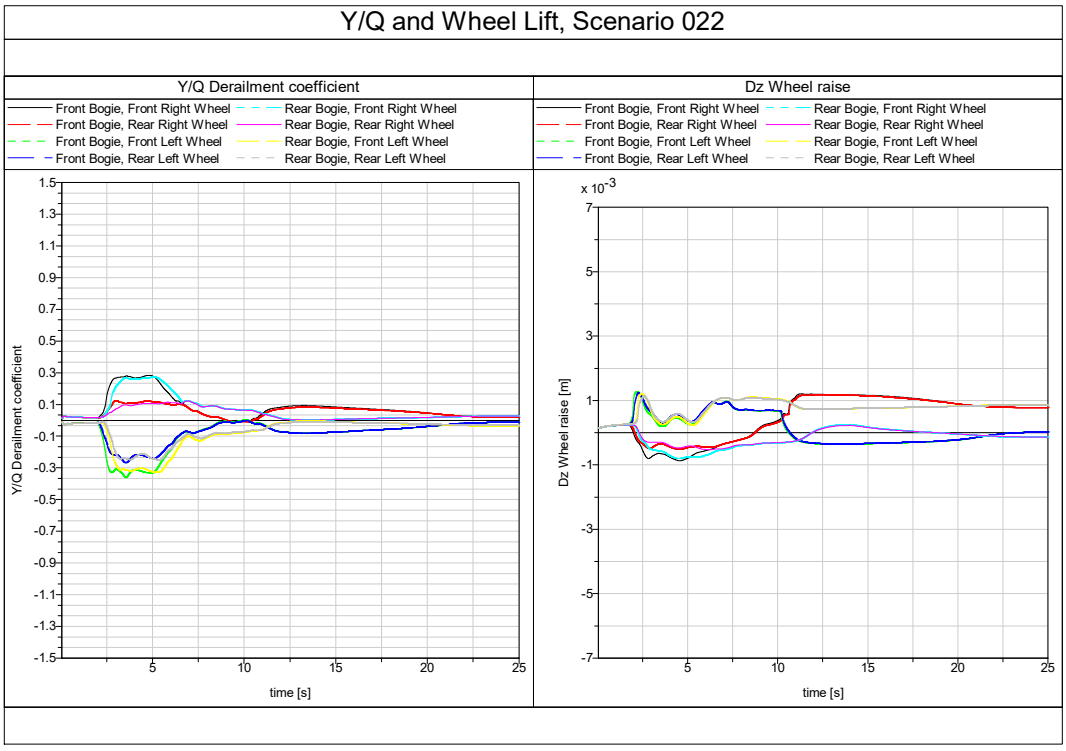

Figure A.54 : Y/Q and Wheel Lift for Scenario 022.

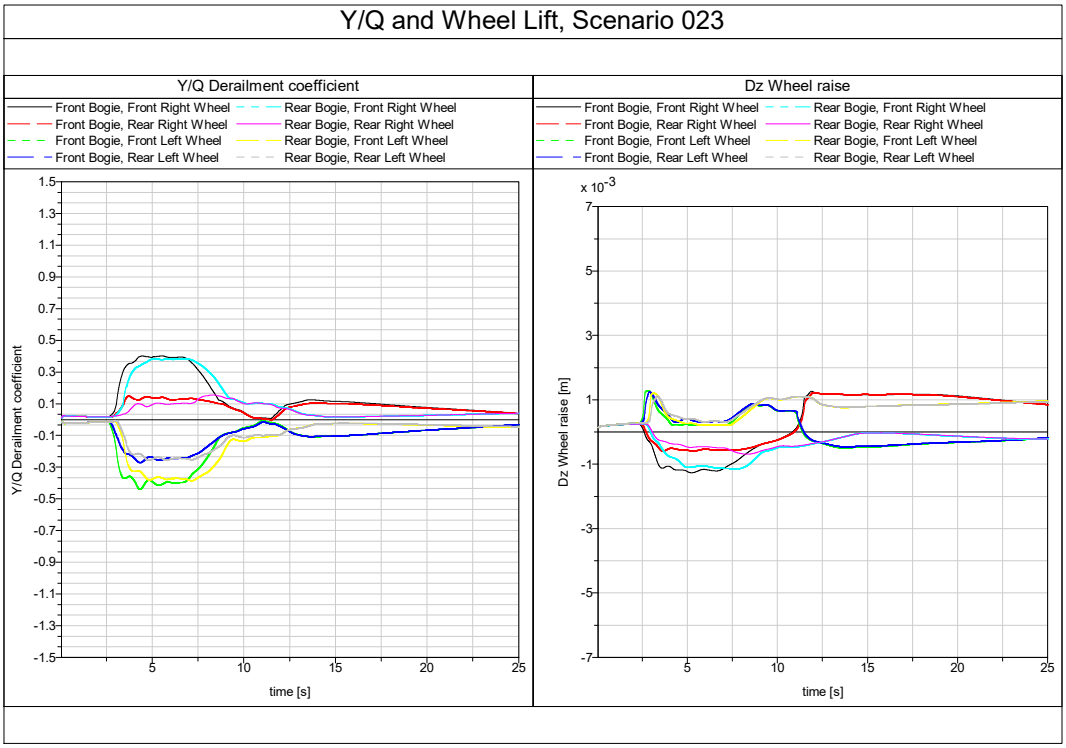

Figure A.55 : Y/Q and Wheel Lift for Scenario 023.

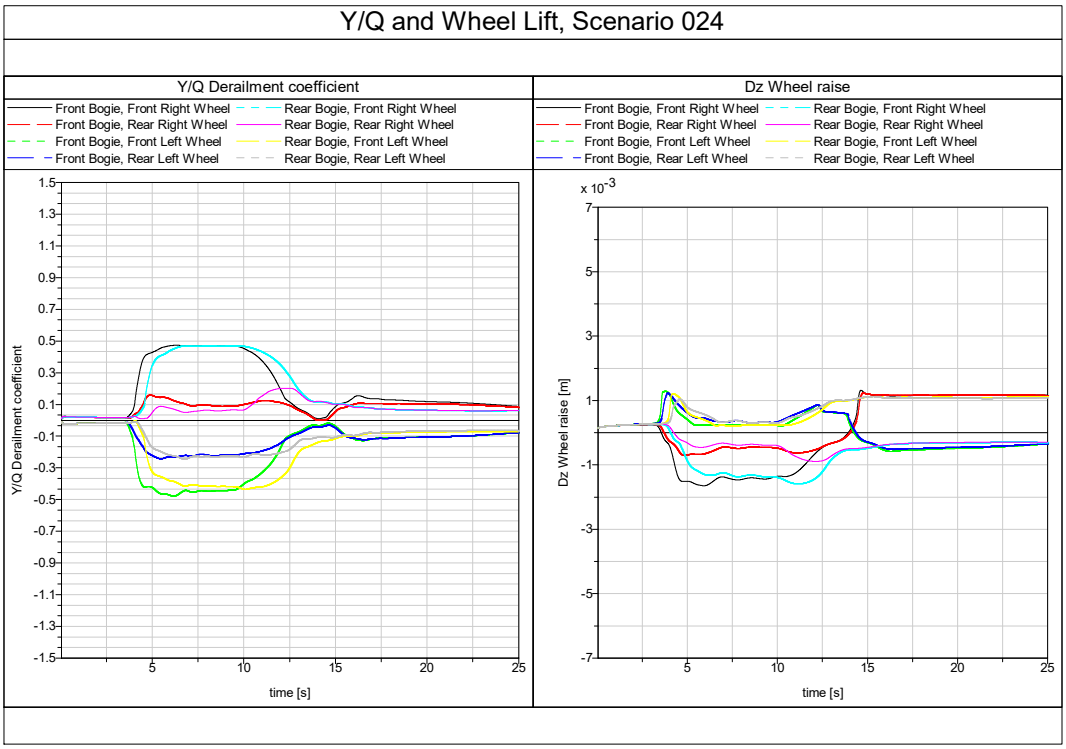

Figure A.56 : Y/Q and Wheel Lift for Scenario 024.

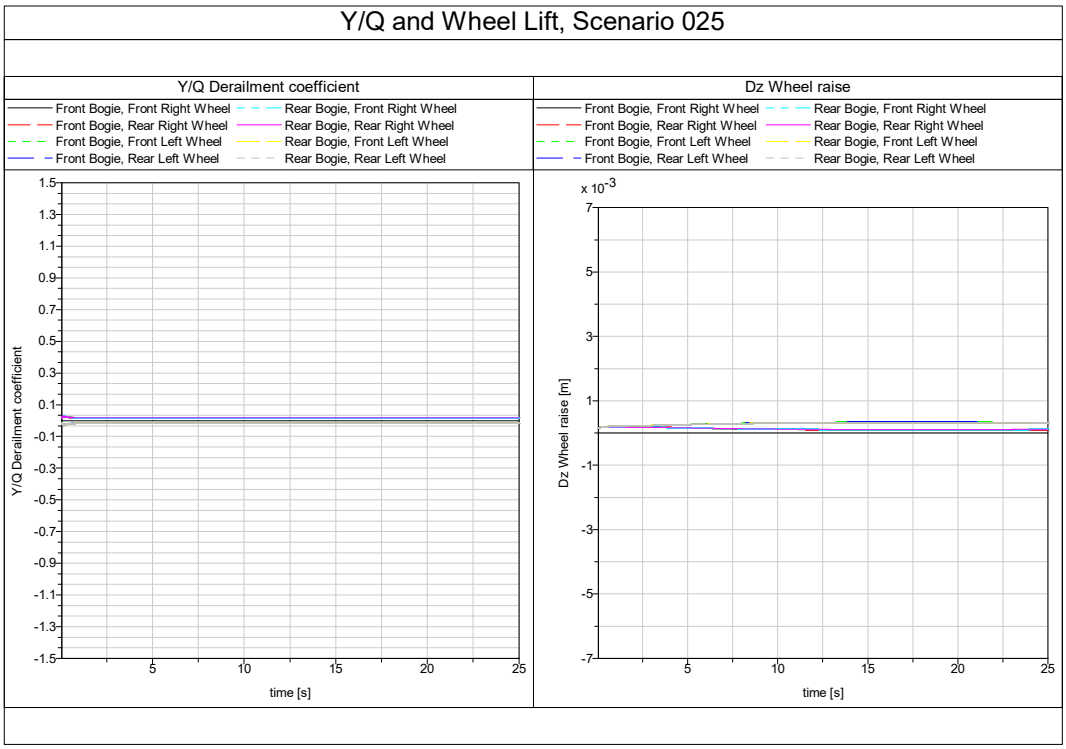

Figure A.57 : Y/Q and Wheel Lift for Scenario 025.

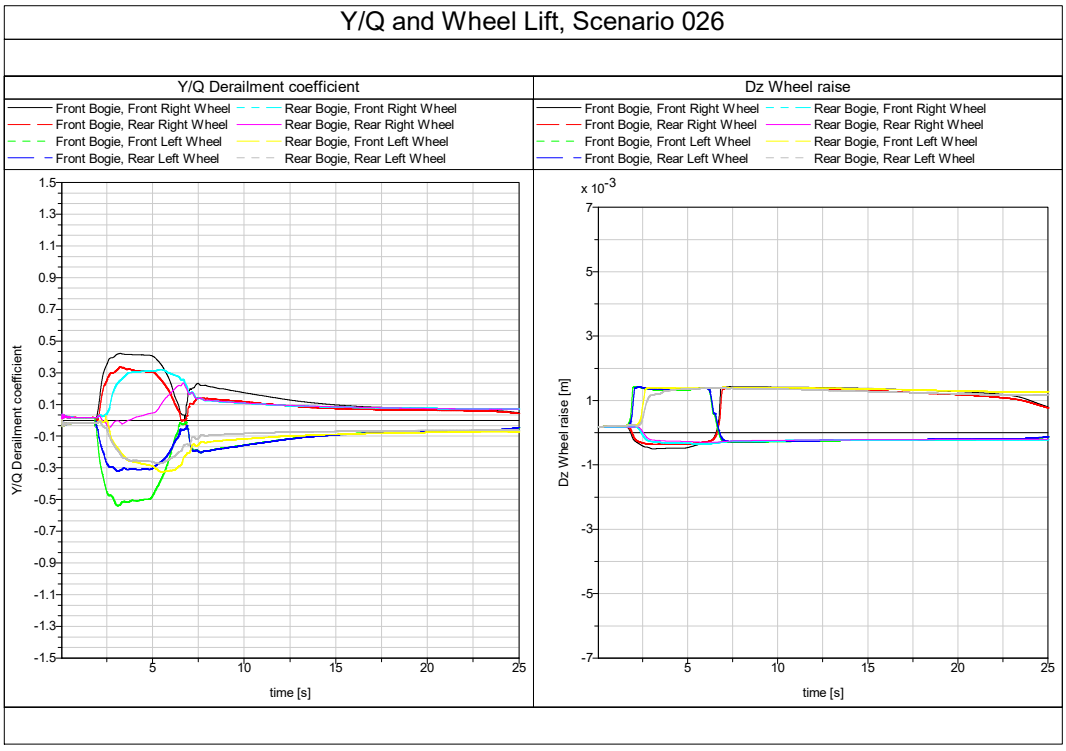

Figure A.58 : Y/Q and Wheel Lift for Scenario 026.

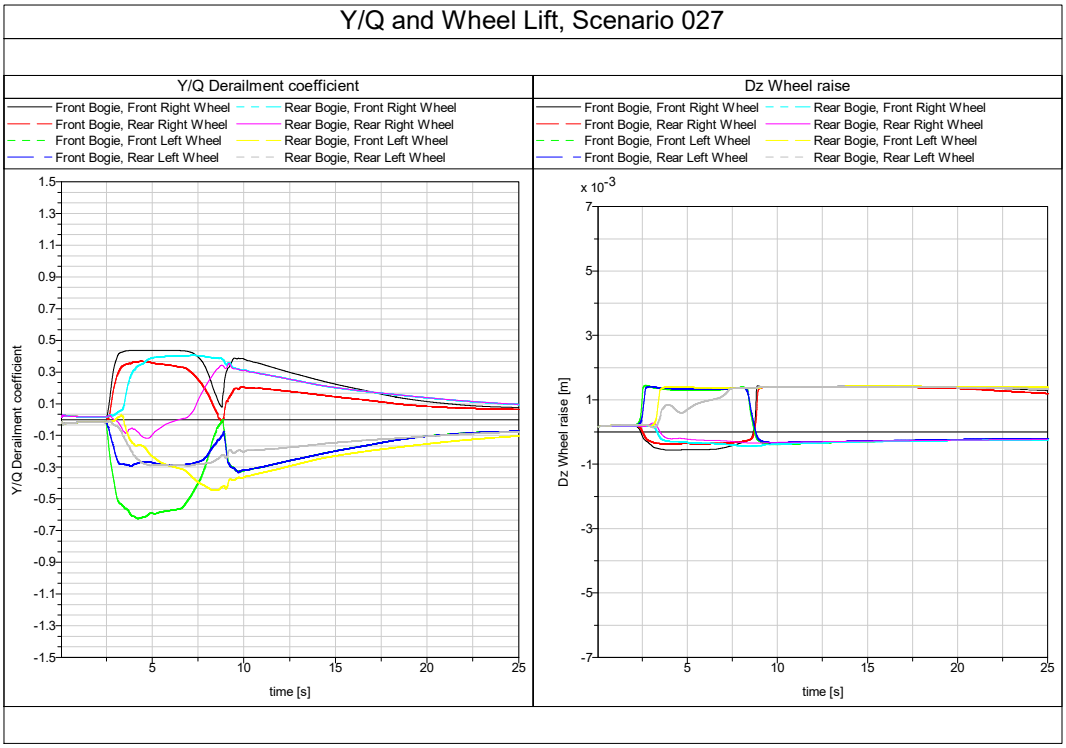

Figure A.59 : Y/Q and Wheel Lift for Scenario 027.

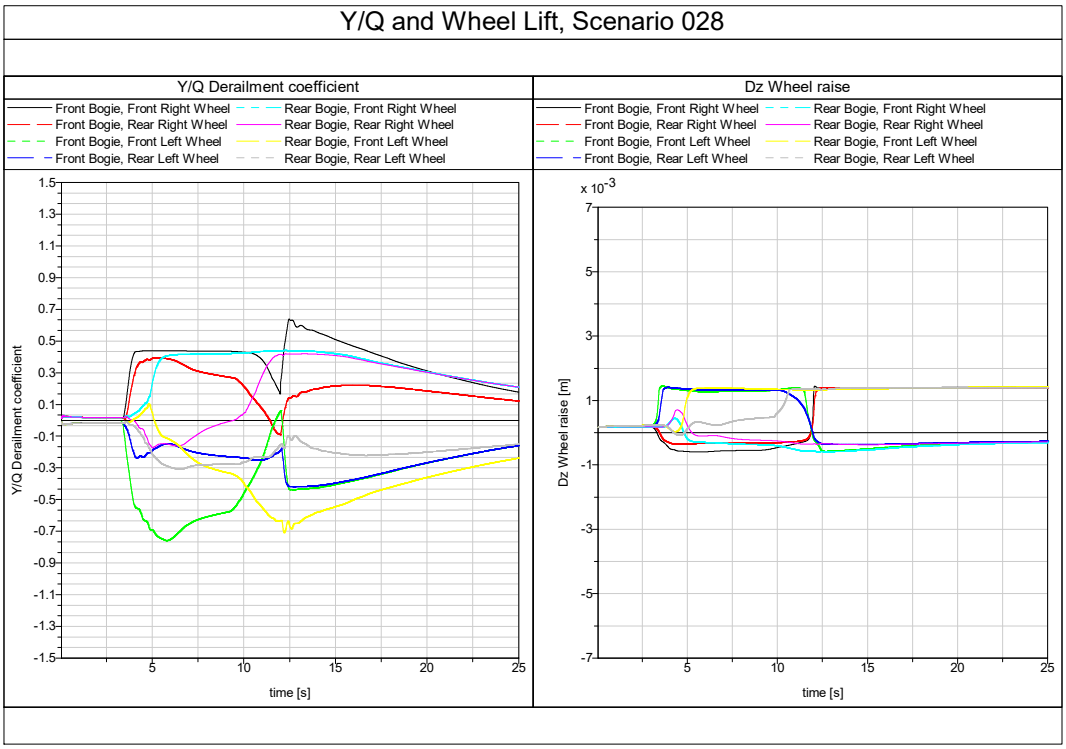

Figure A.60 : Y/Q and Wheel Lift for Scenario 028.

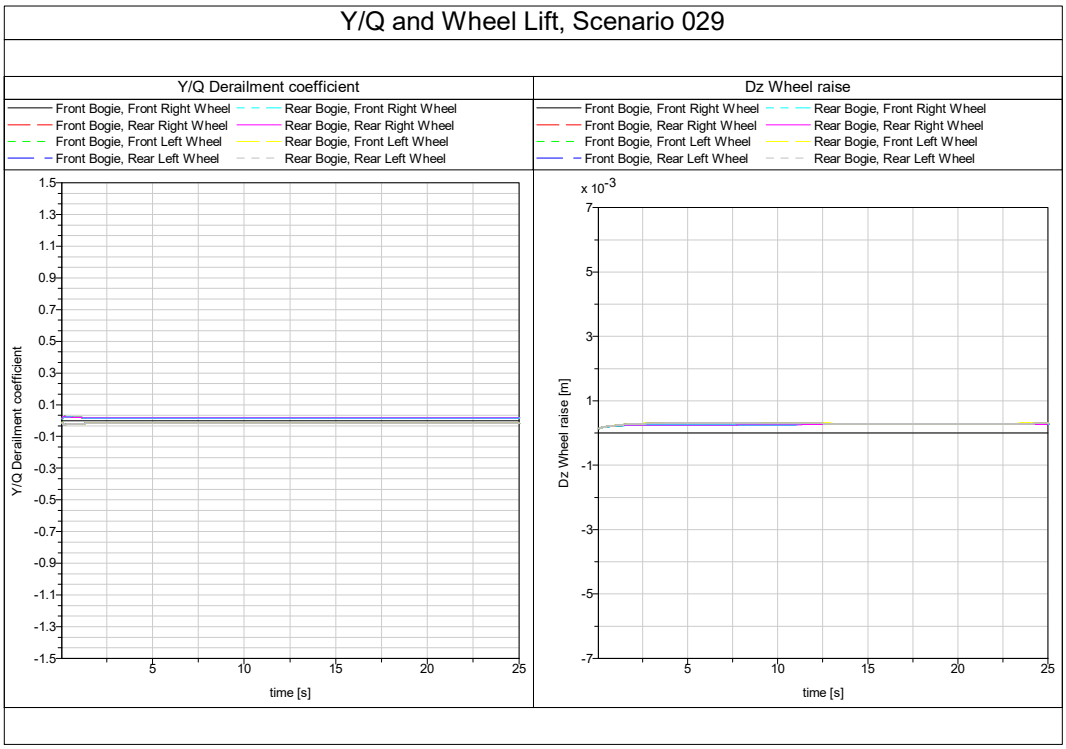

Figure A.61 : Y/Q and Wheel Lift for Scenario 029.

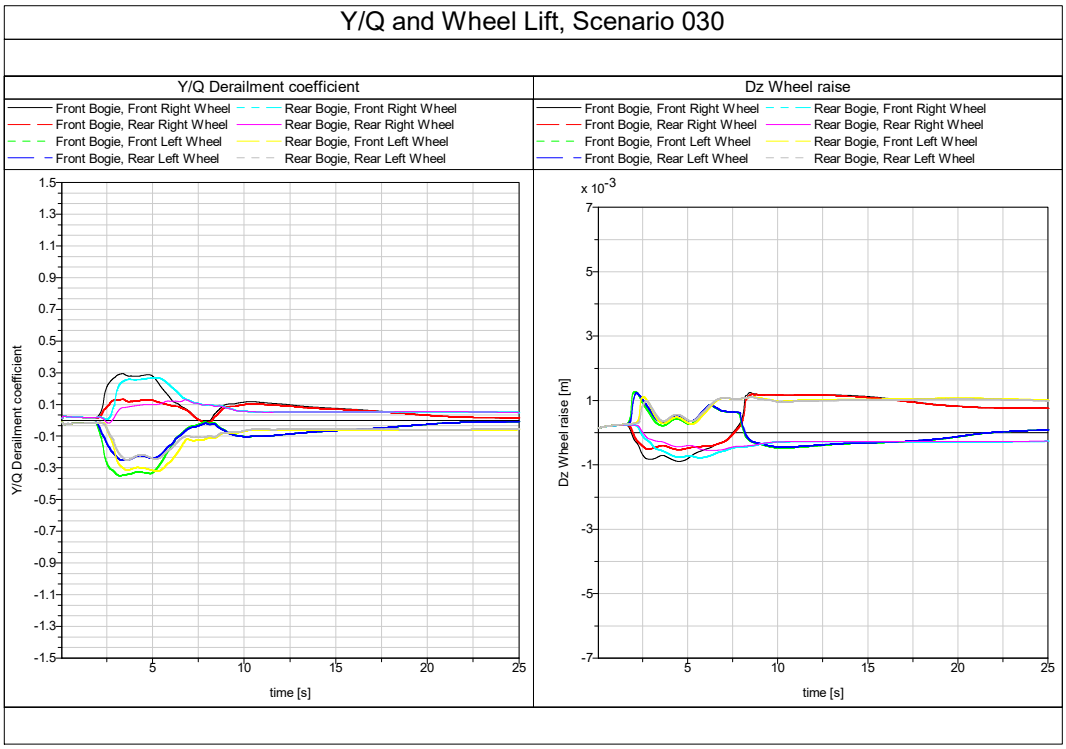

Figure A.62 : Y/Q and Wheel Lift for Scenario 030.

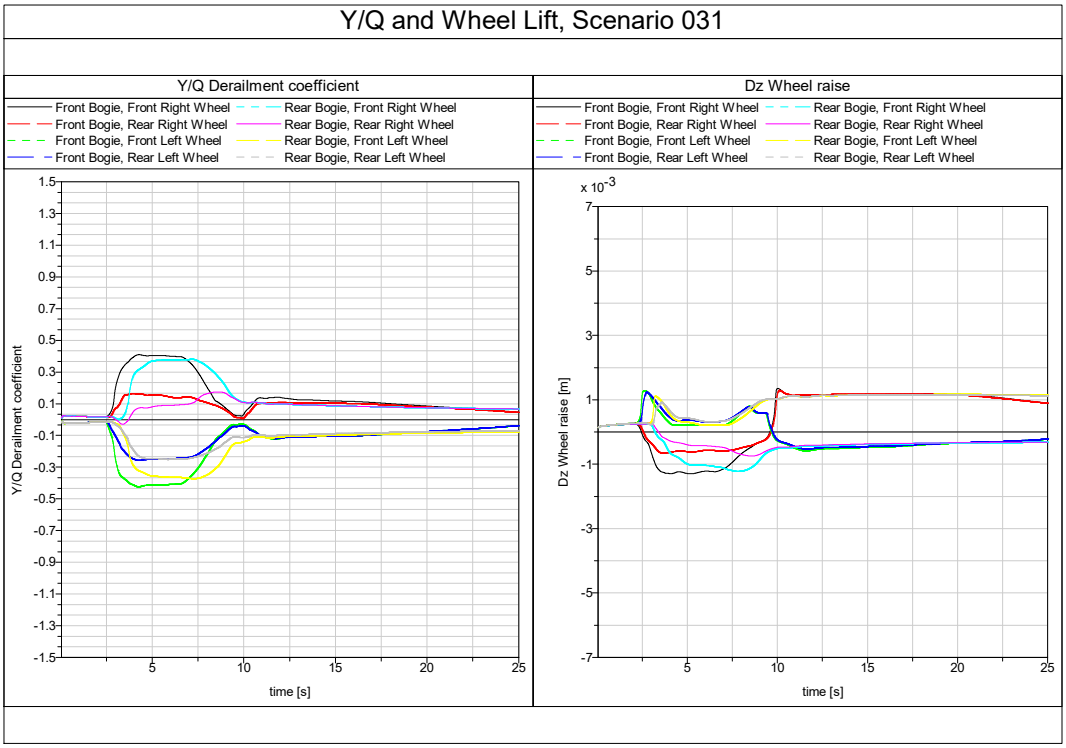

Figure A.63 : Y/Q and Wheel Lift for Scenario 031.

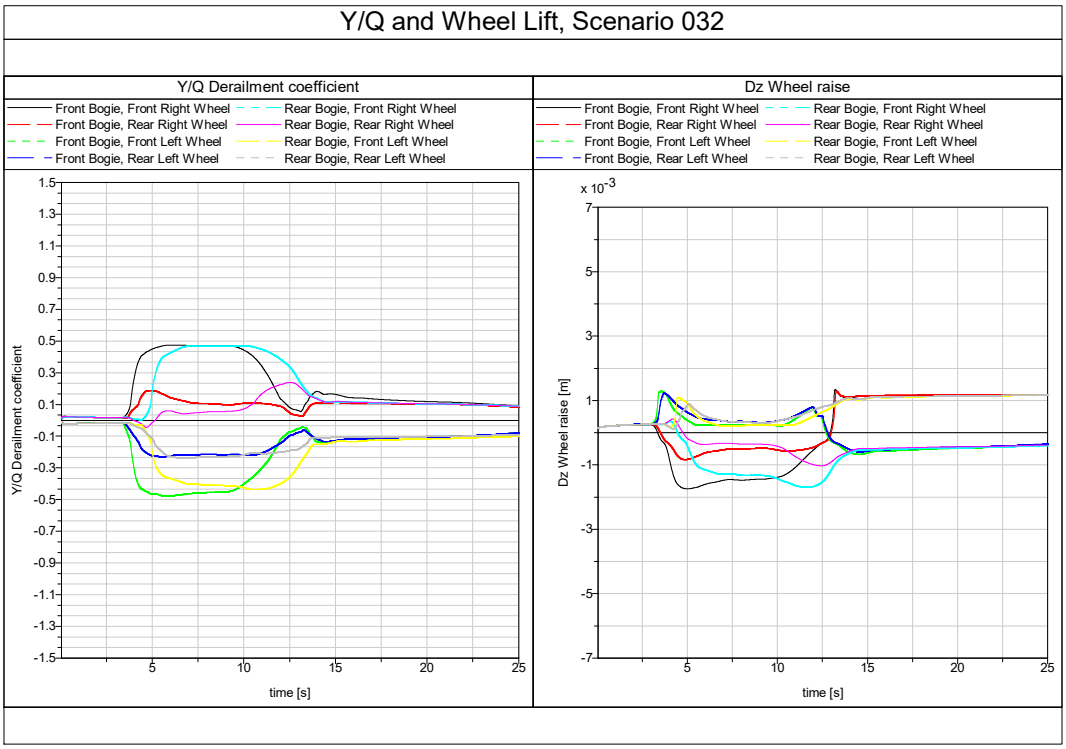

Figure A.64 : Y/Q and Wheel Lift for Scenario 032.

CURRICULUM VITAE

Name Surname : Gökhan KARAKAŞ

EDUCATION :

- **B.Sc.** **:** 2017, Karabük University, Faculty of Engineering, Railway Engineering

PROFESSIONAL EXPERIENCE AND REWARDS:

- 2017 Armin Elektrik Catenary Technical Office Engineer
- 2021 A-Ztech Ltd. CAE and Simulation Engineer